Svoluji k zapůjčení své disertační práce ke studijním účelům a prosím, aby byla vedena přesná evidence vypůjčovatelů. Převzaté údaje je vypůjčovatel povinen řádně odcitovat.

I consent to borrow my doctoral thesis for study purposes and I ask for keeping the exact records of the borrowers. The borrower is obliged to cite all the taken data.

Charles University
Faculty of Science

Study program: Molecular and Cellular Biology, Genetics and Virology

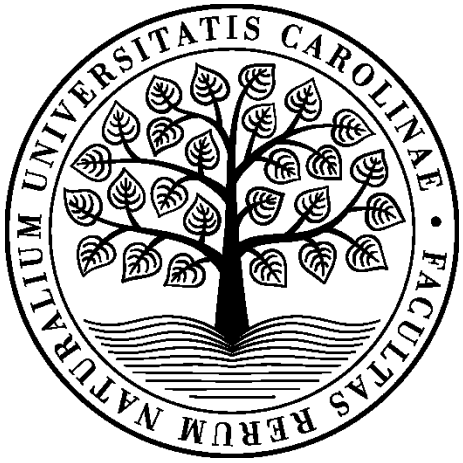

Mgr. Jiřina Žáčková Suchanová

Targeting of viral nanoparticles to cancer specific receptors

Cílení virových nanočástic na specifické nádorové receptory

Doctoral thesis

Supervisor: RNDr. Hana Španielová, Ph.D.

Prague, 2018

Prohlášení:

Prohlašuji, že jsem závěrečnou práci zpracovala samostatně a že jsem uvedla všechny použité informační zdroje a literaturu. Tato práce ani její část nebyla předložena k získání jiného nebo stejného akademického titulu.

Statement:

I declare that I prepared the PhD thesis independently and I stated all used sources of information and literature. This thesis or its substantial part has not been submitted to obtain another or equivalent academic degree.

V Praze/ In Prague 29.6.2018

.....

Acknowledgements

I would like to thank to my supervisor RNDr. Hana Španielová, Ph.D. for the invaluable help, advice and comments that she have provided me during the elaboration of this doctoral thesis. Additionally, I would like to thank to doc. RNDr. Jitka Forstová, CSc. for precious advice and support. I very thank to all my friends and colleagues from the Laboratory of Molecular Virology for very friendly and kind attitude to me and also to other colleagues from our collaborating groups from the Institute of Organic Chemistry and Biochemistry. My special thanks belong to Mgr. Jitka Neburková and Mgr. Petr Cígler, Ph.D. for helping me with chemical part and progression of my research and to Mgr. Pavel Šácha, Ph.D. for providing me of cancer cell lines and SPR equipment. Finally, I would like to thank to my husband and family for their unlimited love, patience, support and trust.

This work was supported by the League Against Cancer Prague and by the Grant Agency of the Czech Republic (GAČR 305/17-11397S).

Abstract

The aim of this thesis is to reveal the potential of mouse polyomavirus (MPyV) based virus-like particles (VLPs) as possible nanocarriers for directed delivery of therapeutic or diagnostic compounds to specific cells or tissues. We have chosen mouse polyomavirus VLPs because they do not contain viral DNA and are considered safe for utilization in bio-applications.

In our research, we used a chemical approach for retargeting of MPyV based VLPs from their natural receptor to cancer cells. The chemical modification of the capsid surface exposed lysines by an aldehyde-containing reagent enabled conjugation of VLPs to selected molecules: transferrin and inhibitor of glutamate carboxypeptidase II (GCPII). Transferrin, as a transporter of iron to metabolically active cells, targeted VLPs to numerous types of cancer cells overexpressing the transferrin receptor. On the other hand, GCPII serves as a transmembrane marker specific for prostate cancer cells and conjugation of its inhibitor to VLPs resulted in successful recognition of these cells. Electron microscopy was used for visualization of modified VLPs and flow cytometry together with confocal microscopy for investigation of cell specific interactions and VLP uptake. Furthermore, we explored the influence of serum proteins on VLPs. The abundance of serum proteins in the blood stream is a major problem of *in vivo* targeting of various types of nanoparticles because these proteins interact with nanoparticle surface and form so called protein corona. The protein corona then masks the targeting ligands and prevents the specific targeting of nanoparticles. We used ELISA assays and flow cytometry to prove that the targeting of prepared VLPs is not affected by protein corona formation.

In conclusion, we demonstrated that polyomavirus based VLPs could be retargeted to either broadly distributed or type-specific cancer markers. This makes the VLPs an universal tool for addressing a wide range of tumors. The strong avidity and binding selectivity of VLP conjugates have a tremendous potential to increase the sensitivity and specificity of cancer therapies.

Key words: polyomavirus, virus-like particle, VLPs, nanoparticle, GCPII, transferrin

Abstrakt

Úkolem této práce bylo prozkoumat potenciál umělých virových částic (virus-like particles, VLPs) odvozených od myšího polyomaviru (MPyV) jako možných nanonosičů pro řízenou dopravu terapeutických a diagnostických látek do specifických buněk či tkání. Vybrali jsme VLPs myšího polyomaviru, protože neobsahují virovou DNA a jsou považovány za bezpečné pro využití v bioaplikacích.

Při našem výzkumu jsme použili přístup chemické modifikace pro přesměrování VLPs z jejich přirozeného receptoru na nádorové buňky. Lysinové zbytky exponované na povrchu částice byly modifikovány aldehydickým činidlem pro následnou konjugaci vybraných molekul, transferinu a inhibitoru glutamát karboxypeptidázy II (GCPII), na povrch částice. Transferin, transportér iontů železa do metabolicky aktivních buněk, pomohl k přesměrování VLPs do různých druhů nádorových buněk nadměrně produkujících transferinový receptor. Na druhou stranu, GCPII slouží jako transmembránový antigen specificky se vyskytující na buňkách nádoru prostaty a připojení malé molekuly inhibitoru k VLPs vedlo k úspěšnému rozpoznání těchto buněk. Použili jsme metodu elektronové mikroskopie k vizualizaci obou typů modifikovaných VLPs a metody průtokové cytometrie a konfokální mikroskopie pro studium specifických buněčných interakcí a internalizace nanočástic. Dále jsme také zjišťovali vliv sérových proteinů na modifikované polyomavirové VLPs. Velké množství sérových proteinů vyskytujících se v krevním řečišti je totiž jedním z hlavních problémů cílení různých nanočástic *in vivo,* protože tyto proteiny interagují s povrchem nanočástice a formují takzvanou proteinovou koronu. Proteinová korona pak zakryje směrující ligand a zabrání specifickému zacílení dané nanočástice. Použili jsme průtokovou cytometrii a ELISA analýzu, abychom prokázali, že směrování VLPs není ovlivněno vytvořením proteinové korony.

Závěrem lze říci, že polyomavirové VLPs lze přesměrovat jak na široce distribuované, tak na typově specifické nádorové markery. To činí z VLPs univerzální nástroj pro cílení širokého spektra nádorů. Silná avidita a vazebná specificita konjugátů VLPs má ohromný potenciál pro zvýšení senzitivity a specificity nádorových terapií.

Klíčová slova: polyomavirus, umělé virové částice, VLPs, nanočástice, GCPII, transferin

Table of Contents

List of Abbreviations

AA	Amino Acid
AF488	Alexa Fluor 488
AuNPs	Gold Nanoparticles
BKPyV	BK Polyomavirus
bp	Base Pairs
BSA	Bovine Serum Albumin
CCMV	Cowpea Chlorotic Mottle Virus
CHO	Cell line from Chinese Hamster Ovary
CPMV	Cowpea Mosaic Virus
CPV	Canine Parvovirus
CPZ	Chlorpromazine
dH_2O	Distilled water
ddH_2O	Deionized water
dpi	Days Post Infection
DLS	Dynamic Light Scattering
DTT	Dithiotreitol
EDC	Ethyl(Dimethylaminopropyl) Carbodiimid (EDC)
EGF	Epidermal Growth Factor
FBS	Fetal Bovine Serum
GCPII	Glutamate Carboxypeptidase II
GFP	Green Fluorescence Protein
HPV	Human Papillomavirus
iGCPII	Inhibitor of Glutamate Carboxypeptidase II
JCPyV	JC Polyomavirus
LT	Large T-antigen
MALDI	Matrix Assisted Laser Desorption/Ionization
MCPyV	Merkel Cell Polyomavirus
MNPs	Magnetic iron oxide-based Nanoparticles
MPyV	Mouse Polyomavirus
MT	Middle T-antigen
NHS	N-hydroxysuccinimidyl ester
NLS	Nuclear Localization Signal
NPs	Nanoparticles
OD	Optical Density

PCV2 Cap	Capsid protein from Porcine Circovirus Type 2
PEG	Polyethylene Glycol
PFU	Plaque Forming Units
PSMA	Prostate Specific Membrane Antigen
QDs	Quantum Dots
rpm	Rotates per minute
SA10	10 mM sodium acetate, pH = 5
SDS	Sodium Dodecyl Sulphate
SDS-PAGE	SDS Protein Electrophoresis
Sf	Spodoptera frugiperda
SPR	Surface Plasmon Resonance
ST	Small T-antigen
SV40	Simian polyomavirus (Simian vacuolating Virus 40)
TAMRA	Tetramethylrhodamine
TBS	Tris Buffer Saline
TEM	Transmission Electron Microscopy
TEMED	N,N,N´,N´-tetramethylethylendiamin
TMV	Tobacco Mosaic Virus
Tf	Transferrin
TfR	Transferrin Receptor
TRIS	Tris-(hydroxymethyl)-aminomethan
uPAR	Urokinase-type Plasminogen Activator Receptor
VLPs	Virus-like Particles
VLP*	Virus-like Particles conjugated with AF488
VLP*	Virus-like Particles conjugated with rhodamine
VLP*-iGCPII	Virus-like Particles conjugated with AF488 and iGCPII
VLP*-PEG	Virus-like Particles conjugated with AF488 and PEG
VLP*-Tf	Virus-like Particles conjugated with AF488 and Tf
VLP*-Tf*	Virus-like Particles conjugated with rhodamine and Tf with AF488
VLP*-T.Red	Virus-like Particles conjugated with AF488 and Texas Red
VP1	Viral Protein 1 (Major capsid protein of Mouse Polyomavirus)
VP1 VLPs	Virus-like Particles containing only VP1 protein

1. Introduction

Detailed study of viruses and understanding of the molecular mechanisms utilized during the infection serve to develop effective drugs against infections but also to find new approaches for drug development. Nowadays, virus-like particles (VLPs) are in the spotlight of many research groups because they have the unique ability to self-assemble into nanostructures similar to viral capsids. Thanks to their structural stability, tolerance to manipulation and fast, easy and cheap production, VLPs are highly utilized not only for studying of virus – host cell interactions but also for production of vaccines or new vehicles for specific delivery of therapeutic or diagnostic compounds. They are able to effectively enter the cells with appropriate receptor. However, due to the absence of the viral genome, they cannot be replicated. On the other hand, VLPs retain their ability to encapsidate foreign nucleic acids and small molecules. This makes them promising tools of gene therapy and diagnostics, where they can serve for targeted delivery of therapeutic DNA, drugs, antigens and contrast agents to cells or tissues. Nevertheless, the clinical application of VLPs derived from viruses infecting humans could be significantly limited by the strong immune response; therefore it is favorable to chose VLPs derived from animal viruses due to the absence of their pre-existing immunity in human population.

This thesis is focused on retargeting of VLPs derived from the mouse polyomavirus (MPyV) to specific cancer cells by chemical modification. We have chosen two different ligands for conjugation onto the surface of VLPs. Firstly; we used the transferrin protein, which is an iron transporter in metabolically active cells. Accordingly, its receptor is overexpressed on numerous types of cancer cell, e.g. bladder, lungs and breast cancer. For chemical conjugation, we used naturally exposed lysine residues on the MPyV VLP surface and created amidic bond between carboxyl group and amino group through N-hydroxysuccinimidyl ester (NHS). Thereafter, the transferrin molecule was attached to VLPs by so called “click” chemistry. The effectivity of conjugation and interaction of prepared VLPs with cancer cells were further tested. Secondly, we decided to examine the possibility of retargeting the VLPs by a small molecule. For this, the inhibitor of glutamate carboxypeptidase II (GCPII) was selected as it was proven to be a powerful system for targeting prostate cancer cells, where GCPII is overexpressed. The same system of modification was used and prepared VLPs were characterized. Both molecules confirmed to be efficient in retargeting of polyomaviral VLPs from their natural receptor to specific cancer cells and thus could serve as potent nanocarriers for biomedical applications.

The third goal of this thesis was to analyze the behavior of polyomaviral VLPs in the presence of serum proteins. These proteins are naturally present in blood stream and could form the protein/biomolecule corona that influences the nanoparticle behavior in physiological conditions, especially the targeting capacity of nanoparticles. Hence we incubated our VLPs with various serum proteins and tested the selectivity of interactions with cells. Surprisingly, we found out that the VLPs bound to cells without being restrained by the formation of protein corona.

2. Literature Overview

2.1 Mouse Polyomavirus

Mouse polyomavirus (MPyV) belongs to the *Polyomaviridae* family of small DNA tumor viruses. This family comprises about a hundred polyomaviral species which infects mammals, birds, fishes and arthropods (Buck et al., 2016; Moens et al., 2017). The model representatives are MPyV and Simian vacuolating virus 40 (SV40), both mostly studied from the molecular biology aspect. SV40 infects mostly monkeys, however, its sequences were found also in human cells. Therefore we have focused our research on MPyV that will not be recognized by the pre-existing antibodies in human immune system. From polyomaviruses infecting humans are currently the most significant BK polyomavirus (BKPyV), JC polyomavirus (JCPyV) and Merkel cell polyomavirus (MCPyV). Mammalian polyomaviruses usually after primary infection induce lifelong persistence and are not linked to acute infection. The major sites for persistence are skin (MCPyV), kidney (BK virus), central nervous system and hematopoietic system (JC virus). However, immunosuppression can serve as a stimulus for reactivation, leading to several disease patterns (Dalianis and Hirsch, 2013). Productive polyomaviral infection proceeds as follows: early antigens are expressed in the cell and induce the S-phase of cell cycle to provide replication of the viral genome. After generation of new progeny, viruses are released by the cell lysis.

2.1.1 Genome organization

The covalently closed circular genome of MPyV consists of double-stranded DNA with 5297 bp. The genome is separated into 3 regions: early, late and regulatory (Fig. 2.1). Products of the early region are created from the reverse chain unlike products from the late region and are transcribed early after the cell entry. However, the expression is not limited only by the early stage but continues also during the late stages of infection.

The early region encodes 3 viral regulatory tumorogenic proteins (so called T-antigens). All T-antigens have a common N-terminal part of mRNA because they are created by alternative splicing from pre-mRNA molecule. T-antigens are important for induction of viral replication and transformation of infected cell. LT stimulates the cell cycle and interacts with its regulators and therefore is responsible for immortalization of the cell. However, in contrast to other Polyomaviridae species, MPyV could transform the cell only when LT cooperates also with MT antigen (Dilworth, 1990). MT associates with many proteins of signal transduction and regulators of cell growth. ST antigen provides interaction with protein phosphatase 2A and therefore activate the MAP kinase signaling pathway and cell growth (Sontag et al., 1993).

The regulatory region contains replication origin, promoters and enhancers (ENH/ORI). The origin of replication is important for initiation of DNA replication and is composed of internal sequence (core) and 2 side sequences that serve as enhancer of transcription and binding site for LT antigen.

Late region is composed of genes encoding 3 structural viral proteins VP1, VP2 and VP3. Similarly to early proteins, structural proteins are also created by alternative splicing from common pre-mRNA molecule. The sequence of minor protein VP3 is all encompassed in the C-terminal sequence of minor protein VP2. The major capsid protein VP1 is read from another open reading frame and therefore the amino acid (AA) sequence is different.

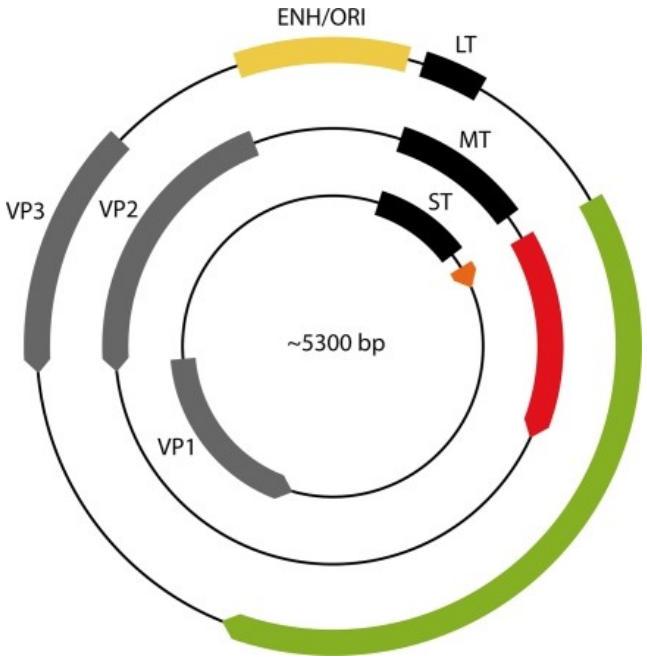

Figure 2.1: **Map of MPyV genome**
Early and late regions are separated from each other by regulatory region (ENH/ORI). Colors illustrate the positions of early tumorogenic antigens LT, MT and ST (black color determines the common N-terminal part) and late structural proteins VP1, VP2 and VP3 (Fluck and Schaffhausen, 2009).

2.1.2 Major capsid protein VP1

The major capsid protein VP1 mediates specific interaction with cell receptor and following internalization of the virus into the cell. Probably it is taking part also in attaching the viral genome to the nuclear matrix and beginning of early transcription (Carbone et al., 2004). VP1 with its molecular weight of 45 kDa is the major protein of viral capsid.

The tertiary structure of VP1 protein was described by RTG diffraction (Liddington et al., 1991; Stehle and Harrison, 1996). According to the tertiary structure, VP1 could be separated into 3 regions: N-terminal, central and C-terminal. The N-terminal domain is hidden inside the pentamer and contains nuclear localization signal and DNA binding domain

(Chang et al., 1993) that interacts with DNA unspecifically (Moreland et al., 1991). The central part of VP1 protein is organized into α-helixes and antiparallel β-sheets that are connected with 6 loops. The most important loops, BC, DE, EF and HI are described in the figure 2.2A. Loops BC and HI are important for specific VP1/receptor interaction, EF loop is located on the side of VP1 proteins and serves as a part of binding site for Ca^{2+} ions (Stehle et al., 1994; Stehle and Harrison, 1996). The DE loop contains the major immunodominant epitope and mediates the interaction with MPyV co-receptor α4β1 integrin (Caruso et al., 2003). C-terminus of VP1 protein is very flexible, mediates the interaction between pentamers (Fig. 2.2A,B) and is also a part of Ca^{2+} ions binding site (Liddington et al., 1991; Stehle et al., 1996).

The important ability of VP1 protein is self-assembling either *in vitro* or *in vivo* into the capsid related structures and creating artificial viral particles (virus-like particles, VLPs). Even though VP1 protein could be intensively posttranslationally modified by phosphorylation, acetylation, sulphonation, methylation and hydroxylation (Bolen et al., 1981), neither of these modifications is needed for VLPs assembly (Salunke et al., 1986). Moreover, the presence of minor capsid proteins VP2 or VP3 is not essential for capsid formation (Montross et al., 1991).

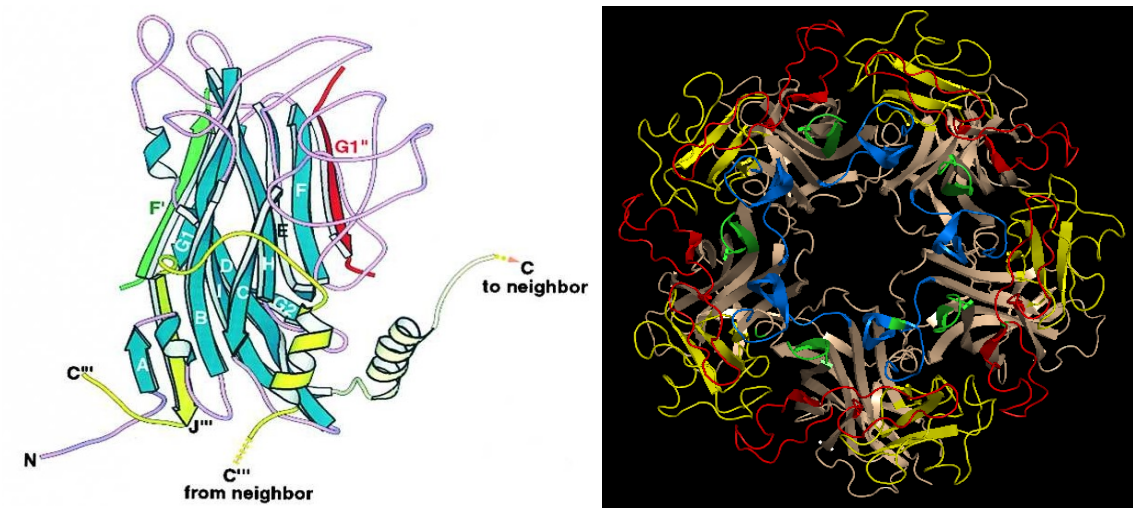

Figure 2.2: **Structure of capsid protein VP1**
(A) Tertiary structure of major capsid protein VP1 with described terminal domains and important loops. The connection to other VP1 monomers is indicated by positions of neighbor C-terminus. Taken from Chen et al., 2000. (B) Ribbon drawing of pentamer composed of 5 monomeric VP1 proteins. The most important loops of VP1 protein are visualized by various colors: BC loop (red color), DE loop (blue color), EF loop (yellow color) and HI loop (green color). The cavity in the middle of the pentamer serves for connection of minor protein. Taken from Suchanova et al., 2015.

2.1.3 Structure and morphogenesis of virion

The MPyV capsid has 45 nm in diameter, icosahedral symmetry and is formed from 3 structural proteins: VP1 (45 kDa), VP2 (35 kDa) and VP3 (23 kDa). It is composed of 360 molecules of VP1 protein which creates 72 pentamers, 60 hexavalent and 12 pentavalent (Fig. 2.3). The central cavity of VP1 pentamer serves for conjugation of minor protein; however, as it was mentioned above, capsid could be formed also without the presence of minor proteins.

The morphogenesis of virion starts with translocation of structural protein complexes that were synthesized in cytoplasm and transported into the nucleus. The process of morphogenesis is described as sequential assembly of virion. Structural proteins of the virion cover genomic DNA in a form of chromatin because it is associated with cellular histones H2A, H2B, H3 and H4 and the condensed minichromosome is called "nucleocore". According to Griffith et al., 1992, the condensation of capsomeres is dependent on the presence of minor proteins which direct capsomeres to the viral minichromosome. It is supposed that during the final part of morphogenesis there is a conformational change which changes immature virion to stable mature virion. Nevertheless, the big question was how the specific polyomaviral DNA is packed into the virion and which cellular proteins take part in the DNA encapsidation. Oppenheim et al., 1992 discovered so called *ses* sequence (SV40 encapsidation signal) in the regulatory region of viral genome. But for many years the mechanism for MPyV was unknown. After thorough research Spanielová et al., 2014 found out that there is no specific sequence for mouse polyomavirus (*pes*); however, the encapsidation is dependent on the replication rate of circular DNA.

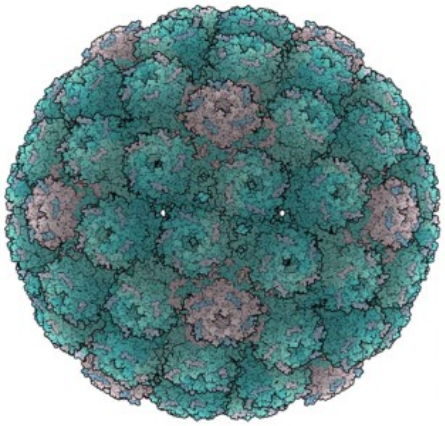

Figure 2.3: **Structure of mouse polyomaviral capsid**
The MPyV capsid composed of VP1 pentamers. Hexavalent pentamers are indicated by green/blue color and pentavalent pentamers by purple color. Taken from Stehle and Harrison, 1996.

2.1.4 Life cycle

The life cycle starts with the binding of viral particle to cellular receptor (Fig. 2.4). For MPyV the receptors are gangliosides GD1a and GT1b containing sialic acid (Tsai et al., 2003) and as a co-receptor was indentified α4β1 integrin (Caruso et al., 2003). The following endocytosis is mediated by smooth monopinocytic vesicles that transport virus to early endosome. The uptake is a fast process, after 30 minutes the majority of the virus is internalized in the cell (Richterova et al., 2001). The mechanism of viral entry into the nucleus still remains unknown, however, it is intensively studied in our laboratory and the involvement of importin β1 was recently published (Soldatova et al., 2018). Immediately after viral entry to the nucleus early genes are transcribed by the host RNA II polymerase and produced T-antigens dysregulate cell cycle and stimulate the transition to S-phase. For initiation of replication the LT antigen has to bind the region of replication origin (ori). The late region of viral genome is not transcribed until replication of viral DNA starts. Increase level of structural proteins is followed by virion assembly and newly produced viral particles are released from the cell by cell lysis (Fields et al., 2007).

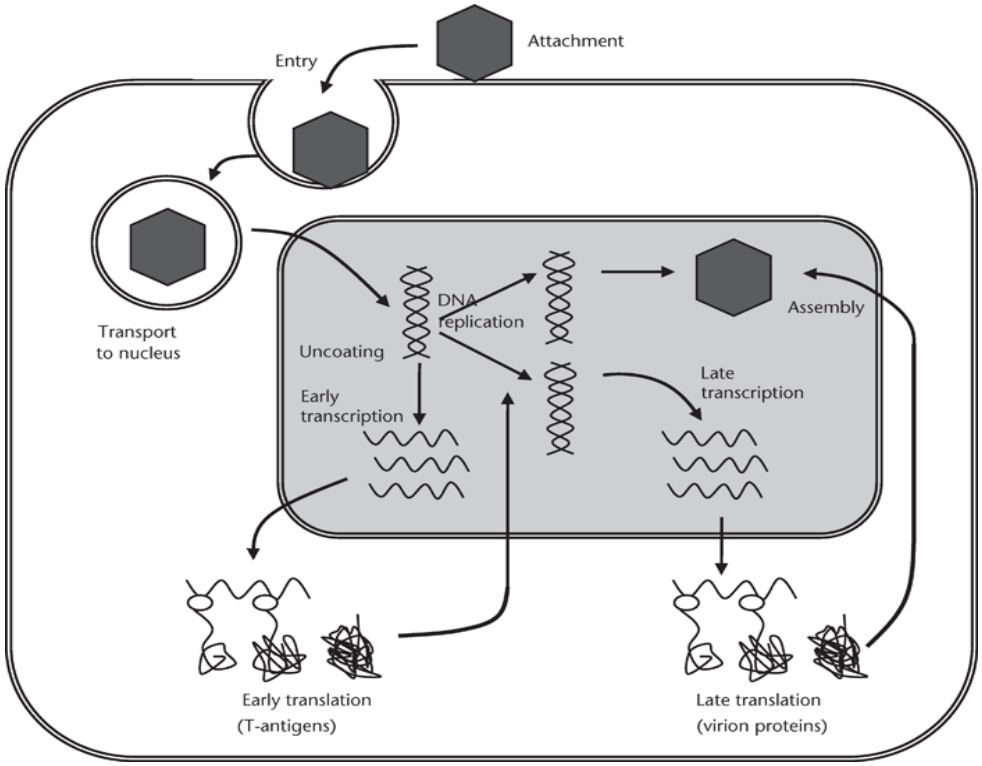

Figure 2.4: **Life cycle of MPyV**
The illustration of mouse polyomavirus life cycle. Taken from (Java et al., 2012)

2.2 Utilization of MPyV VLPs for therapeutic purposes

A number of capsid proteins have the unique ability to self-assemble into artificial viral capsids (VLPs) that are similar to wild type virus, however, do not contain the viral DNA. Therefore they are non-infectious and safe for biomedical applications. VLPs are thanks to their high tolerance to manipulations, structural stability and very cheap and fast production abundantly utilized during the study of virus/host cell or virus/immune cell interactions. Their strong immunogenicity determines also usage in vaccine preparation. Furthermore, VLPs has the ability to encapsidate small molecules and DNA inside of the capsid. This makes them efficient tools for diagnostics, gene therapy and immunotherapy, where they serve for delivery of therapeutic RNA, DNA, drugs, contrast agents or antigens into the targeted cells.

2.2.1 Utilization of MPyV VLPs for delivery of diagnostic and therapeutic molecules

According to the ability of VLPs to incorporate proteins, nucleic acids and other molecular compounds, the possibilities of their usage are very wide. Moreover, VLPs are able to protect the encapsidated heterologous compounds and transport them through plasmatic membrane to eukaryotic cells either *in vitro* or *in vivo*.

2.2.1.1 Utilization of MPyV VLPs for delivery of proteins and peptides

The interior space of VLPs could serve as a nanocontainer for encapsulation of biologically active proteins or peptides, deliver the cargo into targeted cells and protect it from external proteases and recognition by the immune system.

The conjugation of peptide to MPyV VLPs could be realized by two ways: either by fusion of protein to major capsid protein VP1 or to minor capsid proteins VP2/VP3. Conjugation of GFP molecule to VP1 protein was mediated by the 28 AA of the WW domain of the mouse formin-binding protein 11 (Schmidt et al., 2001). This domain binds proline-rich ligands with very high affinity and the name is derived from two essential tryptophan residues. The fusion to N-terminal part of VP1 protein allowed the conjugation of 260 polyproline-tagged GFP molecules (Günther et al., 2001). According to the theoretical calculation 360 globular GFP molecules could be encapsidated into VP1 particles and so the achieved number 260 seems very promising. However, the authors did not attempt to verify the position of GFP protein on the VP1 capsid and therefore GFP molecules could be also exposed on the surface. On the other hand they showed the ability of these VLPs to deliver

GFP to mouse fibroblasts NIH 3T3 (Günther et al., 2001). The C-terminus of VP1 protein served also for conjugation of the entire capsid protein of porcine circovirus (PCV2 Cap), nevertheless, this fusion avoided VLP assembly and allowed only the formation of pentamers (Fraiberk et al., 2017). Despite this fact, the conjugation of the whole PCV2 Cap protein was the most effective vaccine variant from all tested possibilities (Fig. 2.5).

An alternative approach is conjugation of peptide with minor proteins. According to the electron density map it was revealed that 45 AA from the C-terminus of minor proteins VP2/VP3 are essential for the interaction with the cavity of VP1 pentamer (Chen et al., 1998). However, not long ago Dashti et al., 2018 found out that the minimum anchoring C-terminal sequence of VP2/3 proteins is not 45 AA but only 31 AA. In the pioneer work, the 49 AA of the C-terminal part of VP2 protein served as an anchor for conjugation of GFP molecule. Prepared VLPs were stable, regularly shaped and the amount of encapsidated GFP was very high (64) and almost reach the theoretical number of 72 (Abbing et al., 2004). Consequently, GFP was also fused with C-terminal part of VP2 protein (51 AA) and encapsidated to VLPs produced in plants (Catrice and Sainsbury, 2015). Recently, the co-encapsidation of 2 fluorescent proteins, GFP and mRuby3, into one MPyV VLP was realized. These particles successfully delivered these proteins into HUVEC cells (Dashti et al., 2018). VP2 protein anchor served also for efficient transport of a 683 AA long fragment of the receptor Her2 (Tegerstedt et al., 2007, 2005) and entire human prostate specific antigen (Eriksson et al., 2011) into dendritic cells. A similar approach was used for minor protein VP3, where EGFP was fused to N-terminus of truncated VP3 (corresponding to positions 225-324 in VP2 sequence) (Bouřa et al., 2005). This construct was utilized for testing of immune responses to various proteins, for example, EGFP (Frič et al., 2008), Bcr-Abl (Hrusková et al., 2009) and PCV2 Cap (Fig. 2.5, Fraiberk et al., 2017).

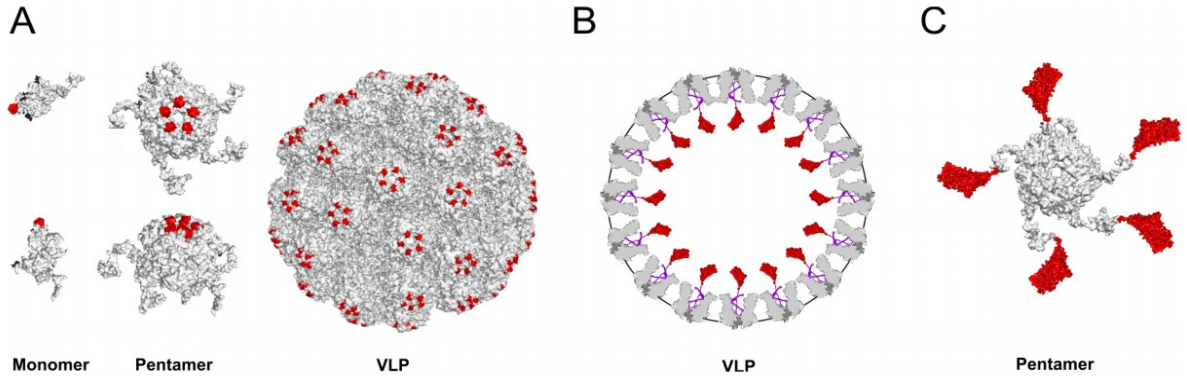

Figure 2.5:**Design of chimeric structures based on MPyV capsid proteins, carrying sequences of PCV2 Cap** (A): Monomers, pentamers and VLPs of MPyV (grey) with immunogenic epitopes of PCV2 Cap (red) inserted into the DE loop of MPyV VP1. (B): Entire PCV2 Cap (red) fused with truncated MPyV minor capsid protein—VP3 (violet) is situated inside the MPyV VLP. Cross-section of VLP (grey) is presented. (C): Entire PCV2 Cap (red) fused to the C-terminus of MPyV VP1 (grey) forming a pentameric capsomere. Taken from Fraiberk et al., 2017.

2.2.1.2 Utilization of MPyV VLPs for delivery of nucleic acids

Naturally, nucleic acids are obvious cargos for VLPs. The presence of NLS in the VP1 structure allows the efficient encapsidation of nucleic acids without the need of VP2/3 presence. Historically, VLPs were used exclusively for delivery of DNA for gene expression, nevertheless, today the gene therapy is more focused on direct transfer of mRNA or silencing molecules (Lund et al., 2010). The complex of VLP with specific nucleic acids could be prepared *in vitro* as well as *in vivo*. It was already proved that MPyV VP1 VLPs could interact with heterologous DNA *in vitro* (Štokrová et al., 1999), enter the mammalian cells and deliver the encapsidated DNA to the nucleus with following expression. This process is known as *pseudoinfection* and these VLPs are called *pseudocapsids* (Forstová et al., 1995). Preparation of VP1-DNA complexes is one of the limitation steps for successful gene delivery. It was published that complexes of empty particles and DNA are most effectively produced at a molar ratio of 5:1 capsids:DNA (Krauzewicz et al., 2000). The size of naked exogenous DNA that was stably complexed with VP1 protein and protected against DNases was approximately 3 kbp (Forstová et al., 1995). However, in complex with histones, the size of encapsidated DNA increases up to 5 kbp (Gillock et al., 1997). The major advantage of polyomaviral VLPs is their ability to deliver DNA into cells, where the DNA is expressed for relatively long time. The wild type mice expressed the DNA for few months and the immunosuppressed mice expressed even higher amounts of DNA for longer time period (up to 6 months) (Heidari et al., 2000). Effective delivery of transgenes into cells is mediated by interaction with sialic acid because the neuraminidase treatment led to inhibition of gene transfer. After the binding to receptors, pseudocapsids are transferred along microtubules to the nucleus and the inserted gene is transferred (Krauzewicz et al., 2000). Even though, the efficiency of VLP binding and entry does not alter from infectious virions (Richterová et al., 2001), in case of successful delivery of DNA to the nucleus the situation is different. Only minor part of VLP particles is able to transport the incorporated DNA into the nucleus, what is probably caused by the absence of minor proteins that are not essential for VLP assembly but play a crucial role in DNA delivery (Mannová et al., 2002; Španielová et al., 2014).

MPyV VP1 VLPs were tested also as a mean for delivery of antisense oligonucleotides; specific drugs for inhibition of gene expression at the transcriptional level. VLPs were loaded with fluorescently labeled oligonucleotides against N-methyl-D-aspartate receptor. These particles were used for transduction of cells overexpressing this receptor and cytotoxicity was measured. However, in comparison to other delivery methods, MPyV VP1

VLPs had only a moderate effect on antisense oligonucleotide functionality cytotoxicity test (Weyermann et al., 2004).

In addition to MPyV, other members of *Polyomaviridae* family were tested for the ability of unspecific nucleic acids binding and their further transportation into cells. The efficient delivery of DNA was achieved also with hamster polyomavirus (Voronkova et al., 2007), SV40 (Enomoto et al., 2011; Kimchi-Sarfaty and Gottesman, 2012, 2004; Nakanishi et al., 2008), human polyomavirus BKPyV (Schowalter and Buck, 2013; Touzé et al., 2001), human polyomavirus JCPyV (Chao et al., 2018, 2015; Chen et al., 2010; Deng et al., 2015) and human polyomavirus MCPyV (Schowalter and Buck, 2013). SV40 and JCPyV were utilized also for effective transfer of interfering RNA. For SV40 it was siRNA (Kimchi-Sarfaty et al., 2005; Kler et al., 2012) and for JCPyV short hairpin RNA (Chou et al., 2010; Lin et al., 2014).

2.2.1.3 Utilization of MPyV VLPs for delivery of other molecular compounds

The internal space of particle could be used for encapsidation of fluorescent probes, diagnostic or therapeutic compounds, leaving the external surface free for interaction with receptor or conjugation of targeting ligand. MPyV VLPs have not been extensively studied for this kind of application, however, some studies exist. Firstly, a fluorescein was conjugated to the VLP interior. All naturally occurring cysteines were replaced by serines and new cysteine was incorporated into GH loop that is faced to the internal space of MPyV VLPs. Then fluorescent dye Texas Red was conjugated through a maleimide linker to the cysteine residue. The prepared VLPs retained their ability to bind the receptor and successfully entered mouse cells C2C12 (Schmidt et al., 1999). Secondly, the drug methotrexate; a well known antifolate utilized in tumor therapy, was covalently linked to the VP2 anchor with loading of 462 methotrexate molecules per VLP. The drug was efficiently delivered to cells CCRF-CEM and demonstrated time and concentration dependent cytotoxicity (Abbing et al., 2004).

Contrary to MPyV VLPs, SV40 and JCPyV VLPs were thoroughly investigated as delivery vehicles of diagnostic and therapeutic compounds. The molecules could be inserted either by a simple encapsidation or through chemical or genetic conjugation. JCPyV VLPs enabled encapsidation of propidium iodide (Goldmann et al., 2000) and fluorescent dye Cy3 (Qu et al., 2004) and loading of hydrophobic cytostatic drug paclitaxel through modified β-cyclodextrin with thiol-reactive group (Niikura et al., 2013). SV40 VLPs were utilized for encapsidation of various nanoparticles: quantum dots (QDs), gold nanoparticles (AuNPs) and magnetic iron-based nanoparticles (MNPs). QDs are nanocrystals with outstanding properties

such as high density (TEM visualization), high absorption coefficient and fluorescence quantum yields (fluorescence microscopy visualization) (Li and Zhu, 2013). Various conditions for QDs assembly into SV40 VLPs were performed; regular assembly buffer (Li et al., 2009), dissociation buffer (Gao et al., 2013) and various charges of QD surface coatings (Li et al., 2010). In all cases VP1 pentamers bound QDs with high affinities, suggesting that QD serves as a scaffold and nucleation center for VLP assembly. The ratio of QD:VLP is 1:1 and their internalization into cells is similar to wild type virus. Other nanoparticles with outstanding optical properties, such as scattering in the visible-near infrared region and strong absorption are AuNPs. These particles were already applied in photothermal therapy, gene therapy and biosensing (Khlebtsov et al., 2013). AuNPs of different sizes were encapsidated into SV40 VLPs, where the efficiency increased with the diameter of the AuNPs (from 10 nm to 30 nm) (Wang et al., 2011). However, the group continued with the research, conjugated AuNPs on the VLP surface and published combinations of this approach with encapsulated QDs (Li et al., 2012, 2011). The last type of nanoparticles are MNPs that are supramagnetic and therefore applicable for diagnostic (magnetic resonance) or therapeutic methods (magnetic hyperthermia) (Gupta and Gupta, 2005). These MNPs were coated with citrate and encapsidated into SV40 VLPs (Enomoto et al., 2013). This process was followed with chemical conjugation of epidermal growth factor (EGF) on the VLP surface that enabled the specific targeting of these VLPs to the cancer cells overexpressing EGF receptor. Recently the micron-sized MNPs were layered through streptavidin of the surface of VLPs containing QDs. The fluorescence of QDs was utilized for the detection of cargo entry and intracellular localization. After 16 hours VLPs were localized in the perinuclear space of Vero cells and therefore could serve as a Trojan horse for MNPs delivery (Gao et al., 2016).

2.2.2 Retargeting of MPyV VLPs to specific cell types

For utilization of VLPs in therapy and diagnostics it is necessary to target the therapeutic compound specifically to damaged tissue and protect it from interaction with healthy cells. Only this could bring the effective therapy with a minimum of side effects mediated by free distribution of the active substance.

Cancer markers and ligands must be used for specific targeting of viral particles. The conjugation to the MPyV VLPs could be realized by two methods, either by genetic modification with alteration of viral genome or by chemical modification, where the ligand is chemically coupled through a reactive group on the VLP surface. The major advantage of VLPs against other therapeutic vehicles is the ability to display a high number of targeting

proteins or molecules and their amount and orientation could be controlled (Gupta et al., 2005).

2.2.2.1 Targeting of MPyV VLPs through genetic modification

Targeting by genetic modification requires the construction of genetic fusion between targeting ligand and the major capsid protein VP1. The limitation of genetic modifications of MPyV VLPs is the necessity of finding the appropriate position in the surface loop that will allow a display of our inserted protein sequence on the VLP surface and at the same time will not have a negative effect on the VLP stability. For SV40 virus these loops are only DE and HI (Takahashi et al., 2008).

The MPyV VLPs were modified by genetic approaches very frequently because it allows the insertion of peptides into 4 surface loops (BC, DE, EF, and HI). The purpose of VLP modification could be either retargeting or immunotherapy. The techniques and success of already realized modifications are summarized in Table 2.1. After insertion of epitope into the surface loop, it is displayed on the exterior in 360 repetitions and therefore it is accessible for numerous interactions. The size limitation of inserted peptide exists and it is usually between 20 to 40 AA. In some cases the flexible linkers (e.g. glycine-serine) are connected to both sides of inserted peptide to facilitate the assembly into proper conformation. The insertion of flexible linkers even enabled internalization of a whole enzyme (dihydrofolate reductase) with 18 kDa (Gleiter et al., 1999). The enzyme showed major changes in comparison to wild type, however, the enzymatic activity remained functional. Very surprisingly the insertion of enzyme did not have detrimental effect on VLPs assembly. The other example of successful incorporation of selected molecule directly into VP1 sequence were fragments of activator of urokinase-type plasminogen receptor (uPAR) that served as targeting moieties the uPAR receptor. The protein uPAR is expressed by many cancer cells and correlates with metastasis and poor prognosis. All four loop were tested for insertion of uPAR activator sequences, nevertheless, only EF loop was able to accept the incorporation without negative effect on protein solubility or particle stability (Shin and Folk, 2003).

Genetic modifications could be used not only for direct conjugation of molecules but also for connection of molecules through insertion of adaptor molecules. Adaptors have dual specificities: one end binds the targeting molecule and the other binds viral protein. The way of designing could be realized by genetic modification of VLPs so that they will display the versatile adaptor binding motif. Many motifs were genetically engineered to MPyV VP1 VLPs. In one study, 9 AA region of polyanionic peptide was inserted into HI loop and served as an adaptor for fusion with complementary polyanionic sequence on Fv fragment of tumor specific antibody. This conjugation did not affect the particle stability and successfully

Table 2.1: **Overview of MPyV VP1 protein modification and their influence on the VLPs assembly**
This table was taken and adjusted from Suchanova et al., 2015**.**

Virus	Insert	Location	Utilization	Expression system	Assembled VLPs	References
MPyV	pre-S1 phil - 2 hydrophilic fragments from HBV pre-S1 sequence (70 AA and 6 AA linkers)	HI loop	immunization	*S. cerevisiae*	Yes	(Skrastina et al., 2008)
MPyV	B-cell epitopes (12 a 14 AA)	BC loop	immunization	*E. coli*	Yes	(Neugebauer et al., 2006)
MPyV	PCV2 Cap epitopes (5 variants: 16, 13, 17, 9 and 18 AA)	DE loop	immunization	Baculovirus	Yes	(Fraiberk et al., 2017)
MPyV	protein Z (antibody binding to a domain of protein A) (57 AA + 17 AA linkers)	HI loop	retargeting	*E. coli*	Yes	(Gleiter and Lilie, 2001)
MPyV	WW domain (from murine FBP11) (38 AA)	DE loop HI loop	retargeting	*E. coli*	No	(Schmidt et al., 2001)
MPyV	peptide with 8 glutamate and 1 cysteine residues	HI loop	retargeting	*E. coli*	Yes	(Stubenrauch et al., 2001)
MPyV	peptide sequence binding uPAR (60 AA) or FLAG sequence (8 AA)	BC loop DE loop HI loop EF loop	retargeting	Baculovirus	No Yes	(Shin and Folk, 2003)
MPyV	peptide sequence binding to GCPII (9 AA)	BC loop	retargeting	Baculovirus	Yes	(Suchanova, 2012)
MPyV	peptide sequence binding to Bcr-Abl (25 AA)	HI loop	retargeting	Baculovirus	No	Spanielová, unpublished results

Abbreviations: AA – amino acids; FBP11 – formin binding protein 11; uPAR – urokinase-type plasminogen activator receptor; PCV2 Cap – capsid protein of porcine circovirus type 2

retargeted VLPs to dendritic cells (Stubenrauch et al., 2001). In other study, the 38 AA domain of protein Z was incorporated into HI loop of VP1 protein. Protein Z is a binding domain derived from protein A of bacteria *Staphylococcus aureus* and therefore has the ability to bind antibody immunoglobulins. This insertion allows the association of chosen antibody type that will determine the targeting specificity of such modified VLPs. The group confirmed that conjugation of herceptin antibody did not affect the particle stability and selectively retargeted VLPs to glycoprotein Her2, which is presented on several different human cancer cells (Gleiter and Lilie, 2001). Schmidt et al., 2001 investigated the insertion of 28 AA of the WW domain of the mouse formin binding protein 11. WW domains bind proline-rich sequences with PPLP consensus motifs; however, their utilization is limited by high dissociation rate and loss of the VLP assembly capacity. In conclusion, the MPyV VLPs could be genetically retargeted to specific cellular markers but only few studies demonstrated stable VLPs with high selectivity. Probably it is not only the size of inserted foreign sequence that affect the particle integrity, the stability of VLPs could be influenced also by the actual position and character of foreign sequence introduced to VP1 protein and therefore it really hard to predict what effect on VLPs will the insertion have.

2.2.2.2 Targeting of MPyV VLPs through chemical modification

Conjugation of molecules on the VLP surface utilizing covalent bonds offers many advantages. Contrary to genetic modifications here we have the possibility to conjugate various different molecules usually without a steric hindrance and could be mostly sure that the molecule will be displayed on the VLP surface. To apply chemical conjugations on VLPs it is necessary to know the crystallographic structure that identifies the AA residues located on the external part of VLPs. Currently most of the viruses have known crystallographic structure and polyomaviruses are not an exception (Liddington et al., 1991; Stehle et al., 1996).

Nowadays the mostly used techniques for chemical modifications of viral particles are based on classical methods used for protein adjustments (Hermanson, 2008; Wong, 1991). The bioconjugation techniques that are currently utilized for covalent modifications of surface exposed amino acids of virus-like particles are thoroughly reviewed in (Strable and Finn, 2009). Briefly, the most used amino acids for modifications are cysteines, lysines and amino acids containing carboxyl group. The most exploited method for conjugation of molecules to the VLP surface is creation of amide bond between amino and carboxyl group. This method allows connection of peptide of fluorophore to surface exposed lysines through carboxyl residues that are firstly activated by carbodiimid (EDC) and N-hydroxysuccinimide (NHS)

and then react with lysine amino residues thus forming the amides. Also thiol residues of cysteines could be utilized as reactive groups for conjugation of molecules. The bond is created by alkylation of thiol group of cysteines by reaction with bromo/iodo acetamide or maleimide.

Chemical modifications are not much explored yet for polyomaviral VLPs. The pioneer work was done for SV40 VLPs, where in fact, it is a combination of chemical and genetic modification. The reactive cysteine group was genetically inserted into DE loop of VP1 protein because the majority of naturally presented cysteines in VLPs are connected with each other through disulfide bonds and therefore do not have a free thiol group. The thiol group of inserted cysteine was further utilized for chemical conjugation of full length human EGF through heterobifunctional cross-linker SM(PEG)2 containing maleimide and succinimide moieties. These modified VLPs showed 10-fold high selective internalization to cells overexpressing EGF receptor compared to unmodified VLPs (Kitai et al., 2011). As there were no published experimental data investigating the potential of polyomaviruses as a backbone for chemical conjugation utilizing naturally occurring lysines, we decided to focus our research on that topic. The results of our two successful conjugations of high molecular weight molecule transferrin (Zackova Suchanova et al., 2017) and low molecular weight inhibitor of GCPII (Neburkova et al., 2018) are presented in this thesis.

2.3 Transferrin

Transferrin (Tf), a 78 kDa monomeric glycoprotein, is found abundantly in the blood and its primary function is to transport iron into the cells (Fig. 2.6). The binding of two ferric atoms to serum transferrin is followed by the conformational change that provides its selective recognition by the transferrin receptor (TfR) (Richardson and Ponka, 1997). The ligand-receptor complex is internalized by the cascade of clathrin-mediated endocytosis (Yashunsky et al., 2010). As iron serves as a cofactor of many proteins involved in cellular metabolism and DNA synthesis, the levels of transferrin receptor are upregulated on highly proliferating cells. Multiple studies confirmed the overexpression of TfR in numerous tumor types including bladder, pancreas, lung, colon and breast cancer. (Kondo et al., 1990; Prutki et al., 2006; Ryschich et al., 2004; Seymour et al., 1987; Walker and Day, 1986) In addition, elevated TfR expression correlates with cancer progression, tumor stage and prognosis. (Daniels et al., 2006; Das Gupta and Shah, 1990; Prior et al., 1990; Yang et al., 2001) The increased level of TfR in malignancies, its extracellular exposure and efficient endocytosis make this molecule an ideal target for delivery of therapeutic or diagnostic compounds to tumors.

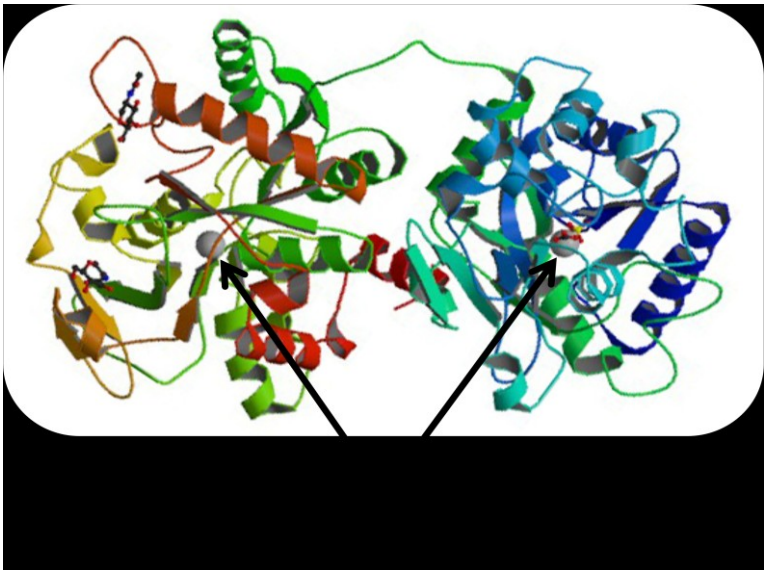

Figure 2.6: **Structure of transferrin glycoprotein**
Three dimensional structure of monomeric transferrin molecule. Binding sites of 2 molecules of Fe3+ ions (grey balls) are indicated with black arrows. Taken and adjusted from RCSB PDB: 3QYT.

2.4 Glutamate carboxypeptidase II

Glutamate carboxypeptidase II (GCPII, Fig. 2.7), also known as prostate specific membrane antigen (PSMA), is a tissue specific glycoprotein highly expressed in prostate cancer cells and cancer associated neovasculature (Liu et al., 1997; Silver et al., 1997). The abundance of GCPII correlates also with the aggressiveness of prostate cancer, metastasis and poor prognosis (Bostwick et al., 1998). In healthy tissue GCPII antigen is located in cytoplasm and only after tumor transformation it is incorporated into plasma membrane and exposed on the cell surface (Su et al., 1995). GCPII is tissue specific marker, it is expressed only in prostate, central nervous system, small intestine and kidney and expression in other tissues is very low (Maurer et al., 2016). According to the location, the function of GCPII differs and so there are various names for this enzyme. In the central nervous system GCPII metabolizes N-acetyl-L-aspartyl-L-glutamate into neurotransmitters N-acetyl-L-aspartate and glutamate and therefore is called NAALADase. In the proximal small intestine GCPII participates in the cleavage of γ-linked glutamate from pteoryl-poly-γ-glutamate, releasing the vitamin folic acid and it is also known as folate hydrolase I (O'Keefe et al., 2001). The substrate and physiological function of GCPII in prostate still remain unknown; however, its overexpression in prostate cancer is well established. Moreover the internalization of GCPII is increased 3-fold after binding of monoclonal antibody (Liu et al., 1998). The efficient internalization and high specificity of expression make GCPII an ideal marker for utilization in prostate cancer targeting therapies.

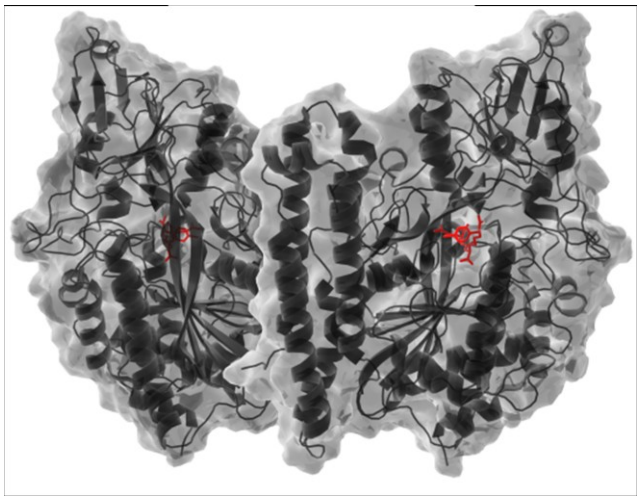

Figure 2.7: **Structure of glutamate carboxypeptidase II**
Three-dimensional structure of the GCP II homodimer. The location of binding site of GCP II inhibitor in each monomer is shown in red color. The position of the structure relative to the membrane is shown. Taken from (Šácha et al., 2016).

2.5 Protein corona

As it was previously mentioned, nanoparticles (NPs) could be functionalized by various targeting molecules such as antibodies, peptides or small chemical molecules that will enable the specific recognition of receptor on the cell surface. In order to improve the efficiency of specificity and sensitivity of interaction, many researchers have focused on understanding the process of nanoparticle behavior in the biological environment such as cells (Jiang et al., 2008), tissues (Choi et al., 2010) and blood (Pitek et al., 2012). However, numerous studies demonstrated that after inoculation of NPs into the blood, serum proteins interact with their surface and form so called protein corona (Lynch and Dawson, 2008; Nguyen and Lee, 2017; Rahman et al., 2013; Treuel et al., 2015) that interferes with nanoparticle targeting (Fig. 2.7). The corona around NPs surface with tightly bound and low dynamic exchange of proteins (in the order of several hours) is called a "hard" corona. This corona could further interact with low affinity bound and dynamically exchanged proteins and form a "soft" protein corona (Casals et al., 2010; Monopoli et al., 2012, 2011).

There are many critical factors of NPs determining the formation and composition of "hard" protein corona such as nanoparticle size, charge surface chemistry, shape, solubility, thickness, curvature and route of administration (reviewed in Docter et al., 2015; Ge et al., 2015; Mahmoudi et al., 2011; Rahman et al., 2013). Among these the most significant nanoparticle parameters that affect protein corona are size (Chithrani et al., 2006; Lundqvist et al., 2008; Piella et al., 2017; Tenzer et al., 2011) and charge (Maffre et al., 2011; Treuel et al., 2014). Better understanding the influence of each physicochemical parameter on protein corona will serve for designing of targeted NPs without losing the targeting specificity.

To suppress the protein corona formation, antifouling flexible hydrophobic polymers from polyethylene glycols (PEG) are often conjugated onto the nanoparticle surface to shield their surface (Dai Qin et al., 2014; Gref et al., 2000; Hamad et al., 2010; Knop et al., 2010; Otsuka et al., 2003). Although PEGylation decreases the non-specific targeting, it does not totally prevent protein adsorption (Pozzi et al., 2014). Moreover, the process of PEG installation onto NPs is not simple as the ideal density of connected PEGs and the length of their side chain has to be optimized (Lee et al., 2015; Perry et al., 2012).

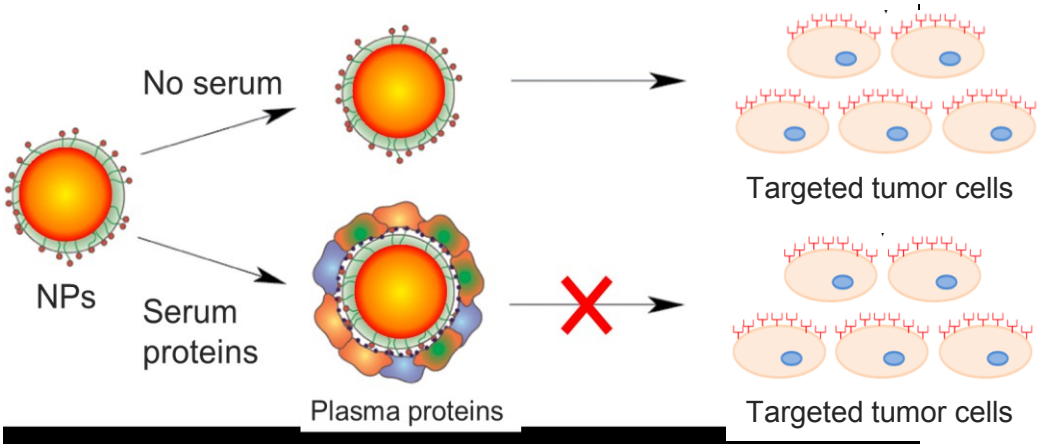

Figure 2.7: **Schematic representation of protein corona formation around the nanoparticle surface** Illustration of nanoparticle behavior with or without the presence of serum proteins and its further influence on the specific targeting of NPs to cancer cells or tissues. Taken and adapted from (Saha et al., 2013).

3. Goals

The main goal of this thesis was to develop mouse polyomavirus based chimeric VLPs as a novel nanomaterial for targeting various types of cancer cells. We intend to examine the approach of chemical modification for conjugation of targeting molecule, compare different strategies of nanoparticle retargeting and study the behavior of polyomaviral VLPs in the context of biological fluids.

Partial goals were realized in the following steps:

Goal 1. Preparation of VLPs with conjugated transferrin and analysis of their efficiency to interact with cancer cells.

a) Produce polyomaviral VLPs in insect cells Sf9 with utilization of baculovirus expression system.
b) Conjugate transferrin protein to the surface of VLPs by "click" chemistry.
c) Analyze the efficiency of modified VLP binding to cancer cells overexpressing transferrin receptor by confocal microscopy and flow cytometry.

Goal 2. Preparation of VLPs with conjugated inhibitor of GCPII and analysis of their efficiency to interact with cancer cells.

Produce polyomaviral VLPs in insect cells Sf9 with utilization of baculovirus expression system.

a) Conjugate inhibitor of GCPII to the surface of VLPs by "click" chemistry.
b) Analyze the binding efficiency of modified VLPs to cancer cells overexpressing GCPII by confocal microscopy and flow cytometry.

Goal 3. Characterization of polyomavirus based VLPs in context of serum proteins.

a) Examine the interaction of unmodified VLPs with serum proteins
b) Prepare VLPs with conjugated transferrin (VLP*-Tf), incubate them in 55% and 10% serum and characterize their properties
c) Analyze the cellular uptake by ELISA assay and flow cytometry

4. Material and Methods

4.1 Material

4.1.1 Instruments

BD LSR II Flow Cytometer (BD Biosciences)

Confocal Microscope TCS-sp (Leica)

Confocal Microscope LSM 780 and LSM 880 (Zeiss)

CO_2 incubator (Forma Scientific)

Epoch microplate spectrophotometer (BioTek Instruments)

Fluorescence microscope BX-60 (Olympus)

Fraction Recovery System (Beckman)

Gradient Master™ Base Unit with MagnaBase™ Tube Holders (Science Services)

GS – 15R Centrifuge (Beckman)

Laminar Flow Box (Forma Scientific)

Magnetic shaker B212 (Bibby)

Megafuge 1.0R Centrifuge (Heraus Sepatech)

Microfuge Centrifuge, rotor F241.5 (Beckman)

Molecular Imager GS-800 Calibrated Densitometer (BioRad)

Molecular Imager PharosFX System (BioRad)

Optima TM L-90K Ultracentrifuge, rotors SW 28, SW 41 (Beckman)

pH meter S20 SevenEasy (Mettler Toledo)

Qubit® fluorometer (ThermoFisher Scientific)

SDS-PAGE Apparatus (BioRad and Hoefer)

Sonicator Soniprep 150 (Schoeller Pharmacia)

SPR sensor platform (PLASMON IV) developed at the Institute of Photonics and Electronics, Academy of Sciences of the Czech Republic

Thermo-Shaker TS-100C (Biosan)

Transmission Electron Microscope JEOL JEM 1200EX

Vortex-Genie 2 (Scientific Industries)

Western Blotting Apparatus (BioRad)

XCell SureLock™ Mini-Cell Electrophoresis System (ThermoFisher Scientific)

4.1.2 Molecular Weight Marker

Spectra™ Multicolor Broad Range Protein Ladder (ThermoFisher Scientific)

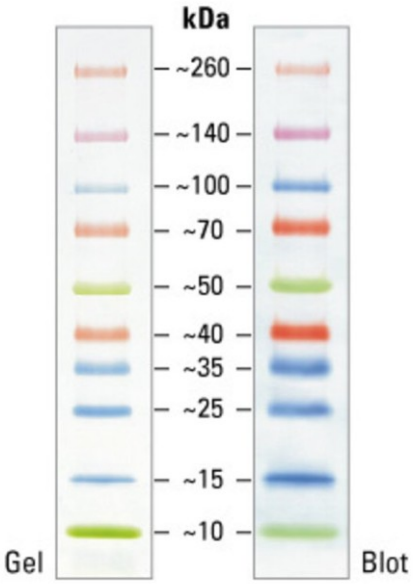

Protein marker visualized on 4-20% Tris-glycine gel (SDS-PAGE) and subsequently transferred to nitrocellulose membrane (ThermoFisher Scientific).

4.1.3 Frequently Used Solutions

PBS (Phosphate Buffered Saline): 4.090 g NaCl
0.1 g KCl
1.79 g $Na_2HPO_4 \cdot 12H_2O$
0.12 g KH_2PO_4
pH was adjusted to 7.4 and the volume was dropped to 500 ml by dH_2O

B Buffer: 10 mM Tris–HCl (pH = 7.4)
150 mM NaCl
0.01 mM $CaCl_2$

1M Tris–HCl: 30.29 g of Tris-(hydroxymethyl)-aminomethan (Serva) was dissolved in 200 dH_2O ml, pH was adjusted by HCl and the volume was dropped to 250 ml by dH_2O.

5 x concentrated Laemli buffer:	1.25% SDS (Sigma) 50 mM Tris–HCl (pH = 6.8) (Serva) 25% ß-mercaptoethanol (Serva) 50% (v/v) glycerol (Lachema) 0.005% bromphenol blue (Lachema)
Insect medium with serum:	TNM–FH insect medium (Sigma) 10% FBS (Sigma) For infection also antibiotics for tissue culture were added (1/100 of the volume)
Insect serum-free medium:	TNM – FH insect medium (Sigma)
DMEM with serum:	DMEM (Dulbecco's Modified Eagle's Medium) (Sigma) 10% FCS - Fetal Bovine Serum (Sigma) 2 mM L–Glutamine (Gibco) For infection also antibiotics for tissue culture were added (1/100 of the volume)
DMEM without serum:	DMEM (Dulbecco's Modified Eagle's Medium) (Sigma) 2 mM L–glutamine (Gibco)

Antibiotics for Tissue Culture (KRD):	100x concentrated	
	1 ml contains:	10000 units of penicillin
		10 mg streptomycin
		25 mg amphotericin B

4.1.4 Cell cultures

Cell culture CCRF-CEM

– Stable lymphoblastic cell line from human peripheral blood (ATCC No. CCL-119)

– Medium: Roswell Park Memorial Institute medium (RPMI-1640; Sigma-Aldrich)

Cell culture HUVEC

– Stable cell line from Human Umbilical Vein Endothelial Cells (ATCC No. CRL-1730)

– Medium: Endothelial Basal Medium-2 with supplements (EBM-2 SingleQuots™ Kit; Lonza)

Cell culture NIH 3T6

– Stable cell line of mouse fibroblasts (prof. Griffin, Royal Postgraduate School, London)

– Medium: Dulbecco's modified Eagle's medium (DMEM, Sigma-Aldrich D5796)

Cell culture Sf9

– Stable cell culture of insect cells derived from the ovarian tissue of moth *Spodoptera frugiperda* (ATCC No. CRL-1711)

Cell culture U2OS

– Stable human bone osteosarcoma cell line (ATCC No. HTB-96)

– Medium: Dulbecco's modified Eagle's medium (DMEM, Sigma-Aldrich D5796)

Cell culture U-251 MG with switchable GCPII expression

– Stable human glioblastoma cell line (supplied by ATCC as U373 MG cells, ATCC No. HTB-17 – misidentified cell line)

– Production of U251 MG cell line with switchable GCPII expression was already published (Neburkova *et al.,* 2018). Briefly, U251 MG cell line were stably transfected with pTet-Off® Advanced vector (Clontech) using FuGENE® HD transfection reagent (Roche) and after selection of monoclonal populations the U251 MG +/- clone with highest/lowest GCPII expression was chosen. The ideal concentration of doxycycline for turning GCPII expression off was achieved at 100ng/ml.

– Medium: Dulbecco's modified Eagle's medium (DMEM, Sigma-Aldrich D5796)

4.1.5 Viruses

MPyV

- Mouse polyomavirus BG strain (GenBank, accession number: AF442959), the VP1 sequence from this type of polyomavirus is utilized for production of VLPs
    - Sequence of the major capsid protein is coded on the complement strand of the genome
    - VP1 (genome sequence 2932 - 4086)

AcVP1

- Recombinant baculovirus producing the major capsid protein VP1 of mouse polyomavirus

4.1.6 Baculovirus Expression System

VLPs assembled from the major capsid protein VP1 were produced in Sf9 insect cells through baculovirus expression system. Baculovirus containing the VP1 gene of mouse polyomavirus was previously prepared in our laboratory (Forstova et al., 1993) and the acquired media containing baculovirus was used for insect cell infection.

4.1.7 Antibodies

4.1.7.1 Primary Antibodies

- MαMPyV-VP1: mouse monoclonal antibody against VP1 protein, clone D4 (prepared by RNDr. Alena Drda Morávková, MBA, Ph.D.), (dilution 1:20)
- RbαMPyV-VP1: rabbit polyclonal antibody against VP1 protein, produced in EXBIO company by immunization of rabbits with VP1 VLPs (dilution 1:5000)
- MαMPyV-dnVP1: mouse monoclonal antibody against denaturated VP1, isotope IgG1 (dilution 1:100) (Forstova et al., 1993)
- MαHuman-Tf: mouse monoclonal antibody against human transferrin, HTF-14, isotope IgG1 (dilution 1:1000) (Exbio)

4.1.7.2 Secondary Antibodies

- Goat immunoglobulins against mouse immunoglobulins conjugated with horseradish peroxidase (dilution 1:1000) (BioRad)
- Goat immunoglobulins against rabbit immunoglobulins conjugated with Alexa Fluor (dilution 1:1000) (BioRad)

4.2 Methods

4.2.1 Sterilization

Solutions, Eppendorf tubes and Micropipette tips were sterilized in autoclave (30 min, 120 kPa, 127 °C). Solutions that could not be sterilized by autoclaving were sterilized by filtration through 0.2 μm filters. Laboratory glass was covered by aluminium foil and sterilized in 180 °C for 3 hours.

4.2.2 Protein methods

4.2.2.1 Preparation of samples for SDS-PAGE

Protein samples were mixed with Laemli buffer (4:1), incubated for 5 minutes in 100 °C and centrifuged for 10 s (short spin).

Material:

5 x concentrated Laemli buffer

4.2.2.2 SDS polyacrylamide electrophoresis (SDS-PAGE)

Electrophoretic glasses were thoroughly washed with detergent, dH_2O and denaturated ethanol. Dried glasses were tightly fixed in the apparatus and lower gel was poured between the glasses (0.5 cm under the end of comb). The gel was covered with ddH_2O and polymerized approximately 30 minutes. Then the upper gel was poured onto the lower gel and the comb was installed into the upper gel. After 15 minutes the comb was taken out and glasses with gel were transferred to electrophoretic apparatus. Wells were washed with electrophoretic buffer and the rest of it was poured into the apparatus. Samples were loaded into the wells together with the molecular weight marker.

Electrophoresis firstly ran for 30 minutes with the voltage 80V/cm and then with 120V/cm, until samples reached the bottom of the glass (approximately 1.5 hours).

Material:

Lower gel:	4 ml 30% acrylamide (Serva)
	4.5 ml Tris-HCl (pH = 8.8) (Sigma)
	120 µl 10% SDS (Sigma)
	3.25 ml ddH_2O
	40 µl 10% APS (Serva)
	8.5 µl TEMED (Sigma)
Upper gel:	0.5 ml 30% acrylamide (Serva)
	0.375 ml Tris – HCl (pH = 6,8) (Sigma)
	30 µl 10% SDS (Sigma)
	2.11 ml ddH_2O
	20 µl 10% APS (Serva)
	5µl TEMED (Sigma)

APS and TEMED were added just before pouring of the gel.

Electrophoretic buffer:	25 mM Tris (Serva)
	192 mM glycine (Sigma)
	0.1 % SDS (Sigma)
	pH = 8.3

4.2.2.3 Gel staining after SDS – PAGE

Acrylamide gel after protein electrophoresis was washed 3 times for 5 minutes in ddH_2O and then stained in GelCode Blue Stain Reagent for one hour to overnight with light shaking. After incubation the gel was washed few times in dH_2O and scanned on densitometer.

Material:

GelCode Blue Stain Reagent (ThermoFisher Scientific)

4.2.2.4 Dot blot

Protein samples (1-2 µl) were dropped onto the nitrocellulose membrane. Dried samples on the membrane were further visualized by immunological detection.

Material:

Nitrocellulose membrane Amersham Prothran (GE Healthcare)

4.2.2.5 Western blot

Acrylamide gel after SDS-PAGE was incubated 10 minutes in blotting buffer. Whatman and nitrocellulose membrane were cut according to the size of the gel and poured into the blotting buffer. Blotting sandwich was assembled as follows: the grid was layered into the blotting buffer and foam, whatman and gel was put onto it. Then nitrocellulose membrane, whatman, foam and grid and the sandwich was secured against opening by plastic locker. Afterwards the sandwich was inserted into the blotting apparatus that was filled with blotting buffer. Blotting lasted 1 hour in 250 mA and then the membrane was washed with dH_2O.

Material:

Nitrocellulose membrane Amersham Prothran (GE Healthcare)

Whatman (GE Healthcare)

Blotting buffer: 25 mM Tris (Serva)
195 mM glycine (Sigma)
20% methanol (Lachema)
pH = 8.3

4.2.2.6 Immunodetection of proteins immobilized on nitrocellulose membrane

Membrane with immobilized proteins was incubated for 30 minutes in low-fat milk (5% solution in PBS). Afterwards the membrane was incubated 1 hour with primary antibody diluted in low-fat milk solution, then washed 3 times with PBS (each wash lasted 10 minutes) and incubated 30 minutes in secondary antibody diluted in low-fat milk solution. The membrane was again washed 3 x 10 min with PBS. The detection of enhanced chemiluminiscence was realized in the dark room. The membrane was poured

with developing solution (mixed A+B), incubated for 30 s and then dried on the cellulose wadding. Afterwards the membrane was inserted into plastic foil, the X-ray film was layered onto the foil and the exposition lasted from 15 s to 30 min. The X-ray film was developed by developer and fixator.

Material:

5% low-fat milk in PBS

Luminol (3-aminophthalydrazide; Sigma A 8511): 250 mM solution in DMSO, aliquoted and deposited in -70 °C

Coumaric acid (Sigma C 9008): 90 mM solution in DMSO, aliquoted and deposited in -70 °C

Developing solution A	80 µl p-coumaric acid (90 mM) 200 µl luminol (250 mM) 2 ml 1M Tris-HCl (pH = 8.5) (Sigma) 18 ml dH_2O
E Developing solution A	12 µl H_2O_2 (30%, Sigma) 2 ml 1M Tris-HCl (pH = 8.5) (Sigma) 18 ml dH_2O

Both solutions were mixed (1:1) just before usage.

PBS

X-ray films (Foma)

Developer (Foma)

Fixator (Foma)

4.2.2.7 Gradient SDS-PAGE

Prepared VLPs were separated on SDS-PAGE (NuPAGE Novex 4-12% Bis-Tris precast polyacrylamide gels, ThermoFisher Scientific) according to manufacturer's protocol. The running time in SDS-PAGE was 50 min with constant voltage 200 V. Proteins were then stained with colloidal Coomassie dye G-250 (see 4.2.2.3).

4.2.2.8 Densitometry analysis

Coomassie-stained SDS-PAGE gels were scanned on a Molecular Imager GS 800 densitometer (Bio-Rad). The quantification of densities was done by Quantity One image analysis software, version 4.5.0 (Bio-Rad). For calculation of protein to particle ratio, two gels with standards were prepared. VP1 protein and transferrin were loaded onto SDS-PAGE in various concentrations and consequently a standard curve was made for calculation of protein concentrations from measured densities.

4.2.2.9 Fluorescence scanning of the electro-transferred proteins

Proteins were electro-transferred (1 h, 250 mA) onto a nitrocellulose membrane (GE Healthcare Life Sciences). For details see 4.2.2.5. The membrane was scanned for rhodamine (excitation at 552 nm) and Alexa Fluor 488 (excitation at 488 nm) fluorescences on a PharosFX Molecular Imager (Bio-Rad).

4.2.2.10 Measurement of protein concentration

Protein concentration was measured by Qubit Protein Assay Kit (ThermoFisher Scientific) according to the manufacturer's protocol.

4.2.2.11 Ultracentrifugation through sucrose cushion

Centrifuge tubes (Beckman) were filled with VLP solution in B buffer that was underlayered with 1–1.5 cm of sucrose (10% or 20%) dissolved in B buffer. The tubes were then transferred into centrifuge cuevettes and balanced with B buffer. Centrifugation lasted 3 hours with 35,000 rpm and 4°C (rotor SW41). The pellet was resuspended in B buffer by overnight incubation in 4°C and homogenized by sonication.

Material:

Sucrose (Serva)

B buffer

4.2.2.12 Isopycnic centrifugation in CsCl gradient

Centrifugation in CsCl gradient separates viral particles solely on the basis of their density. Viral particles after pre-purification with centrifugation through sucrose cushion were filled to 8 g with B buffer and then mixed with 3.65 g CsCl. This mixture was overlayed with paraffin oil and then the centrifuge tubes (Beckman) were transferred into

centrifuge cuevettes and balanced. Centrifugation lasted 24 hours with 35,000 rpm and 4°C (rotor SW41). Afterwards the fraction were taken by the fraction recovery system and separated into eppendorf tubes. Refractive index of individual fraction was measured and all fractions were examined by dot blot followed with immunodetection. According to achieved data the fractions were joined into 3 to 5 groups and dialyzed against B buffer.

Material:

CsCl (Serva)

B buffer

Paraffin oil (Roth)

4.2.2.13 Isokinetic centrifugation in sucrose gradient

Centrifugation in sucrose gradient allows the separation of protein material according to the size and therefore viral particles could be separated from disassembled material and low molecular weight compounds. After the centrifugation we could achieve a fraction of purified and homogenous viral particles. Gradient of 10-40 % sucrose was prepared in the Gradient Master with tube holder according to the manufacturer's protocol. Samples (approximately 0.5 ml) were carefully transferred onto the gradient; tubes were inserted into centrifuge cuevettes and balanced. Centrifugation lasted 2 hours with 25,000 rpm and 4°C (rotor SW41).

Afterwards the fractions were taken by the fraction recovery system and separated into flat bottom microtitration plate. All fractions were analyzed by absorbance and fluorescence measurement. According to the achieved data the fractions were joined into two groups and dialyzed against B buffer.

4.2.2.14 Dialysis

Dialysis tube was boiled for 10 minutes in ddH_2O. Joined fractions from isopycnic centrifugation were transferred into the dialysis tube and closed from both sides with clips. Proteins were dialyzed overnight in 6 °C against B buffer with stable stirring. Afterwards the sample was concentrated by ultracentrifugation in sucrose cushion.

If the dialysis was used in preparation of modified VLPs, instead of dialysis tube, minidialyzis columns Slide-A-Lyzer 3,5K MWCO (GeneTICA) were used. The column

was closed with a cap and inserted into a floater. The floater was then transferred into the dialysis buffer and incubated for the desired time in 6 °C with stable stirring of the buffer. During the incubation the buffer was exchanged several times

Material:

B buffer

Dialysis tubes Sevapor (Serva)

Minidialyzis columns Slide-A-Lyzer 3,5K MWCO (GeneTICA)

4.2.2.15 Measurement of binding specificity of VLPs by SPR

The binding specificity of VLPs with conjugated iGCPII were measured by the technology of surface plasmon resonance (SPR). The principal of this technology is based on plasmonic waves that are generated on the metal surface (chip). These waves reflect the incident light on the chip and the detector then according to the angle difference records the height of waves. Plasmon waves increase the height after the attachment of a substance (e.g. polymer, protein or DNA), therefore the reflected light is deflected and the detector records the connection of the substance.

The measurement on SPR was kindly provided by the Mgr. Pavel Šácha, Ph.D. from IOCB AS CR. We used the chip covered with gold and TYGON tubes. The chip contained carboxymethylated dextrans and polyethylene glycol (PEG) on its surface. Dextrans allow binding of the substance through amino groups and PEG covers the surface between dextrans and therefore protect from the steric hindrance during attachment of the substance to the chip. However it is necessary to activate the carboxyl groups of the substances to allow their binding to dextrans. Therefore we used N-hydroxysuccinimidyl ester (NHS) that activates the carboxyl residues and mediates the reaction with amino residues. Together with NHS the ethyl(dimethylaminopropyl) carbodiimid (EDC) is added that enables the creation of very unstable intermediate of the carboxyl group. Nevertheless the acidic pH must be kept in the solution to retain the carboxyl residues active. In that case we used 10 mM sodium acetate buffer of pH=5 (SA10).

The measurement proceeded as follows: The chip was inserted into the SPR instrument and washed with ddH_2O and then with 50 µl NHS together with 50 µl EDC. Excessive NHS/EDC was washed with ddH_2O and the pH was adjusted by the SA10 buffer. Streptavidine (2 µg) was bound to the activated carboxyl groups and the unbound streptavidine was washed with SA10. Afterwards the channels were washed

with these solutions: 0.5 M NaCl in PBS (wash out of non-covalently bound proteins), 1 M ethanolamine (deactivation of residual activated carboxylic groups), SA10 buffer and TBS. After this wash, one half of the channels was treated with solution containing biotinylated extracellular domain of GCPII (Avi-GCPII - prepared according to Tykvart et al., 2012) and the second half with TBS only. All channels were then washed with TBS. Now the solution of various modified VLPs (final concentration 5 nM) was added and finally all channels were washed with TBS. All solutions used during the SPR measurement were degassed prior usage.

Material:

2 mM Ethyl (dimethylaminopropyl) carbodiimid

5 mM N–hydroxysuccinimidyl ester

10 mM sodium acetate buffer, pH=5

Streptavidine

PBS with 0.5 M NaCl

PBS

1 M ethanolamine

TBS (50 mM Tris-Cl, pH 7.6; 150 mM NaCl)

Avi-GCPII in PBS

4.2.3 Work with tissue cultures

4.2.3.1 Passaging of insect cells

Cells in confluency were scratched out and the suspension was transferred into 50 ml conical centrifuge tube. The tube was filled with sufficient amount of TNM-FH insect media with 10% FBS. The final ratio of cells in suspension and fresh medium was 1:4. The cells were resuspended by pipetting and divided into 4 Petri dishes and cultivated in 28°C. The cells were passaged twice a week.

Material:

TNM-FH insect media with 10% FBS

4.2.3.2 Infection of insect cells with baculovirus

Cells were passeged with the ratio 1:3 to serum-free media and cultivated for 30 minutes in 28°C. Then the medium was aspirated and cells were incubated with baculovirus inoculum (10 PFU/cell) was added for 1 hour in room temperature with

constant swinging. Afterwards TNM-FH insect medium with 10% serum was added and the cells were incubated 3-4 days in 28°C. The infected cells were harvested by scratching, collected to 50 ml conical centrifuge tube and centrifuged for 5 min, 2000xg, 4°C. The pellet was washed once with PBS and then either proceeded immediately to isolation or stored in -20°C. The supernatant was stored in 4°C for following infections.

Material:

TNM-FH insect medium with 10% FBS

TNM-FH insect serum-free medium

Baculovirus inoculum

PBS

4.2.3.3 Isolation of VP1 VLPs from insect cells

Cells infected with baculovirus containing the VP1 gene were treated according to previously mentioned protocol (4.2.3.2). The pellet was resuspended in B buffer. The cell suspension was sonicated (amplitude=10) 5 times for 45 s with 30 s pauses and cooling in ice bath. Destruction of nucleus was checked by light microscopy. Sonicated suspension was centrifuged for 15 min, 2000xg, 4°C. Supernatant was centrifuged through 10% sucrose cushion in B buffer for 3 hours, 35,000 rpm, 4 °C (rotor SW41). The pellet was resuspended in B buffer by overnight incubation in 4°C and homogenized by sonication. The suspension was subjected to isopycnic centrifugation (see 4.2.2.11). Fractions resuspended in B buffer were characterized by electron microscopy, the concentration was measured by Qubit and the rests of these fractions were stored in -20°C.

Material:

CsCl (Serva)

B buffer

PBS

Sucrose (Serva)

4.2.3.4 Passaging of mammalian cells

The medium from confluent cells grown on Petri dish (6 cm) was aspirated and the cells were washed with 2 ml of 0.03% EDTA solution in PBS and incubated in 37 °C, 5% CO_2 for 3-10 min in 500 µl 0.25% trypsine solution in PBS. The detached cells were

thoroughly resuspended in DMED with 10% FBS. The suspension was divided onto 6 Petri dishes and filled with DMED medium with 10% FBS. The cells were incubated in 37 °C, 5% CO_2. The cells were passaged twice a week.

Material:

DMED with 10% FBS (or other medium appropriate for the cell type)
0.03% EDTA solution (Sevac) in PBS
0.25% trypsine solution (Sigma) in PBS

4.2.3.5 Confocal microscopy

The cells were detached from the dish, counted and the desired number of cells were transferred either into 24-well plate with microscopic glasses or into 4-chamber Glass Bottom Microwell Dishes (Cellvis, D35C4-20-1.5-N). Afterwards the cells were supplemented with DMED with 10% FBS and incubated overnight in 37 °C, 5% CO_2. Next day the medium was aspirated and cells were treated with VLPs for 1 hour in 37 °C, 5% CO_2.

For confocal microscopy of VLPs conjugated with transferrin and further experiments with serum proteins 0.54 nM concentration of VLPs was used. The cells were fixed with 4% paraformaldehyde in PBS for 15 min followed by extensive washing with PBS. The cover slips were mounted into ProLong Gold Antifade Mountant with DAPI (Invitrogen) and visualized with a Zeiss LSM 880 or Leica TCS-sp confocal microscope.

For confocal microscopy of VLPs conjugated with iGCPII the cells were fixed with 3.7% paraformaldehyde in TBS for 10 min, washed with TBS and counterstained with 500 ng/ml Hoechst 34580 solution (Thermo Scientific). The cells were visualized with a Zeiss LSM 780 confocal microscope.

Material:

DMEM medium with/without 10% FCS (or other medium appropriate for the cell type)
PBS, TBS
VLPs
Paraformaldehyde (Sigma) in PBS
Triton X-100 (Sigma) in PBS

4.2.3.6 Flow cytometry

Cells U-251$^{+/-}$ MG were detached from the dish by trypsinization, resuspended in DMEM with 10% FBS, counted and centrifuged (300xg, 5 min, 4˚C). Subsequently, the cells were dissolved in serum-free DMEM medium without phosphate, transferred into a 96-well plate ($6 \cdot 10^4$ cells per well) and incubated with VLPs (4 nM) for 1 h at 37 ˚C, 5% CO_2. The experiment was done in triplicates and with negative controls (serum-free DMEM only). After the treatment, cells were washed with TBS and resuspended in 200 µl TBS.

Cells U2OS and HUVEC were counted and an appropriate amount of cells was seeded on either 12-well or 24-well plate. The cells were incubated overnight in medium with 10% FBS at 37 ˚C, 5% CO_2. The medium was replaced with 800 µl of serum-free medium. One part of the cells was pre-treated with Tf (Sigma-Aldrich, 100µg/ml) for 30 min, 37 ˚C, 5% CO_2. Subsequently, the cells were incubated with VLPs (0.54 nM) for 1 h at 37 ˚C, 5% CO_2. The experiment was performed in duplicates and with negative control (serum-free medium only). After the treatment, cells were harvested by trypsinization and the activity of trypsine enzyme was subsequently blocked by soybean trypsine inhibitor (ThermoFisher Scientific, 0.5 mg/ml). The cells were washed twice with PBS, resuspended in 300 µl of PBS, and filtered through 35-µm nylon mesh.

Cells CCRF-CEM were suspended, counted, centrifuged (300xg, 5 min, 4˚C), dissolved in 800 µl of serum-free medium, and transferred into a 12-well dish. The treatment with VLPs was the same as for the previously mentioned cells. The experiment was also performed in duplicates and with negative control (serum-free medium only). After the treatment, cells were harvested by scraping. The cells were washed twice with PBS, resuspended in 300 µl of PBS, and filtered through 35-µm nylon mesh.

All cells were with a BD LSRFortessa flow cytometry analyzer (Becton, Dickinson and Company). The data were further analyzed with BD FACSDiva Software, version 6.0. The R program was utilized for statistical analyses.

Material:

DMEM medium with/without 10% FCS (or other medium appropriate for the cell type)

0.03% EDTA solution (Sevac) in PBS

0.25% trypsine solution (Sigma) in PBS

Soybean trypsine inhibitor (ThermoFisher Scientific)

PBS, TBS

VLPs, Tf, iGCPII

4.2.4 Preparation of chemically modified VLPs

4.2.4.1 Labeling of VLPs with NHS-fluorophore

Unmodified VP1 VLPs were dialyzed against 0.1 M HEPES, pH 7.9 and treated with either NHS-rhodamine (ThermoFisher Scientific, final concentration 34 nM, 0.1 equivalents per surface lysine) or NHS-Alexa Fluor 488 (AF488, ThermoFisher Scientific, final concentration 34 nM, 0.2 equivalents per surface lysine) at room temperature overnight with gentle shaking (250 rpm, TS-100C, Thermo-Shaker, Biosan). Excess dye was removed by dialysis against 0.1 M HEPES, pH 7.9 (4 °C, overnight with two buffer changes). A part of the prepared VLP mixture was used for subsequent conjugation of molecules and the rest was purified and concentrated by centrifugation through two successive 20% sucrose cushions (35,000 rpm, 3 hours, rotor SW41, Beckman) and dissolved in B buffer, thus providing the conjugates of VP1 VLPs used as a negative controls; **VLP*** (rhodamine), VLP* (AF488).

Material:

VLPs

NHS-rhodamine ester (ThermoFisher Scientific)

NHS-Alexa Fluor 488 ester (ThermoFisher Scientific)

0.1 M HEPES, pH 7.9

B buffer

4.2.4.2 Conjugation of alkyne to fluorescently-labeled VLPs

Labeled-VLPs were modified with heterobifunctional linker containing propargyl and N-hydroxysuccinimidyl ester moieties (Sigma). VLPs in 0.1 M HEPES, pH 7.9 were treated with the linker (35-fold excess per surface lysine) dissolved in DMSO (10% final concentration of DMSO). The reaction mixture was incubated at room temperature overnight with gentle shaking (250 rpm, TS-100C, Thermo-Shaker, Biosan). Excess reagents were removed by dialysis against 0.1 M HEPES, pH 7.4 (4 °C, overnight, first two buffer changes contained 10% DMSO) and concentrated in an Amicon Ultra centrifugal filter device (Millipore), providing VLP-alkyne conjugate.

Material:

N-hydroxysuccinimidyl ester (Sigma)

0.1 M HEPES, pH 7.9

0.1 M HEPES, pH 7.4

DMSO (Sigma)

4.2.4.3 Preparation of VLP-conjugates by click reaction

VLP-alkyne (51.5 nM) in 0.1 M HEPES buffer, pH 7.4, containing 10 mM copper sulfate, 100 mM aminoguanidine, 50 mM tris(3-hydroxypropyltriazolylmethyl)amine (THPTA, synthesized according to a previously published procedure by Hong et al., 2009) freshly prepared 100 mM sodium ascorbate and either Tf-azide (12.6 µM), **Tf*-**azide (24.9 µM), T.Red-azide (37.1 µM, ThermoFisher Scientific) or iGCPII-azide (35.6 µM) were used for click reactions. Copper sulfate and THPTA were mixed in a separate tube in a 1:5 concentration ratio prior to addition to the reaction mixture. The reaction mixture was well-sealed, mixed, and allowed to stand undisturbed at room temperature for 3 h. Excess transferrin or inhibitor were removed from the resulting VLP conjugates by dialysis (cellulose ester membrane, 300 kDa, Biotech) against 0.1 M HEPES, pH 7.4 (4 °C, overnight) and B buffer (4 °C, overnight). Finally, the VLPs-conjugates (**VLP*-Tf***, VLP*-Tf, VLP*-T.Red, VLP*-iGCPII) were purified and concentrated by centrifugation through two successive 20% sucrose cushions (see 4.2.2.10).

Material:

0.1 M HEPES buffer, pH 7.4
Copper sulfate
Aminoguanidine
THPTA
Sodium ascorbate
Tf*-azide, Tf-azide, T.Red-azide, iGCPII-azide
VLP-alkyne (**VLP*-**alkyne, VLP*-alkyne)
Cellulose ester membrane, 300 kDa (Biotech)
Sucrose (Serva)

4.2.4.4 Preparation of Tf-azide conjugate (Tf)

Holotransferrin (30 mg, Sigma) was dissolved in 15 ml acetate buffer (0.1 M, pH 5.5). Sodium periodate (1 mM) was added on ice and kept in the dark for 30 min. The resulting Tf-aldehyde was purified with 0.1 M HEPES buffer, pH 7.4 using an ultrafiltration cell and concentrated to 10 ml. 3-Aminooxypropylazide (16.2 mg in 500 ml DMSO) was added to Tf-aldehyde solution, and the mixture was gently stirred for 5 h. The product was purified with HEPES (0.1 M, pH 8) in an ultrafiltration cell and concentrated

to 3 ml (Rehor et al., 2015). The resulting Tf-azide was utilized for production of VLP-Tf* conjugates.

In case of double labeled **VLP*-Tf*** conjugates, transferrin (30 mg) was conjugated also with Alexa Fluor 488. Lysine residues of Tf-azide were labeled with AF488 SDP ester (0.6 mg) by stirring overnight and then purified with HEPES (0.1 M, pH 7.4) in an ultrafiltration cell, providing the **Tf*-**azide conjugate.

Material:

Human holotransferrin (Sigma)

Acetate buffer (0.1 M, pH 5.5)

Sodium periodate

0.1 M HEPES buffer, pH 7.4

0.1 M HEPES buffer, pH 8.0

3-Aminooxypropylazide

AF488 SDP ester (ThermoFisher Scientific)

4.2.4.5 Preparation of VLP-PEG particles

VLPs labeled with AF488 (VLP*) were dialyzed against 0.1 M HEPES, pH 8.0, with 0.01 mM $CaCl_2$ (4 °C, overnight). Then, the solution of particles (0.38 mg) was treated with 0.47 mg Acid-PEG_{13}-NHS ester (Broadpharm, BP-22330, 35-fold excess per surface lysine) at room temperature for 5 h with stable stirring. Excess reagents were removed by dialysis against TBS with 0.01 mM $CaCl_2$ (4 °C, overnight).

Material:

TBS (20 mM Tris-HCl, 150 mM NaCl, pH 7.4)

VLP*

0.1 M HEPES buffer, pH 8.0

0.01 mM $CaCl_2$

Acid-PEG_{13}-NHS ester (Broadpharm)

4.2.5 Dynamic light scattering

The hydrodynamic diameter of VLPs (0.1 mg/ml) was measured by a Zetasizer Nano ZS system (Malvern Instruments) at 25 ˚C.

4.2.6 Electron microscopy

For morphology analysis, VLPs were visualized by electron microscopy. Electron micrographs presented in this doctoral thesis were achieved mostly by the author; however, the micrographs of VLPs with iGCPII conjugation were prepared by Mgr. Jitka Neburkova, IOCB AS CR.

4.2.6.1 Negative staining

The samples (VLPs, 7 µl) were dropped on parafilm and adsorbed on carbon-coated formvar copper grids (Electron Microscopy Sciences) for 5 min. Grids were washed twice in redistilled H_2O (30 s each wash) and then contrasted on two drops of 2% solution of phosphotungstic acid, pH=7.3 (1 min for each incubation). The grids were visualized with a JEOL JEM-1011 transmission electron microscope.

Material:

Cu grids (200 mesh) covered with parlodion membrane with steamed layer of carbon

2% phosphotungstic acid, pH=7.3 (Fluka)

Parafilm (American National Can Company)

0.2 µm filtered ddH_2O

4.2.7 ELISA

4.2.7.1 Binding assay on recombinant human TfR

The half-area ELISA 96-well plate (Greiner Bio-One) was loaded with recombinant human transferrin receptor (125 ng/well; R&D systems; 2474-TR-050) and incubated overnight in 4 °C. The wells were washed four times with PBS containing 0.1% Tween-20 and incubated 2 hours with blocking solution (5% low fat milk in PBS). The wells were washed with PBS+0.1% Tween-20 before VLP*-Tf particles (16 ng/µl), with or without serum (10% or 55%), were added. After incubation for 1 hour at RT, the plate was washed four times with PBS+0.1% Tween-20. The primary antibody (Rabbit polyclonal anti Mouse VP1 protein) was diluted in blocking solution (1:5000), loaded on the plate (100 µl/well) and incubated for 1 hour, RT. The plate was washed four times with PBS+0.1% Tween-20 and incubated with secondary antibody (Goat anti Rabbit with horseradish peroxidase; Bio-Rad) for 30 min, RT. After four washes with PBS+0.1% Tween-20 the ATBS substrate (Sigma) in 0.1M citrate buffer, pH=4.0 with hydrogen

peroxide was added, followed by absorbance measurement (Epoch microplate spectrophotometer; BioTek Instruments).

Material:

Recombinant human transferrin receptor (R&D systems)

PBS

Tween-20 (Sigma)

VLP*-Tf

ATBS substrate (Sigma)

Citrate buffer, pH=4.0

Hydrogen peroxide (Roth)

4.2.7.2 Binding assay on U2OS or 3T6 cells

The half-area ELISA 96-well plate (Greiner Bio-One) was loaded either with U2OS cells or 3T6 cells and incubated overnight in 37°C, 5% CO_2. The wells were washed two times with PBS and incubated for 1 hour in 37°C, 5% CO_2 with either VLP or VLP*-Tf particles (16ng/µl) diluted in DMEM with or without serum (10% or 55%). After incubation the samples were transferred to new 96-well half-area plate and coated for 1 hour in RT. Then the plate was washed four times with PBS+0.1% Tween-20 and incubated 1 hour with blocking solution (5% low fat milk in PBS). The primary antibody (Rabbit polyclonal anti Mouse VP1 protein) was diluted in blocking solution (1:5000), loaded on the plate (100 µl/well) and incubated for 1 hour, RT. The plate was washed four times with PBS+0.1% Tween-20 and incubated with secondary antibody (Goat anti Rabbit with horseradish peroxidase; Bio-Rad) for 30 min, RT. After four washes with PBS+0.1% Tween-20 the ATBS substrate (Sigma) in 0.1M citrate buffer, pH=4.0 with hydrogen peroxide was added, followed by absorbance measurement (Epoch microplate spectrophotometer; BioTek Instruments).

Material:

DMEM medium

PBS

Tween-20 (Sigma)

MPyV VLPs, VLP*-Tf

ATBS substrate (Sigma)

Citrate buffer, pH=4.0

Hydrogen peroxide (Roth)

4.2.8 MALDI measurement

For MALDI measurements, 5 µl of the sample (50 µg, 19.5 pmol) was mixed with 2.5 µl of 100 mM DTT and 2.5 µl of 10 M urea for 10 min to disassemble the particles. MALDI analysis was performed by the Laboratory of Mass Spectroscopy, IOCB AS CR.

4.2.9 UV-Vis spectroscopy

The spectra were recorded using an Epoch microplate spectrophotometer (BioTek Instruments). For the measurement the particle concentration was adjusted to 150 µg/ml

.

5. Results

5.0 Production of polyomaviral VLPs for chemical modification

The main goal of this thesis is preparation of chemically modified MPyV based VLPs with the ability of specific recognition of cancer cells. For this, it was necessary to produce very high amounts of VP1 VLPs of a good quality (homogenous, stable and purified). Mouse polyomavirus VLPs contain 360 molecules of the major structural protein, VP1, self-assembled into 45 nm empty viral capsid–like structures. They could be produced in various expression systems. We have chosen baculovirus expression system and Sf9 insect cells because this system allows the effective production of VP1 and its complex post-translational modification. Sf9 cells were infected (4.2.3.2) with recombinant baculovirus containing VP1 gene (AcVP1). VLPs were released from the cells by sonication and contaminating DNA that could interfere with chemical conjugation was degraded by incubation for 30 min with DNase I (Roche, final concentration 100 μg/ml) and 5 mM $MgCl_2$ in room temperature. VLPs were then isolated by centrifugation through sucrose cushion, followed by isopycnic centrifugation in CsCl gradient according to the chapters 4.2.2.11 and 4.2.2.12. Each of six CsCl gradients was divided into 600 μl fractions (12 -13 fractions per gradient) and the refractive index of each fraction was measured. Measured refractive indexes are listed in the Table 5.1.

Table 5.1: **Refractive indexes of CsCl fractions**
The table presents the refractive indexes of fractions of CsCl gradients. The fractions of all gradients were combined according to the similarity of refractive indexes. Five combined fractions were generated.

Fraction number	Refractive index						Combined fractions
	Gradient A	Gradient B	Gradient C	Gradient D	Gradient E	Gradient F	
1	1,373	1,373	1,372	1,374	1,372	1,373	
2	1,371	1,371	1,370	1,372	1,370	1,371	F1
3	1,369	1,369	1,368	1,369	1,368	1,369	
4	1,368	1,368	1,367	1,368	1,367	1,368	F2
5	1,367	1,367	1,366	1,367	1,366	1,367	
6	1,366	1,366	1,365	1,366	1,365	1,366	F3
7	1,365	1,365	1,364	1,365	1,364	1,365	
8	1,364	1,364	1,363	1,364	1,363	1,364	F4
9	1,363	1,363	1,362	1,363	1,362	1,363	
10	1,362	1,362	1,361	1,362	1,361	1,362	F5
11	1,361	1,361	1,360	1,361	1,360	1,361	
12	1,360	1,360	1,358	1,359	1,359	1,359	
13	1,358	1,358	1,356	1,357	1,357	1,356	

The presence of VP1 protein in obtained fractions was checked by dot blot followed with immunodetection (chap. 4.2.2.4 and 4.2.2.6) (Fig. 5.1). VP1 protein was detected (as we expected) in most fractions. This is due to the fact that VP1 has non-specific DNA binding activity and thus, VLPs can encapsidate larger or smaller fragments of cellular or baculovirus DNA which affect their buoyant densities. For purposes of our experiments, it was not necessary to further purify the "empty" VLPs. However, possible future medical exploitation of the prepared VLPs will require a careful removal of contaminating DNAs.

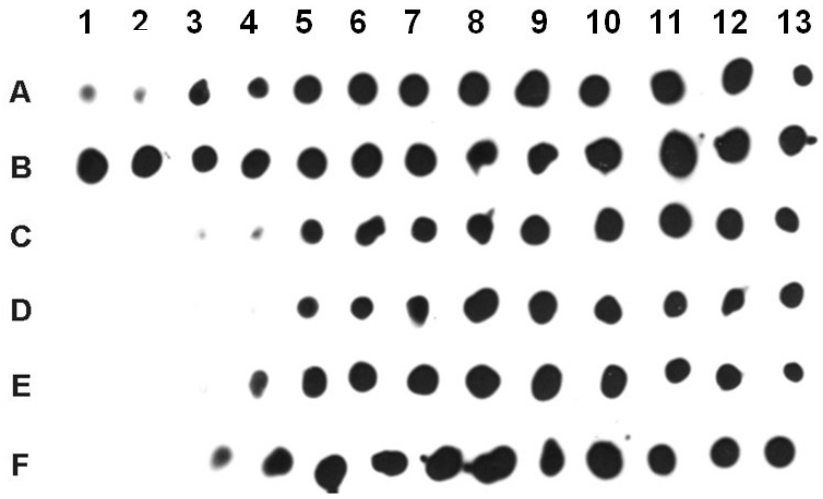

Figure 5.1: **Detection of VP1 protein in CsCl fractions**
Fractions were dropped on the nitrocellulose membrane and their position was defined by the number of fraction and an alphabetical symbol of the gradient (A-F). Proteins were visualized by immnunodetection using VP1-specific antibody and the X-ray film was scanned.

Combined fractions F1-F5 (see Table. 5.1.) were transferred into dialysis tube and dialyzed overnight against B buffer and concentrated by sucrose cushion (chap. 4.2.2.14 and 4.2.2.11). The protein concentration of combined fractions was measured by Qubit Protein Assay Kit (Table 5.2) and the quality of VLPs was verified by electron microscopy (chap. 4.2.6.).

Table 5.2: **Measured concentration of combined fractions**
The table presents the concentration of combined fractions F1-F5 measured by Qubit Protein. The fractions of all gradients were combined according to the similarity of refractive indexes. Five combined fractions were generated.

Combined fractions	Concentration (mg/ml)
F1	0.41
F2	1.85
F3	4.76
F4	2.68
F5	2.32

Electron micrographs (Fig. 5.2) showed the differences between fractions. Fraction F1 contains VLPs of good quality; however, the concentration is too low. In case of fractions F4 and F5 the concentration is high enough but these fractions contain a lot of disassembled material and therefore are not suitable for chemical modifications. The most homogenous VLPs were detected in fraction F2 with refractive index corresponding to buoyant density around 1.348 g/cm^3 and in fraction F3 with refractive index corresponding to the buoyant density between 1.326 -1.337 g/cm^3. Thus only these fractions were further utilized for chemical conjugation of targeting moieties (chap. 5.1 and 5.2).

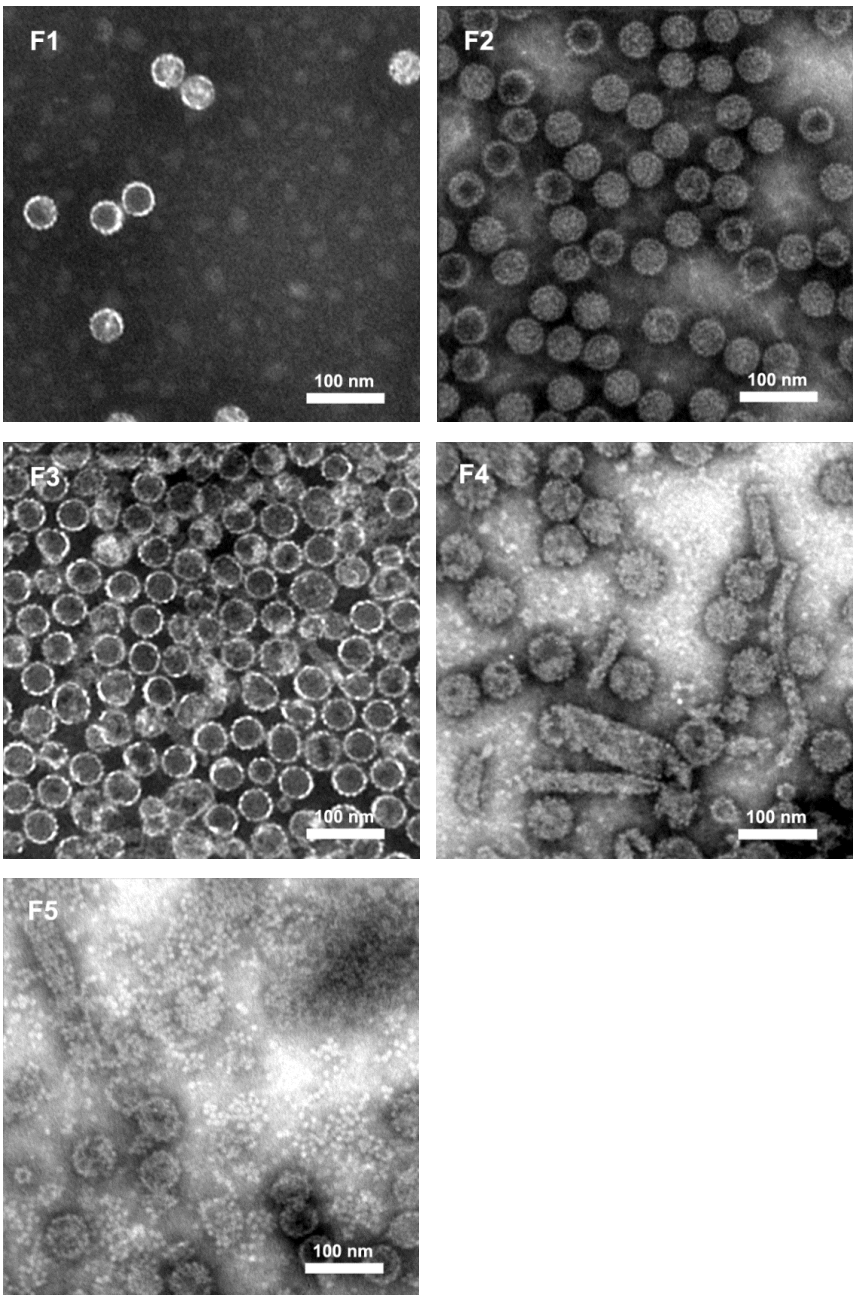

Figure 5.2: **Electron microscopy pictures of prepared VLPs**
Prepared particles were visualized by electron microscopy after negative staining. Fractions (F1-F5) were acquired by joining of CsCl fractions (see Table 5.1). Fractions were diluted 1:10 in B buffer before they were adsorbed onto the grid. Scale bar = 100 nm.

5.1 Preparation of VLPs with conjugated transferrin

The first goal of this thesis was construction of VLPs retargeted to cancer cells by chemical engineering of their surface. Mouse polyomaviral VLPs are superior for the potential clinical usage because of the absence of pre-existing immunity in human population. These VLPs also do not contain polyomavirus genome DNA and therefore they are considered as safe delivery vehicles. We hypothesized that the installation of bulky human transferrin (Tf) on the VLP surface could target the newly prepared particles to cancer cells overexpressing transferrin receptor (TfR). Moreover, it could also create a steric hindrance that would decrease the undesirable binding of VP1 to cell expressing sialic acid residues (Fig. 5.3).

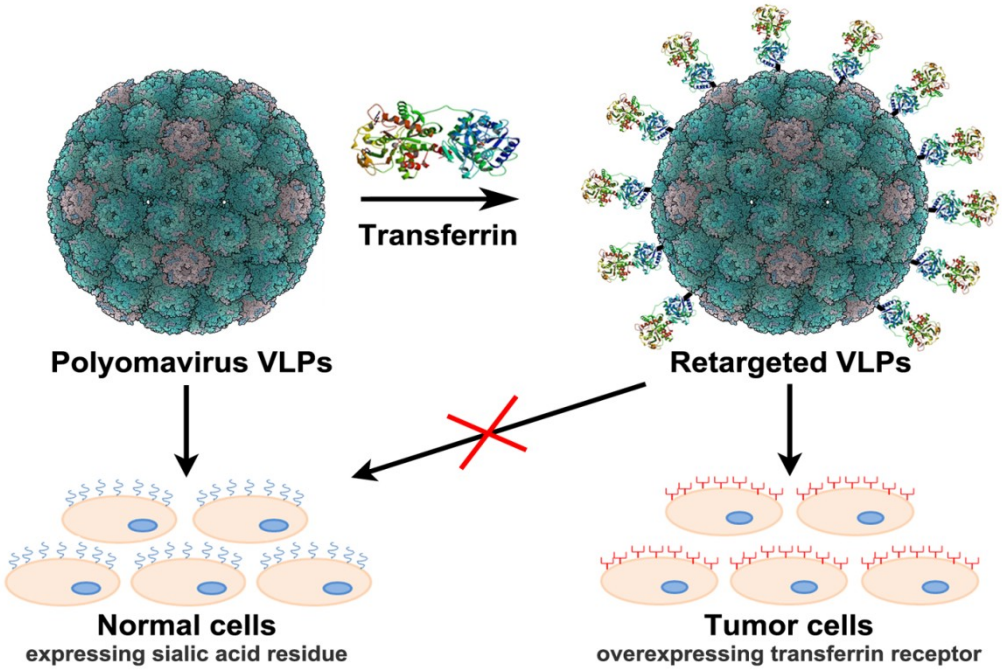

Figure 5.3: **Schematic representation of experimental design.**
The transferrin molecules were installed on the VLP surface by chemical coupling leading to retargeting of these VLPs from cells expressing natural receptor to tumor cells overexpressing transferrin receptor. The scheme was designed in Adobe Photoshop CS4 with utilization of polyomavirus particle prepared by Stehle and Harrison, 1996.

The input VLPs for chemical modification were prepared in sufficient amount (chap. 5.0) and labeled with rhodamine-NHS ester (chap. 4.2.4.1) providing the **VLP*** conjugate for further fluorescence visualization. Then, the remaining lysines were modified with the heterobifunctional linker containing propargyl and NHS ester (chap. 4.2.4.2) thus generating VLP*-alkyne particles. We also labeled human Tf with AF488 (**Tf***) and derivatized its aldehyde with aminooxypropylazide, providing Tf*-azide conjugate (chap. 4.2.4.4). This conjugate was then attached to VLP*-alkyne via Cu(I)-catalyzed azide-

alkyne cycloaddition, so called “click” chemistry (Presolski et al., 2011), obtaining **VLP*-Tf*** conjugate (chap. 4.2.4.3).

We firstly characterized the modified VLPs by transmission electron microscopy (TEM, chap. 4.2.6) and dynamic light scattering (DLS, chap. 4.2.5). TEM analysis proved the homogeneity and stability of both types of VLPs with a diameter of 55 ± 3 nm for **VLP*** and 63 ± 4 nm **VLP*-Tf*** (Fig. 5.4A). Measurement of DLS also ascertained that particles are monodispersed without forming aggregates (Fig. 5.4B). Higher hydrodynamic parameter of **VLP*-Tf*** particles corresponds well with the results from TEM and the obtained values also indicate the deposition of Tf* in one layer, if we consider the hydrodynamic parameter of Tf that is 7.4 nm (Armstrong et al., 2004).

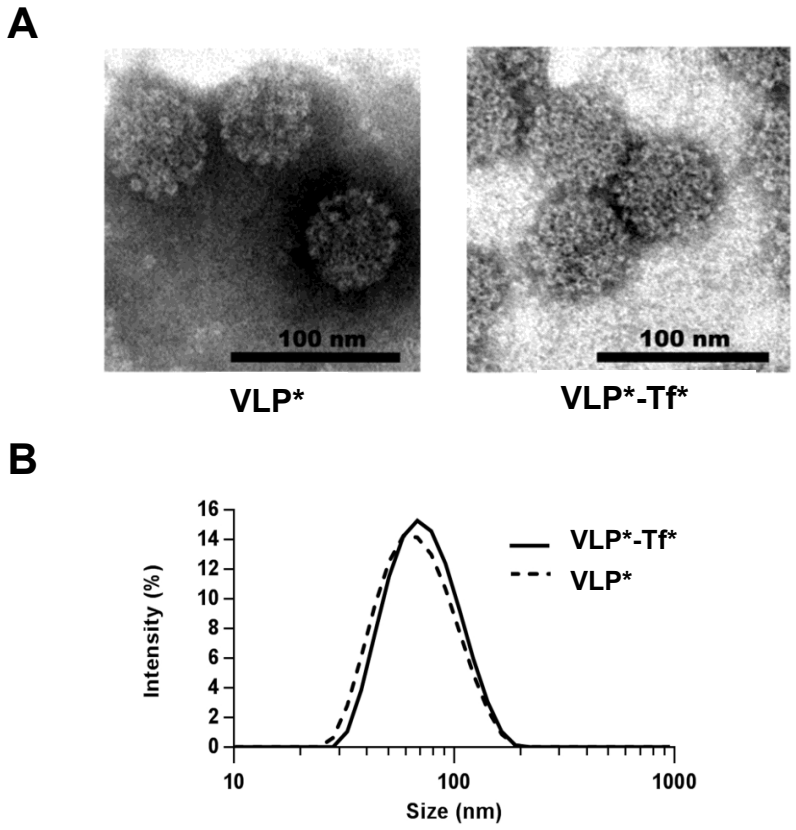

Figure 5.4: **Characterization of prepared VLPs**
(A) Representative TEM images of **VLP*** and **VLP*-Tf*** particles visualized by negative staining with 2% solution of phosphotungstic acid. Scale bar = 100 nm. (B) Hydrodynamic diameters of VLPs measured by dynamic light scattering.

For quantification of surface modification, we measured protein concentration of particles by Qubit protein assay kit and analyzed the Tf load by densitometry analysis of gradient SDS-PAGE (Fig. 5.5A, chap.4.2.2.7 and 4.2.2.8). We obtained approximately 24% coverage of the VLP surface (35 ± 2 **Tf*/VLP*-Tf***). To verify the conjugation of

transferrin, we also obtained extinction spectra. **VLP*-Tf*** particles showed both characteristic absorption bands of rhodamine present in **VLP*** and the Alexa Fluor 488 present in the attached **Tf*** (Fig. 5.5B, chap. 4.2.9).

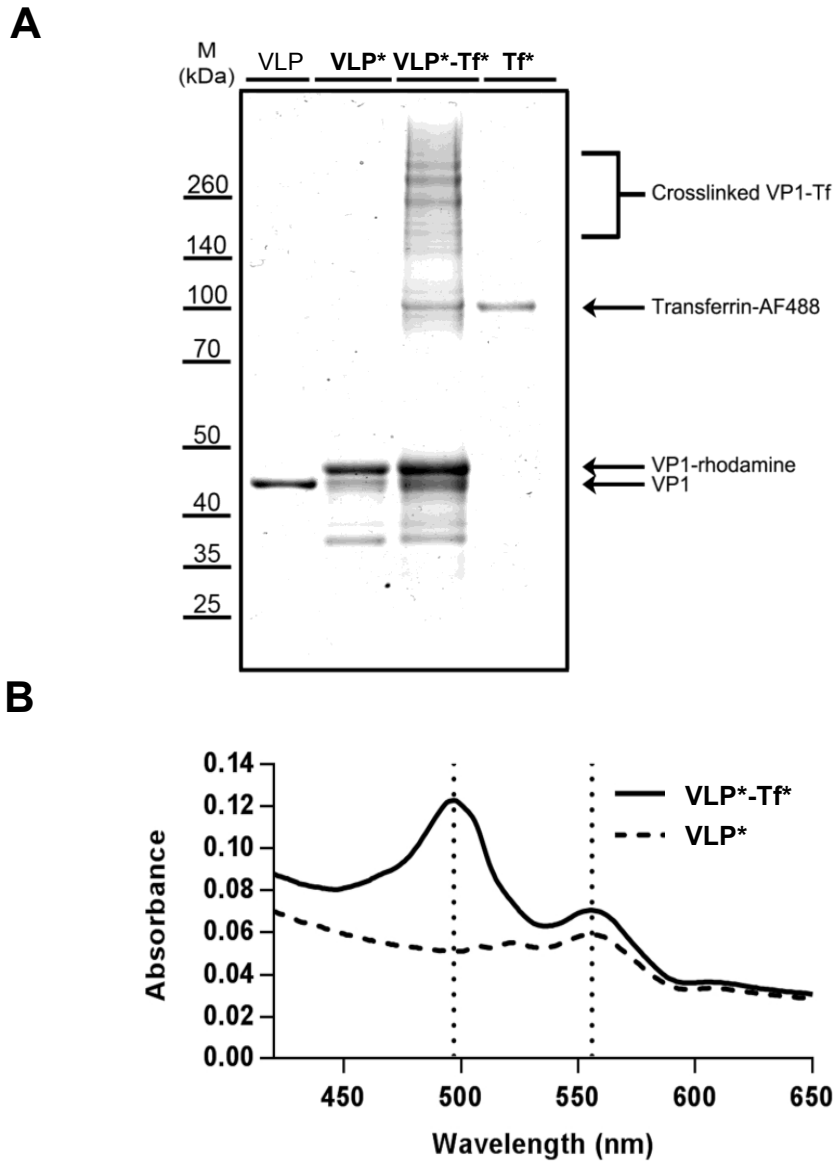

Figure 5.5: **Characterization of VLP surface modifications**
(A) Particles VLP, **VLP***, **VLP*-Tf***, and protein **Tf*** were separated on SDS-PAGE and stained with Coomassie brilliant blue. The molecular weights are indicated on the left. (B) Extinction UV-vis spectra of **VLP*-Tf*** and **VLP*** particles. The first peak defines emission of AF488 and the second peak emission of rhodamine.

After confirmation of successful transferrin conjugation, we examined the ability of particles to selectively target TfR on cancer cells. As a model cancerous cell lines, we used CCRF-CEM lymphoblastic cell line derived from leukemia patient together with U2OS cells derived from osteosarcoma because these cell lines overexpress the TfR on their surface (Nakase et al., 2005; Petrini et al., 1989). As a negative control, we used a non-

cancerous endothelial cell line HUVEC. These cells were incubated with **VLP*** and **VLP*-Tf*** particles for 1 hour and analyzed by flow cytometry (Fig. 5.6, chap. 4.2.3.6). To confirm the binding specificity of **VLP*-Tf*** to TfR, we preincubated the cells with high concentration of free transferrin (Tf+) for 30 min. For both cancer cell lines, we achieved high levels of **VLP*-Tf*** uptake, whereas after preincubation with Tf (Tf+**VLP*-Tf***) the uptake was negligible, verifying the specificity of this interaction. On the other hand, particles without the conjugated transferrin (VLP*) also exhibited interaction with cancer cells, however, this time it was not influenced by free Tf, suggesting the possibility of binding in VP1-specific manner. The data achieved from HUVEC cell line showed very low levels of interaction for both types of particles.

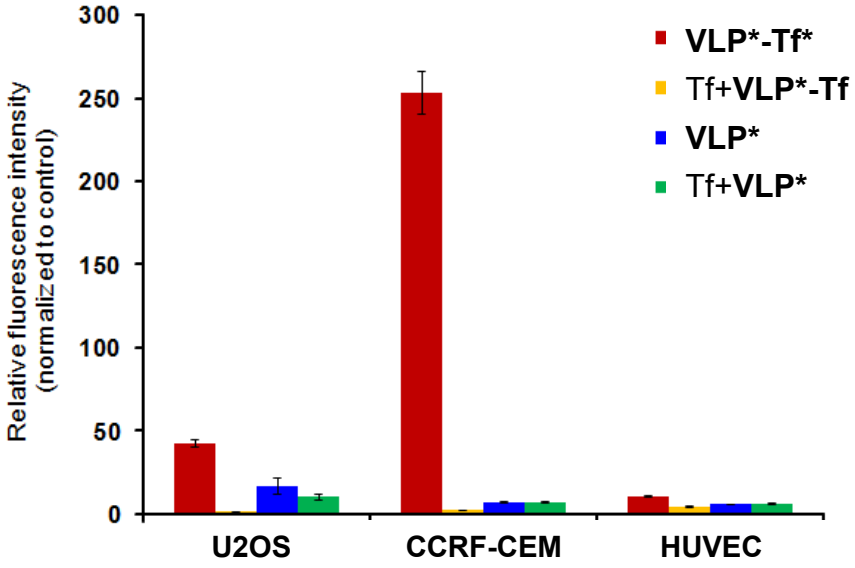

Figure 5.6: **Flow cytometry study of VLPs uptake by CCRF-CEM, U2OS and HUVEC**
The cells were subjected to particles **VLP*** and **VLP*-Tf*** for 60 minutes in 37 °C, 5% CO_2, with (Tf+) or without preincubation with free transferrin (30 min). Data represent the median of fluorescence intensity normalized to autofluorescence of control cells. Standard deviations were calculated from quadruplicates (two independent experiments in duplicates).

To visualize the interaction of particles and cells, we utilized confocal microscopy with fixed U2OS cells (Fig. 5.7, chap. 4.2.3.5). The treatment of the cells was similar to that in previous experiment (**VLP*** and **VLP*-Tf***, 1 hour, with or without Tf preincubation). We observed strong and effective binding of **VLP*-Tf*** particles that was totally blocked by the preincubation with free transferrin (Tf+**VLP*-Tf***). The internalization of **VLP*-Tf*** was relatively fast, only 1 hour after incubation with cells, the particles localized near the perinuclear space. This location is typical for accumulation of polyomaviruses (Richterova et al., 2001), however, these viruses meet the transferrin during the endocytosis 3 hours post infection (Liebl et al., 2006; Mannova and Forstova,

2003). Faster trafficking of **VLP*-Tf*** into the perinuclear area indicates the retargeting of these particles to TfR. The interaction of **VLP*** particles with U2OS cells was negligible and independent on Tf preincubation confirming the unspecific interaction of these VLPs. Finally, we wanted to test the stability of **VLP*-Tf*** during the experiment. So, we utilized the double labeling of **VLP*-Tf*** for colocalization analysis. According to Mander´s colocalization coefficient values (0.747; 0.724), we concluded that **Tf*** molecules do not detach from **VLP*-Tf*** particles during internalization and the linkages remain stable. All data obtained from confocal microscopy are consistent with the flow cytometry data and further testify to the efficiency and selectivity of **VLP*-Tf*** uptake.

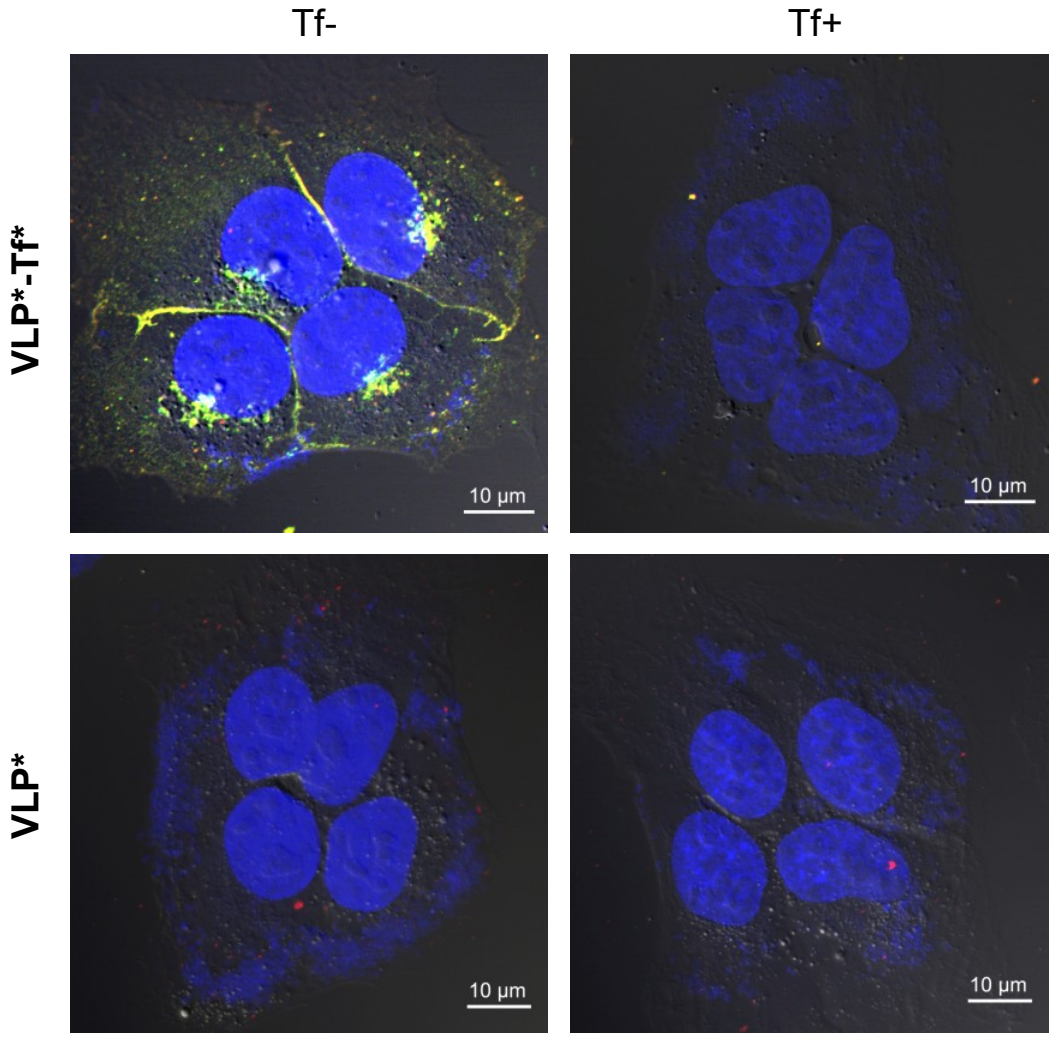

Figure 5.7: **Uptake of modified VLPs by U2OS cells**
U2OS cells were incubated with prepared VLPs **VLP*-Tf*** and **VLP*** for 60 minutes in 37 °C, 5% CO_2 with (Tf+) or without (Tf-) the preincubation with free transferrin. The representative confocal images are presented with corresponding signal in green (Tf conjugated with Alexa Fluor 488 in **VLP*-Tf***), red (VP1 conjugated with rhodamine in **VLP*** and **VLP*-Tf***) and blue (nuclei with DAPI staining). The images are shown as merge of all three channels and bright field with a maximum intensity Z-projection.

5.2 Preparation of VLPs with conjugated inhibitor of GCPII

The second goal of this thesis was construction of VLPs retargeted to cancer cells by chemical engineering of their surface. Previous modification by transferrin proved the possibility of retargeting by installation of relatively huge molecule on the VLP surface. However, the eventuality to utilize small molecule for this purpose still remained undescribed. We hypothesized that the conjugation of appropriate amount of inhibitor of glutamate carboxypeptidase II (iGCPII) on the VLP surface could target the newly prepared particles to cancer cells overexpressing glutamate carboxypeptidase II (iGCPII). Moreover, the sufficient coverage of the VLP surface could also create a steric hindrance that would decrease the undesirable binding of VP1 to cells exposing on their surface sialic acid residues (Fig. 5.8).

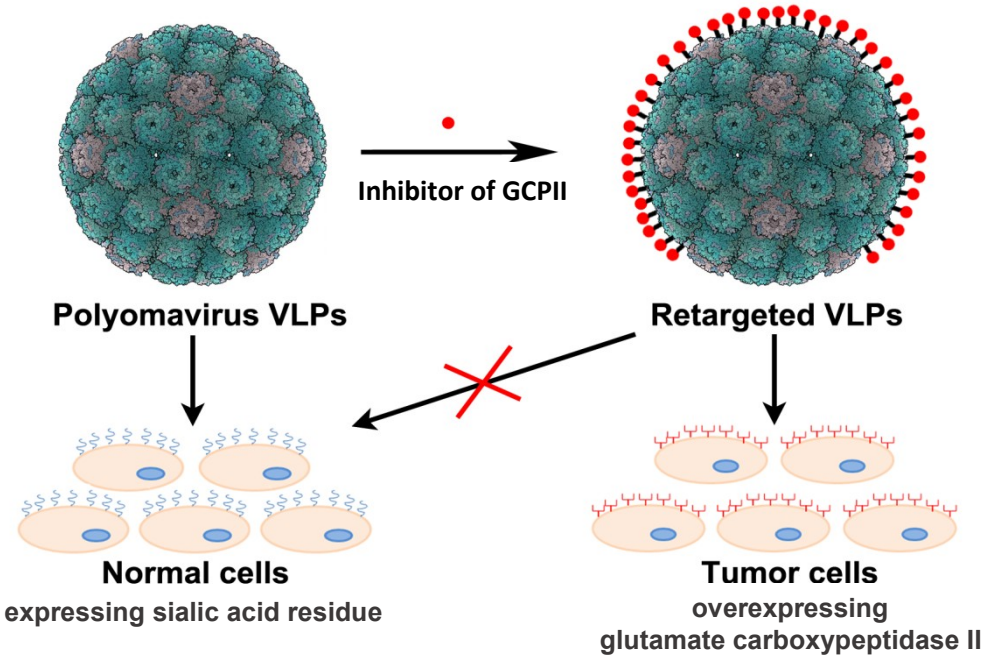

Figure 5.8: **Schematic representation of experimental design.**
The molecules of GCPII inhibitor were installed on the VLP surface by chemical coupling, leading to retargeting of these VLPs form cells expressing natural receptor to cells overexpressing GCPII. The scheme was designed in Adobe Photoshop CS4 with utilization of polyomavirus particle prepared by Stehle and Harrison, 1996.

The input VLPs for chemical modification were prepared in sufficient amount (chap. 5.0) and labeled with Alexa Fluor 488 (AF488) NHS ester (chap. 4.2.4.1), providing the VLP* conjugate for further fluorescence visualization. Then the remaining lysines were modified with the heterobifunctional linker containing propargyl and NHS ester (chap. 4.2.4.2) and generated VLP*-alkyne particles. The iGCPII-azide conjugate (prepared according to Neburkova et al., 2018) was then attached by "click" chemistry to VLP*-alkyne, obtaining VLP*-iGCPII conjugate (chap. 4.2.4.3). We also covered the surface of

VLP* particles with PEG_{13}-carboxyl NHS ester (VLP*-PEG) to avoid the VP1-specific interactions.

Similar methods to previously prepared VLPs with transferrin were used for characterization of modified VLPs. TEM analysis proved that all VLPs were intact, homogenous and stable (Fig. 5.9A). Moreover, DLS ascertained that particles do not form aggregates, thus indicating that the direct conjugation of inhibitor did not change the colloidal stability of modified VLPs (Fig. 5.9B). On the other hand, VLP* without conjugated either iGCPII or PEG showed aggregation that could be visible on DLS measurement as a second peak of hydrodynamic parameter. This is inconsistent with the previously prepared VLPs with conjugated rhodamine (VLP*). Thus, the aggregation could be mediated by conjugation of AF 488 instead of rhodamine. The different behavior is probably due to the charge because high sulphonated dyes such as AF488 are negatively charged in contrast to rhodamine with overall positive charge.

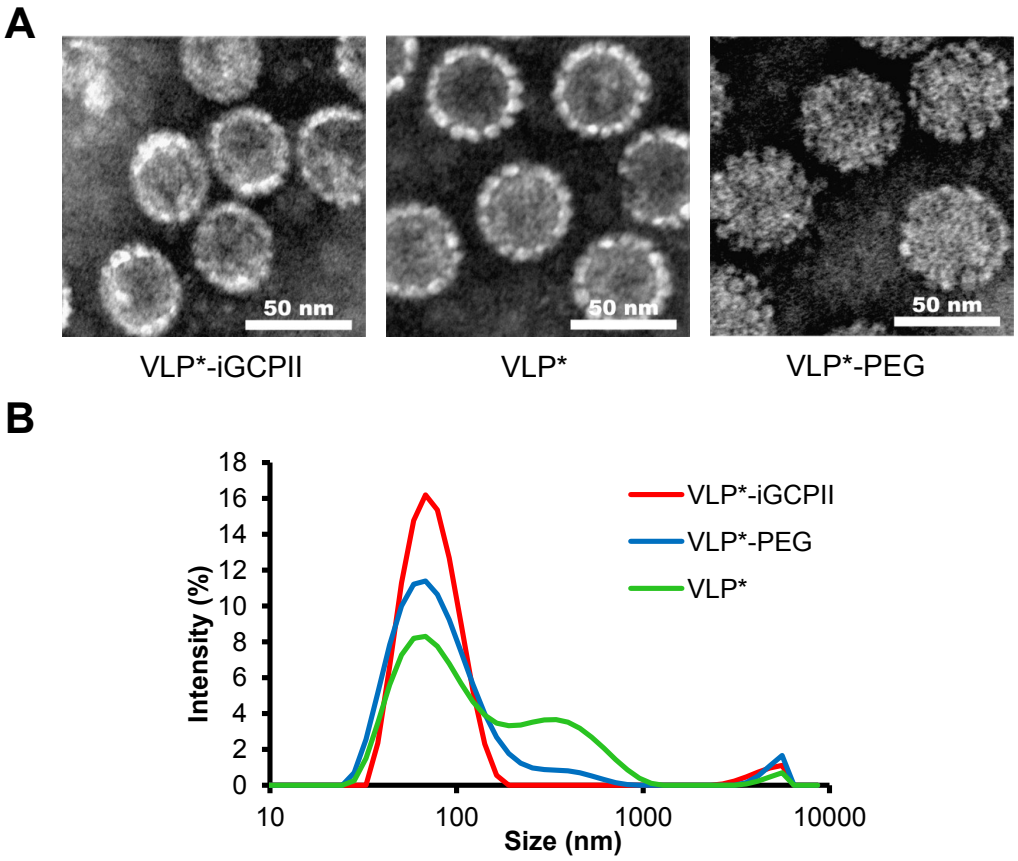

Figure 5.9: **Characterization of prepared VLPs**
(A) Representative TEM images of VLP*-iGCPII, VLP* and VLP*-PEG particles visualized by negative staining with 2% solution of phosphotungstic acid. Scale bar = 50 nm. (B) Hydrodynamic diameters of VLPs measured by dynamic light scattering.

For quantification of surface modification, we measured protein concentration of particles by Qubit protein assay kit and analyzed the number of conjugated ligands by Mass spectrometry (Fig. 5.10, chap. 4.2.8). All types of modified VLPs were disassembled by incubation with urea and dithiotreitol and analyzed by MALDI measurement. The mass spectra of modified proteins were fairly complex; nevertheless, we were still able to quantify the loads. We obtained roughly 540 iGCPII molecules and 1,080 PEG molecules conjugated to VP1 protein. The MALDI measurement also confirmed that both molecules were bound to the VP1 protein covalently.

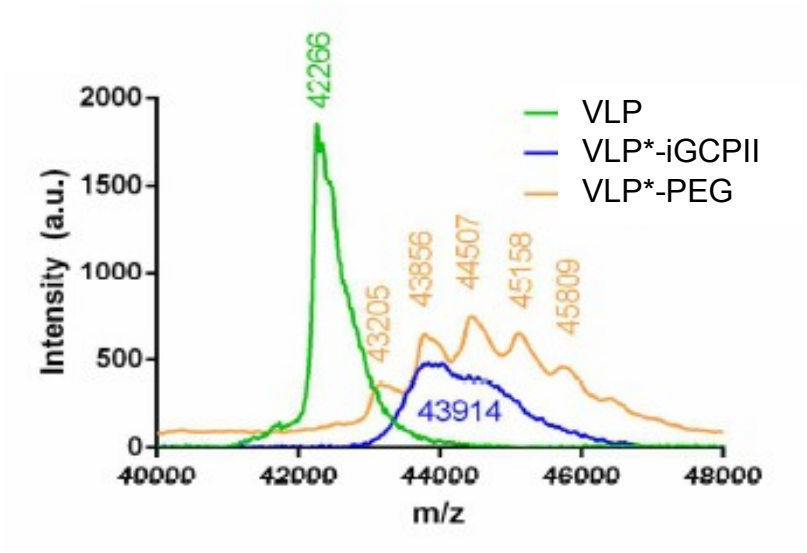

Figure 5.10: **Characterization of VLP surface modifications by MALDI measurement**
VLPs were disassembled to subunits by incubation with high molar urea. Unmodified VLPs (VLP) and VLPs conjugated either with inhibitor of GCPII (VLP*-iGCPII) or PEG (VLP*-PEG) were subsequently analyzed by MALDI. The marked peaks indicate the corresponding mass.

Following the characterization of iGCPII conjugation, we wanted to ascertain their capability to interact with GCPII *in vitro*. We utilized the technology of surface plasmon resonance (SPR, chap. 4.2.2.15). This technology enables to detect the binding of specific molecule and the speed of its washing by the shift in layer thickness. These data could be further evaluated to determine the binding strength and its affinity constant.

For SPR detection, we used a golden chip and GCPII was immobilized in one half of the channels by neutravidin-biotin interaction (GCPII+). As a negative control, we used channels with neutravidin alone (GCPII-). To follow the process of VLP interaction, all channels have to be washed with storage solution of VLPs (B buffer) because even small change of salt concentration is detected. The degree of connection was analyzed by SPR measurement (Fig. 5.11). Only VLP*-iGCPII in the channel containing GCPII (GCPII+, orange color) bound GCPII selectively and with strong affinity. However, in channel containing only neutravidin (GCPII-) and VLP*, we noticed also a weak interaction (blue color). It might be mediated by the off-target binding between VP1 protein and neutravidin because we observed the same interaction during tests with streptavidin (Suchanova, 2012).

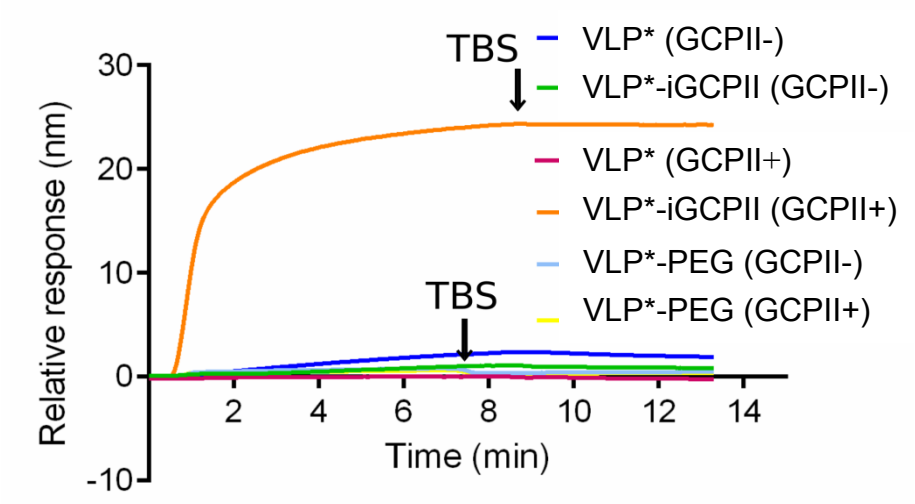

Figure 5.11: **Testing of binding capacity of prepared VLPs to GCPII by SPR measurement**
VLP-GCPII interaction was recorded by SPR measurement. GCPII positive lines (GCPII+) contained GCPII immobilized on the chip through a neutravidin-biotin interaction and negative lines (GCPII-) were covered only by neutravidin. Three types of particles at final concentration 5 nM were utilized for the measurement; VLP*, VLP*-iGCPII, VLP*-PEG. After injection, VLPs were left to associate for several minutes and then, the channels were washed with Tris buffer (TBS). The channels were computationally normalized on a zero level of layer thickness for better demonstration of binding differences.

Once we verified the interaction of VLP*-iGCPII with GCPII, we examined the ability of these particles to selectively target GCPII in context of cells. As a model cell line, we used U251 MG cells from human glioblastoma. This cell line was modified by Tet-Off advanced system to overexpress GCPII on their surface depending on the presence of doxycycline in the media (Gossen and Bujard, 1992; Tykvart et al., 2014). Cells with (U251 MG^+) or without (U251 MG^-) GCPII expression were incubated for 1 hour with VLP*-iGCPII, VLP*-PEG and VLP* and analyzed by flow cytometry. Since phosphate is a weak inhibitor of GCPII, during the experiment, only phosphate-free medium was used to block eventual detaching of VLPs from the cell surface. If we compare the data from VLP*-iGCPII and VLP*-PEG uptake, we observed that conjugation of inhibitor formed strong and specific interaction with GCPII because these particles showed negligible interaction with U251 MG^- (Fig. 5.12A). Very weak binding of VLP*-PEG to both types of cells indicates that the installation of PEG-carboxyl onto the VLP surface prevents the VP1-specific interaction with cells.

On the other hand, the comparison of VLP*-iGCPII with VLP* brought very surprising data (Fig. 5.12B). The iGCPII negative particles, VLP*, showed very high binding efficiency to U251 MG cells, irrespectively to GCPII expression. This observation could be explained by overexpression of complex gangliosides (MPyV natural receptors) on the surface of glioblastoma cells. However, conjugation of PEG, with or without

iGCPII, facilitated the masking of VP1-specific interactions and selective retargeting of these VLPs.

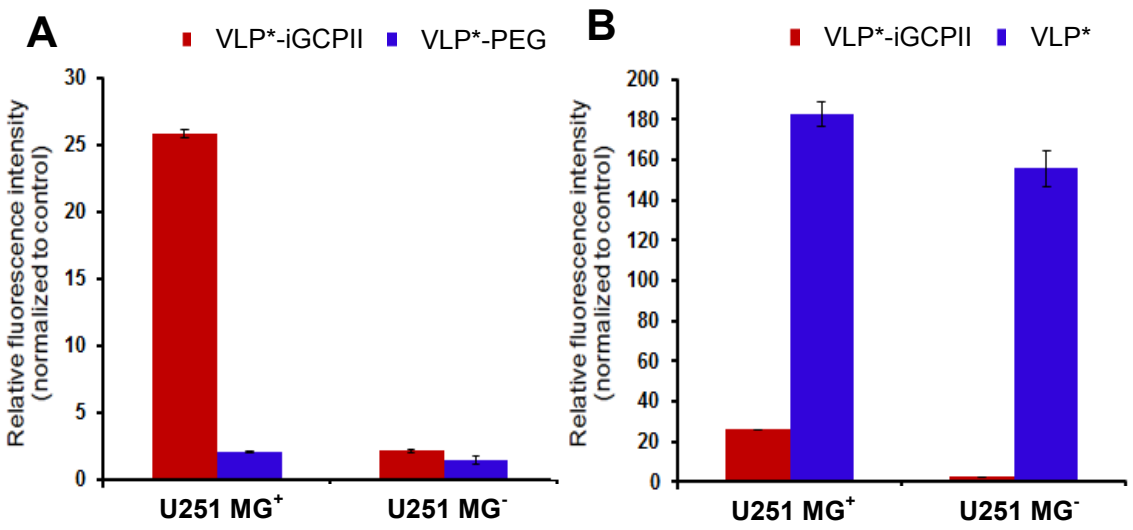

Figure 5.12: **Flow cytometry study of VLPs uptake by U251 MG cells**
The cells with (U251 MG^+) or without (U251 MG^-) GCPII expression were subjected to VLP*-iGCPII, VLP*-PEG, VLP* for 60 minutes in 37 °C, 5% CO_2. (A) Comparison of VLP*-iGCPII and VLP*-PEG, (B) Comparison of VLP*-iGCPII and VLP*. Data represent the median of fluorescence intensity normalized to autofluorescence of negative cells. Standard deviations were calculated from triplicates.

We further visualized the interaction of all three types of VLPs by confocal microscopy with fixed U251 MG cells with (U251 MG^+) or without (U251 MG^-) GCPII expression (Fig. 5.13, chap. 4.2.3.5). The treatment of the cells was similar to previous experiment (VLP*-iGCPII, VLP*-PEG and VLP*, 1 hour). We observed high internalization rate of VLP*-iGCPII particles in U251 MG^+ that was blocked on cells without GCPII expression (U251 MG^-). Negligible interaction with U251 MG cells was visible in case of VLP*-PEG in contrast to VLP* that bound U251 MG cells very effectively. Nevertheless, the majority of VLP* particles was localized on the cell periphery. This indicates that VLP* particles are mostly trapped on the membrane, but do not enter the cells. We even cannot rule out the possibility that the particles visible inside the cell are actually located on the wrinkled surface of the membrane. All data obtained from confocal microscopy are consistent with the flow cytometry data and further testify the efficiency and selectivity of VLP*-iGCPII uptake mediated by surface exposed iGCPII.

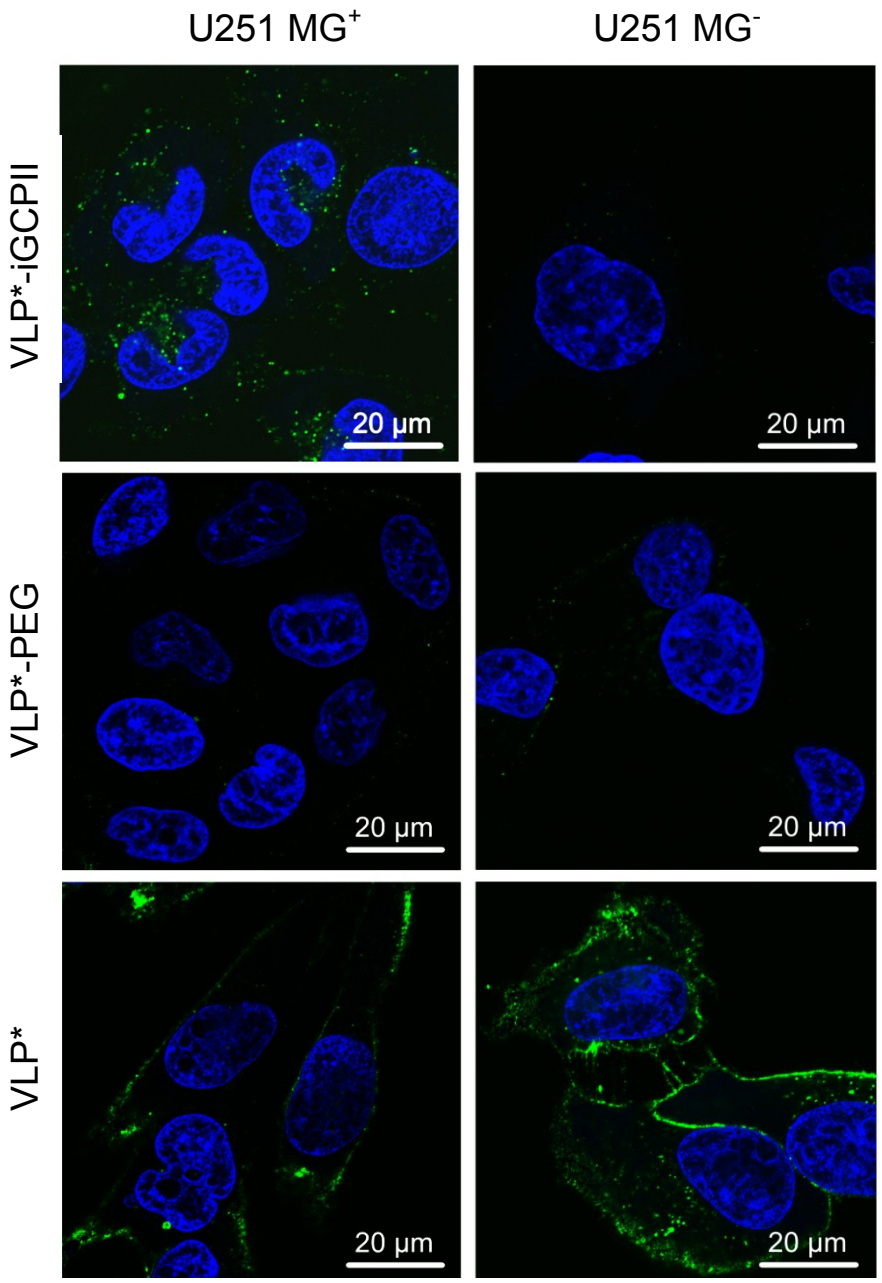

Figure 5.13: **Uptake of modified VLPs by U251 MG cells**

U251 MG cells with (U251 MG^+) or without (U251 MG^-) GCPII expression were incubated with VLP*-iGCPII, VLP*-PEG and VLP* for 60 minutes in 37 °C, 5% CO_2. The representative confocal images are presented with corresponding signal in green (VP1 conjugated with Alexa Flour 488) and blue (nuclei Hoechst staining). The images are shown as merge of both channels and with a maximum intensity Z-projection.

5.3 Characterization of polyomavirus VLPs in context of serum proteins

The third goal of this thesis was to test the influence of protein corona on targeting of MPyV VLPs and their behavior in the presence of serum proteins. We performed the comparative study of MPyV VLPs and polystyrene nanoparticles (Beads). These Beads were chosen as a control nanoparticles for two reasons; the composition of associated protein corona around the Beads is known (Blundell et al., 2016; Lundqvist et al., 2008) and Beads can be provided in a diameter around 50 nm (similar size of MPyV capsids). For this study, unmodified MPyV VLPs were used first and then, we examined also how the presence of serum proteins can affect binding efficiency of modified VLPs with conjugated targeting ligand. For that, we prepared new stocks of MPyV unmodified VLPs and VLPs with conjugated transferrin, new negative controls and tested the binding by flow cytometry and ELISA.

The input material for comparative study was either produced in baculovirus expression system (MPyV VLPs, chap. 5.0) or obtained from Polysciences, Inc (Beads). The experiment was inspired by the previously published protocol for silica and polystyrene nanoparticles (Tenzer et al., 2013), where particles were incubated in the presence of plasma proteins and consequently, Beads with formed hard corona around their surface were purified from the unbound proteins by centrifugation through sucrose cushion. Both VLPs and Beads were incubated for 1 hour in the 55% human serum (Sigma-Aldrich, H6914), then dialyzed against B buffer for 2 days in dialysis tubing (300 kDa, Biotech) with several buffer changes. We added this purification step for nanoparticles with corona as the data revealed the equilibrium dialysis as sufficient method for removal of unbound proteins from various drugs with formed protein corona (Kristensen and Gram, 2009; Lin et al., 2005; Zeitlinger et al., 2011). Following the dialysis, samples were purified by ultracentrifugation in 20% sucrose cushion (20% SC; chap. 4.2.2.11). The particles were analyzed after each purification step by TEM (Fig. 5.14A), SDS-PAGE (Fig. 5.14B) and DLS (Fig. 5.14C) and compared to particles without the serum treatment. As could be seen from the TEM pictures, after dialysis, both Beads and MPyV VLPs contained a high amount of serum proteins, proving that equilibrium dialysis does not lead to dissociation of loosely associated proteins. However, the effect of purification by sucrose cushion differed between the particle types. Protein composition of MPyV VLPs was similar as that in the serum untreated control in contrast to Beads that were aggregated and covered with a relatively thick layer of proteins (Fig. 5.14A). These data were confirmed also by the SDS-

PAGE analysis. The MPyV VLPs without serum proteins showed multiple bands of VP1 protein, its dimer and few, probably degradation or contamining products. The untreated Beads were invisible by Coomassie blue staining because these particles do not consist of protein. After incubation with serum and dialysis step, the samples contained still lots of serum proteins. However, the substantial change accured after further purification of particles by centrifugation in sucrose cushion. SDS profile of MPyV VLPs became practically identical with that of untreated VLPs. On the other hand, Beads were suddenly visible by protein staining and were covered with various serum proteins, with the major band of protein with similar molecular weight to bovine serum albumin (Fig. 5.14B). The proteins adsorbed to the particles were also analyzed by DLS. This method allows the determination of hydrodynamic diameter and convenient observation of the protein corona formation on compact particles (Pino et al., 2014). From the graph of MPyV VLPs, we could see that their hydrodynamic diameter around 60 nm was not changed by the presence of serum, contrary to Beads, where the hydrodynamic diameter was increased from 65 nm to 745 nm.

Therefore, we could conclude that MPyV VLPs are not influenced by formation of hard corona because they were not aggregated, their hydrodynamic diameter was not increased and not additional proteins in comparison with untreated VLPs were visible by coomassie blue staining. The analysis of Beads confirmed the formation of hard protein corona as was published previously (Blundell et al., 2016; Lundqvist et al., 2008).

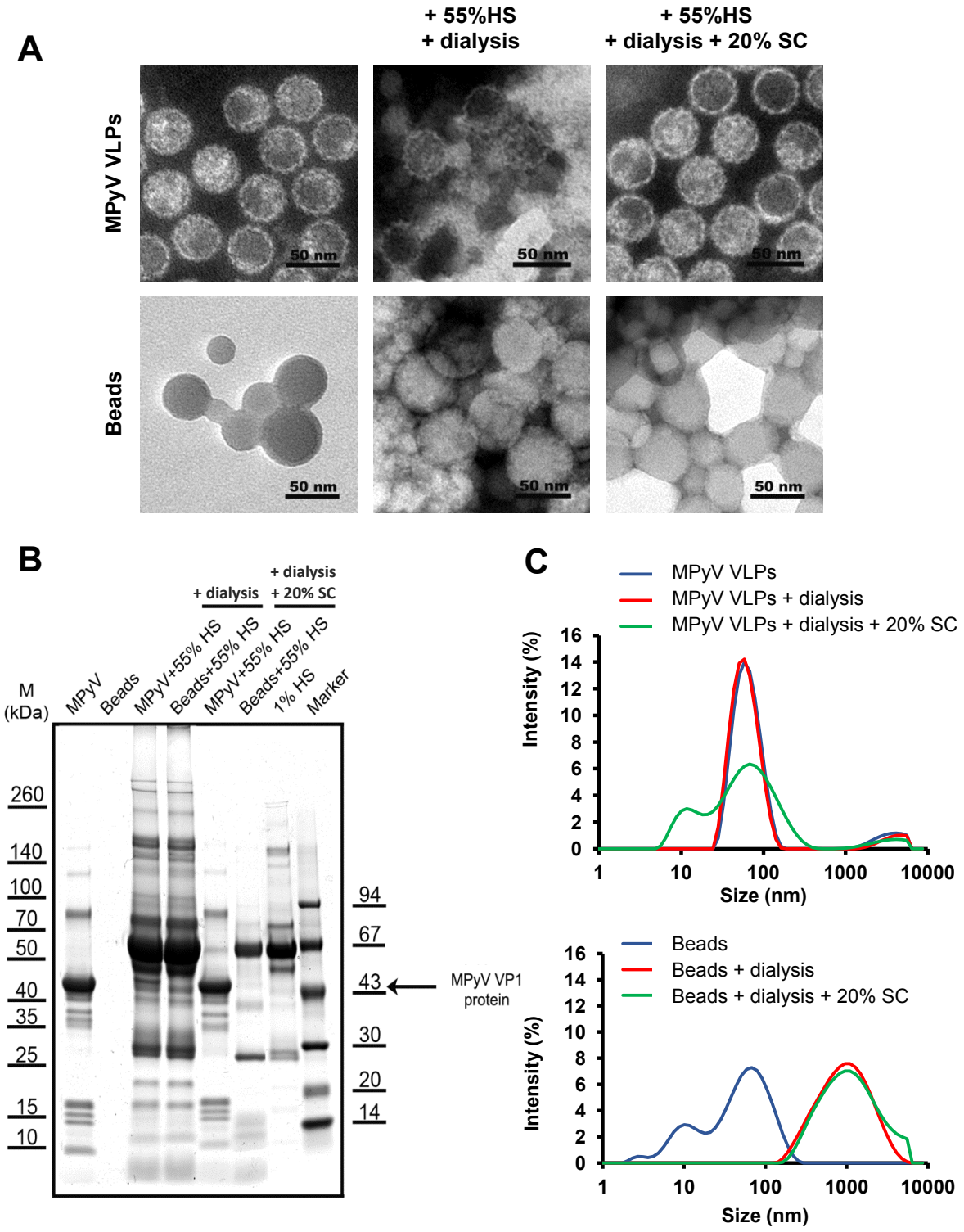

Figure 5.14: **Comparison of VLPs and Beads behavior in the presence of human serum**
(A) Representative TEM images of MPyV VLPs and Beads visualized by negative staining. The pictures without serum addition and after serum addition (+55% HS) and dialysis or both dialysis and centrifugation purification steps are also shown. Scale bar = 50 nm. (B) Fractions of MPyV VLPs and Beads untreated, or incubated with serum, or incubated with serum and purified, or 1% human serum were separated on SDS-PAGE and stained with Coomassie brilliant blue. The molecular weights are indicated on the left. On the right, the molecular weight marker (Pharmacia Fine Chemicals) containing bovine serum albumin (67 kDa) as a control is shown. (C) Hydrodynamic diameters of MPyV VLPs and Beads before or after incubation with human serum or after incubation with serum followed by one or two purification steps, measured by dynamic light scattering.

After we confirmed that MPyV VLPs do not form a hard corona, we analyzed also the behavior of these VLPs in context of cells. We set up the ELISA based binding assay to figure out the influence of serum proteins on VLP interaction with cells. We utilized two cell types; adherent mouse 3T6 fibroblast cells and human osteosarcoma cells,U2OS (chap. 4.2.7.2). Mouse fibroblasts were selected as a positive control of this experiment as these cells are naturally infected by mouse polyomavirus and contain the GD1a and GT1b ganglioside receptors. Human osteosarcoma cells U2OS were used as a model human cancer cell line that is adherent and overexpress transferrin receptor (chap. 5.1). The interaction of MPyV VLPs was studied not only in human serum but also in serum from various animals. We aimed to find out, if the formation of protein corona could be serum species specific, as it was published that the relative proportion of protein composition of serum differs among mammalian species (Zeitlinger et al., 2011). MPyV VLPs with cells (3T6 or U2OS) were incubated (in 37°C, 5% CO_2 in the presence of human (HS), mouse (MS), chicken (ChS), bovine (FBS) or rat (RS) sera, applied in two concentations, 10% or 55 % (Fig. 5.15). Then, the unbound VLPs were transferred onto 96-well plate and detected by ELISA assay (chap. 4.2.7.2). The obtained data showed very low influence of serum proteins on VLP/cell interaction. Even the highest inhibition of VLP binding in 55% human serum reached only 6.4% on 3T6 cells or 9.1% on U2OS cells. These results suggest that serum proteins do not affect interaction of MPyV particles with the natural virus receptors and support the observations that stable protein corona is not formed around MPyV VLPs (Fig. 5.14).

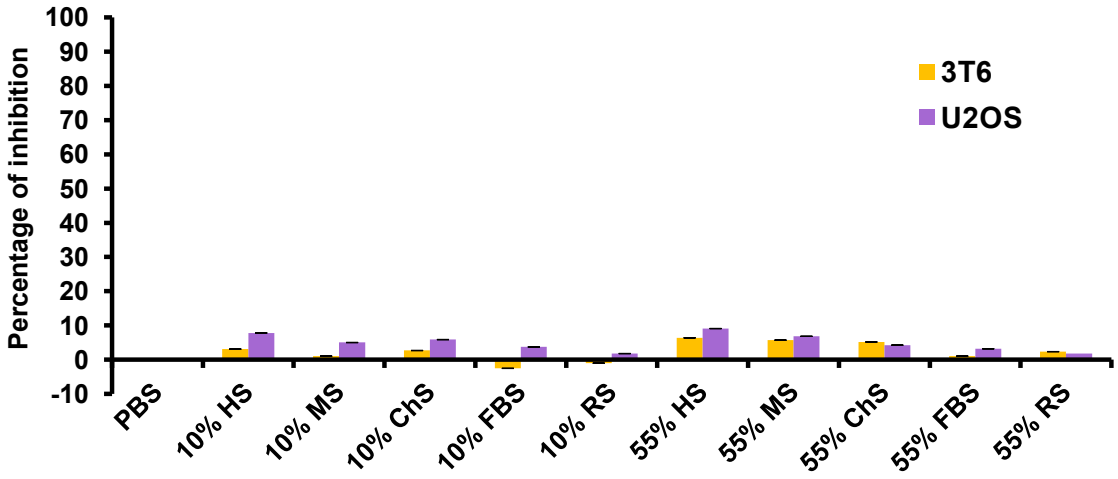

Figure 5.15: **Binding assay on 3T6 and U2OS cells**
The graph represents data from binding assay performed with 3T6 and U2OS cells. These cells were subjected to MPyV VLPs and incubated with or without presence of serum. The unbound VLPs were coated on plates and detected by ELISA assay. The data were normalized by calculation of the difference in absorbance values between VLPs with and without serum. Standard deviations were calculated from triplicates.

Next, more importantly, we examined whether the presence of serum proteins can affect the binding efficiency of VLPs with conjugated targeting ligand. For this purpose, we have prepared a new stock of transferrin modified VLPs. VLPs were prepared in sufficient amount (chap. 5.0) and labeled with Alexa Fluor 488 (AF488) NHS ester (chap. 4.2.4.1) providing the VLP* conjugate. Then, the remaining lysines were modified with the heterobifunctional linker containing propargyl and NHS ester (chap. 4.2.4.2) and generated VLP*-alkyne particles. The transferrin molecule or Texas Red dye conjugated with azide were then attached to VLP*-alkyne by "click" chemistry, obtaining VLP*-Tf or VLP*-T.Red conjugate (chap. 4.2.4.3). Texas red dye was conjugated to VLP* particles as a control of click reaction efficiency as this time the transferrin molecule was not fluorescently labeled.

We characterized the modified VLPs by various methods. The stability and homogeneity of VLPs were analyzed by TEM (Fig. 5.16B) and DLS (Fig. 5.16C). TEM analysis proved the stability of all types of VLPs. Measurement of DLS ascertained that particles are monodispersed and do not aggregate, except of particles labeled with AF488 (VLP*) where an additional peak with higher hydrodynamic diameter was present, indicating the aggregation of these particles. Higher hydrodynamic parameter of VLP*-Tf in comparison with parameters of other particles confirmed the conjugation of transferrin to the VLP surface. For quantification of surface modification by Tf, we measured protein concentration of particles by Qubit protein assay kit and analyzed the Tf load by densitometry analysis of gradient SDS-PAGE gel after Coomassie blue staining (Fig. 5.16A, chap.4.2.2.7 and 4.2.2.8). We obtained 51 ± 3 Tf/VLP*-Tf that provided approximately 35% coverage of the VLP surface. The calculation of the coverage was based on a simple spherical model of VLPs with diameter of 45 nm and the footprint of Tf as a circle of 7.4 nm in diameter (Armstrong et al., 2004). To verify the labeling of VLPs by fluorescent dyes, we also obtained extinction spectra. Particles showed both characteristic absorption bands of Alexa Fluor 488 present in all VLP* and the attached Texas Red to VLP*-T.Red particles (Fig. 5.16D, chap. 4.2.9).

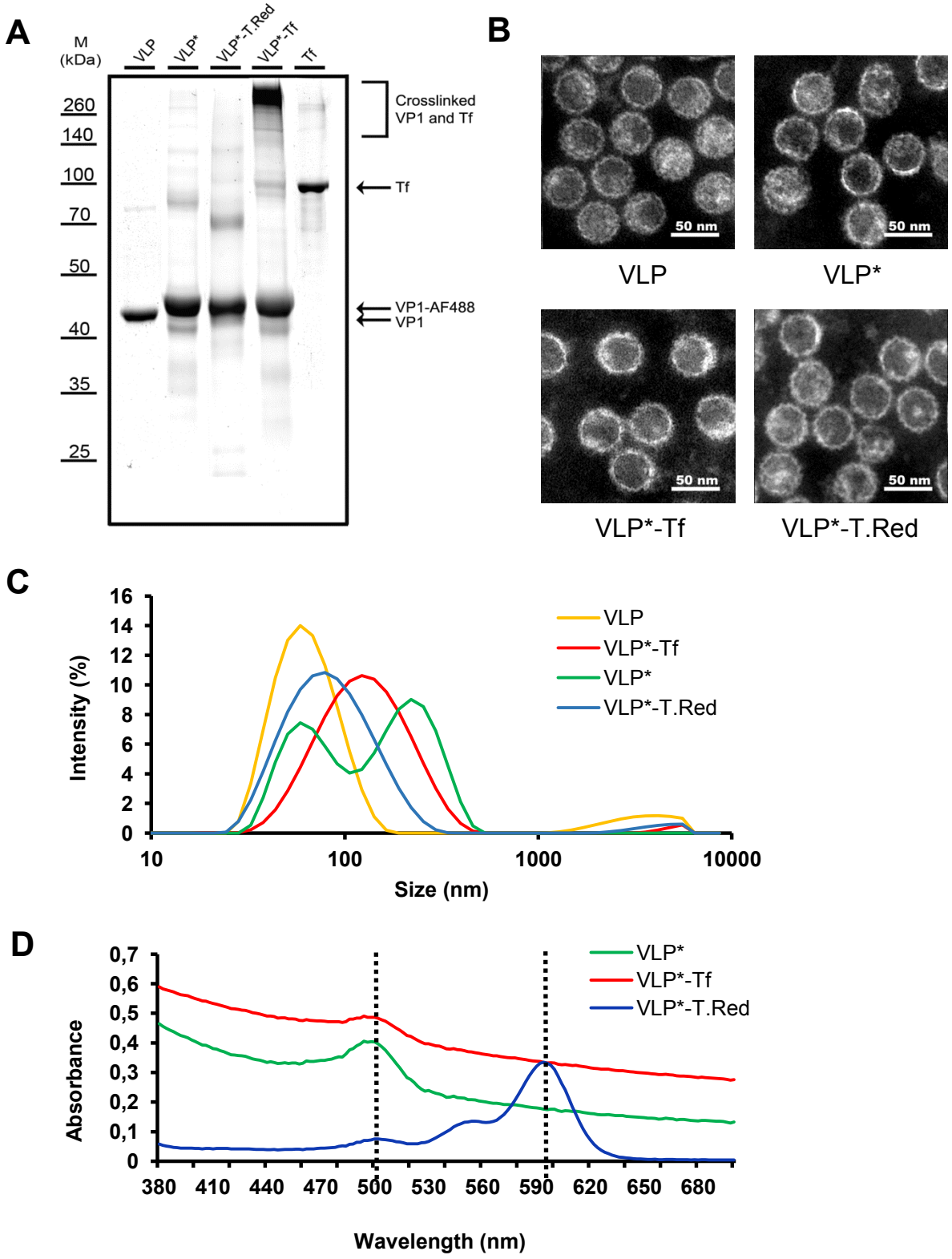

Figure 5.16: **Characterization of prepared VLPs**
(A) Particles VLP, VLP*, VLP*-T.Red, VLP*-Tf, and protein Tf were separated on SDS-PAGE and stained with Coomassie brilliant blue. The molecular weights are indicated on the left. (B) Representative TEM images of VLP, VLP*, VLP*-Tf and VLP*-T.Red particles visualized by negative staining. Scale bar = 50 nm. (C) Hydrodynamic diameters of VLP, VLP*, VLP*-T.Red and VLP*-Tf particles measured by dynamic light scattering. (D) Extinction UV-vis spectra of VLP*, VLP*-T.Red and VLP*-Tf, particles. The first peak defines emission of AF488 and the second peak emission of Texas Red.

The characterized VLP*-Tf particles were utilized also in the confocal study of the clathrin pathway inhibition and serum influence on the way of their internalization by human cancer cells. Transferrin is known to enter cells via clathrin-mediated pathway (Dautry-Varsat, 1986) whereas MPyV utilize non-clathrin pathway (Richterová et al., 2001) We used a clathrin-specific inhibitor, chlorpromazine, that translocates clathrin from the cell surface to intracellular endosomes (Dutta and Donaldson, 2012) and blocks clathrin-mediated endocytosis and HeLa cells that were used previously for studying the inhibition of transferrin uptake by clathrin-mediated endocytosis (Sun et al., 2005).. The cells were incubated for 30 minutes in DMEM without serum, then the medium was aspirated and 0, 10 or 30 μg/ml of chlorpromazine (CPZ) in DMEM with 10% FBS was added. After incubation for 1 hour in 37°C, 5% CO_2 the cells were treated for 30 minutes with Tf-AF488, VLP*-Tf or VLP* in 37°C, 5% CO_2, then washed twice in PBS and fixed (chap. 4.2.3.5). The confocal images (Fig. 5.17) showed that VLP*-Tf as well as free transferrin (Tf-AF488) were dependent even in the presence of 10% FBS on functional clathrin mediated endocytosis since the pre-incubation of cells with chlorpromazine (CPZ 30 μg/ml) inhibited their cellular uptake. The lower concentration (CPZ 10 μg/ml) decreased the interaction but was insufficient to completely diminish it. On the contrary, the uptake of VLPs with AF488 (VLP*) was not influenced by either presence of serum or CPZ pre-incubation. These data confirmed that MPyV VLP*-Tf can be efficiently redirected via transferrin molecule not only to bind cells overexpressing TfR, but also to utilize clathrin mediated endocytosis. Moreover, this behavior is not influenced by the presence of serum.

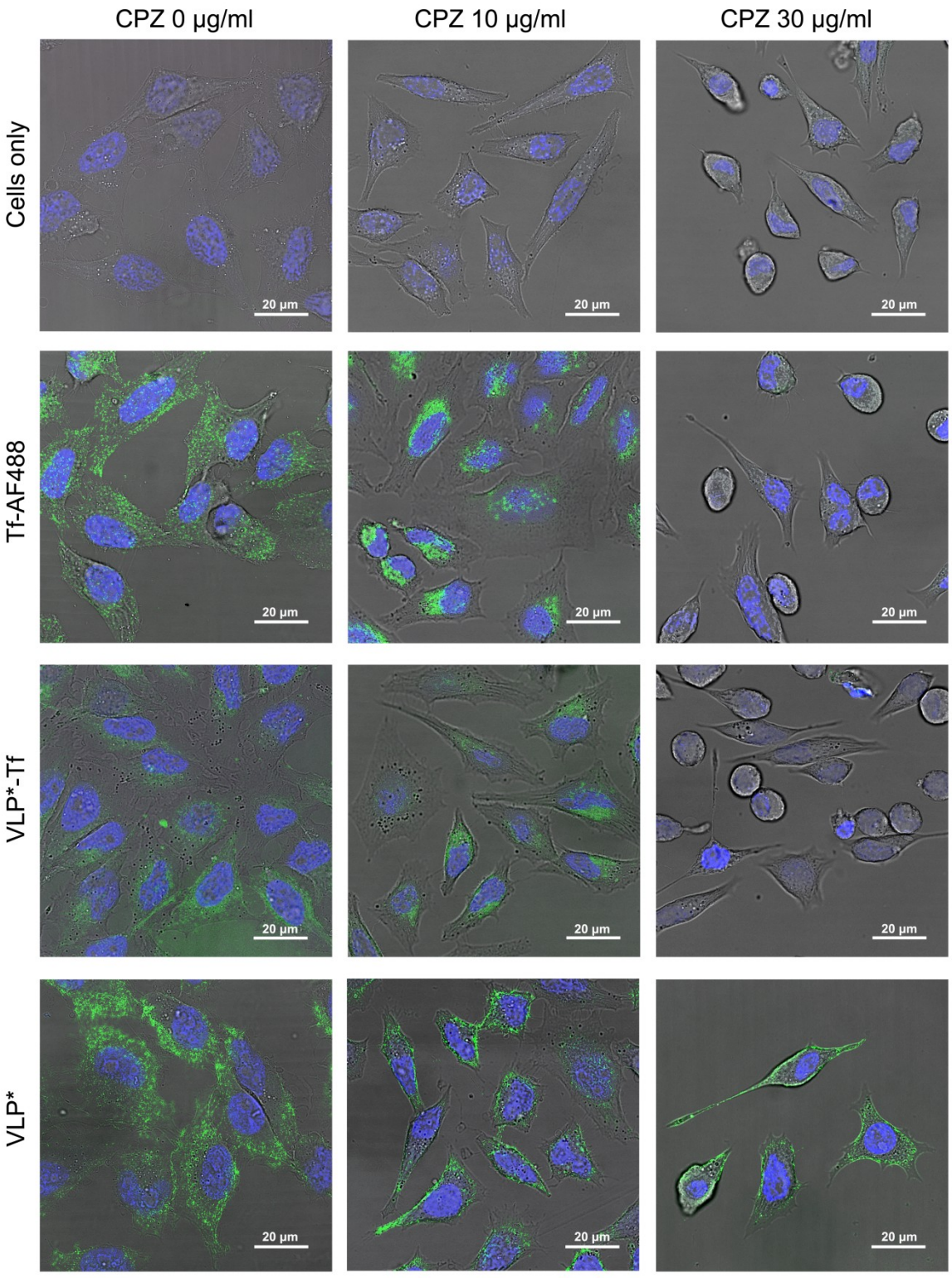

Figure 5.17: **Uptake of modified VLPs by HeLa cells**
HeLa cells with or without inhibition of clathrin-mediated endocytosis by chlorpromazine presence. The cells were incubated with **Tf***, VLP*-Tf, VLP* or B buffer (cells only) for 1 h. Confocal sections of representative cells with corresponding signal in green (conjugation of Alexa Fluor 488) and blue (nuclei with DAPI staining) channels are shown. Merged images are composed of both channels and bright field image.

Following the characterization of VLP*-Tf conjugation and endocytosis, we aimed to prove the capability of these particles to interact with transferrin receptor (TfR) in the presence of serum proteins. We utilized the ELISA assay for testing the direct (out of the context of cells) interaction of VLP*-Tf with TfR and the influence of serum proteins. TfR was coated on plates and incubated for 1 hour with VLPs that were either in PBS, in serum or in serum with added Tf (chap. 4.2.7.1). As sera can contain a high concentration of free transferrin that may inhibit the interaction of VLP*-Tf and TfR (5.1), the sera from three different species; human (HS), mouse (MS) and bovine (FBS), were examined in this assay (Fig. 5.18). These species were chosen according to similarity of transferrin molecule. Mouse transferrin has 73% sequence homology with human transferrin and also their receptors were shown to be very similar (van Agthoven et al., 1984). On the other hand, bovine transferrin has low sequence identity and it was proved that this Tf does not interact with human TfR. To estimate the influence of Tf during interaction of VLP*-Tf with TfR, the free human Tf was added in control serum samples. The obtained data were normalized to absorbance of input VLP*-Tf without serum for calculation of percentage of binding inhibition. The highest inhibition were achieved by combination of serum with free Tf, indicating that the interaction of VLP*-Tf with TfR is specific and mediated by installed Tf molecules on the VLP surface. Human serum had similar effect on these VLPs as it contains a high amount of free human transferrin. Partial inhibition was achieved with mouse serum indicating the possible low-affinity interaction of mouse Tf and human TfR. The presence of FBS did not interfere with the binding; however, surprisingly, it slightly increased the efficacy of particle/receptor interaction.

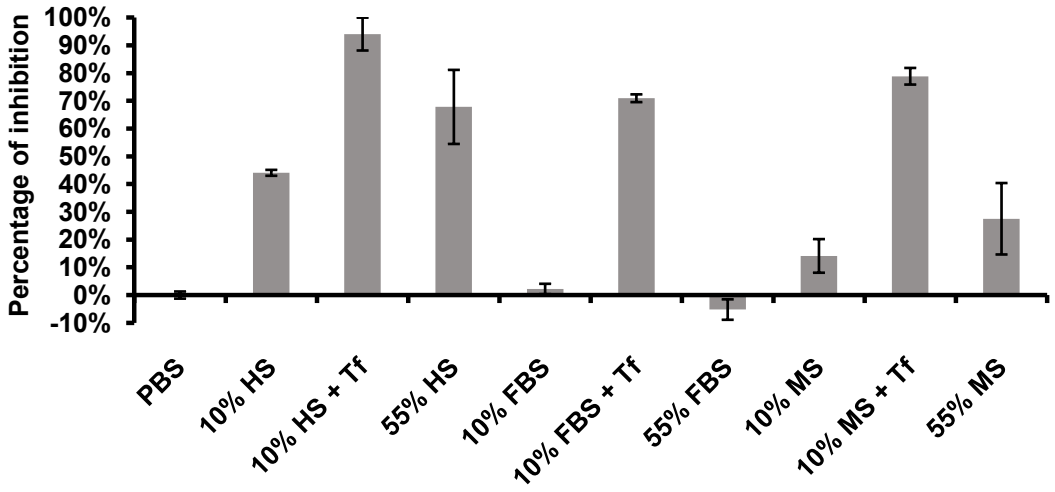

Figure 5.18: **Interaction of VLP*-Tf with TfR**
The graph represents data from ELISA assay performed with transferrin receptor (TfR) coated on ELISA plate. TfR was subjected to VLP*-Tf particles with or without the presence of serum. The specificity of interaction was verified by co-incubation with free transferrin (+ Tf). The data were normalized by calculation of the difference in absorbance value between VLPs with and without serum. Standard deviations were calculated from triplicates.

Finally, we examined the ability of these particles to target TfR in the context of cells by the ELISA based binding assay and by flow cytometry. As a model cell line, we used U2OS from human osteosarcoma as these cells overexpress TfR. The binding assay was performed with U2OS cells (chap. 4.2.7.2) and as previously, HS, MS, FBS and free human Tf were used. Cells were incubated for 1 hour with VLP*-Tf particles in the presence of serum or free Tf (in control samples), then, the unbound VLP*Tf particles were washed, coated on plates and analyzed by ELISA assay (Fig. 5.19). The obtained data were normalized to absorbance of input VLP*-Tf without serum (PBS) for calculation of percentage of binding inhibition. Fig. 5.19 shows that, similarly to data from ELISA test with recombinant TfR, the interaction of VLP*-Tf particles with cells was inhibited by HS to the similar extend as by free human Tf. The effect was dose dependent. Interestingly, we observed opposite trend for MS. The higher concentration of FBS also slightly supported the VLP*-Tf interaction with cells. These data indicated, that specific interaction of VLP*-Tf with target receptor on cells is primarily influenced by free transferrin in sera and not by serum proteins *per se*. Since transferrin in FBS apparently does not inhibit these interactions, we used FBS for subsequent analysis.

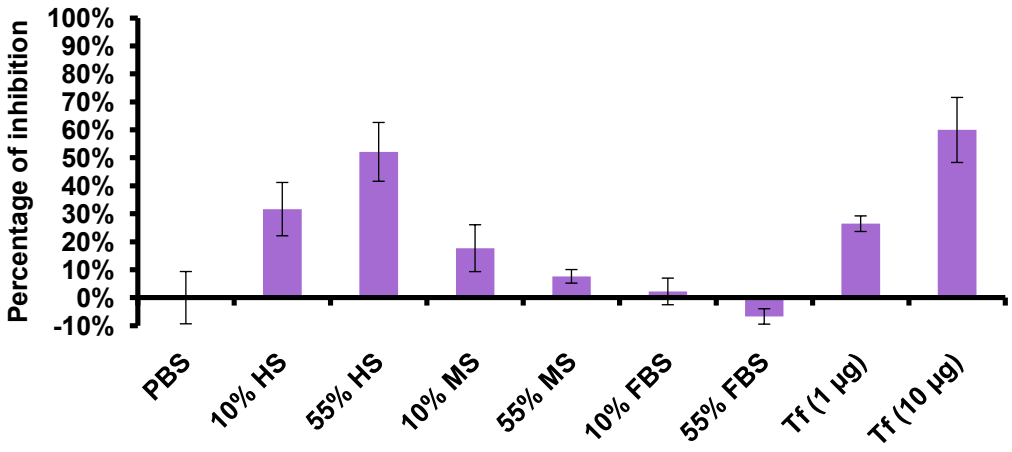

Figure 5.19: VLP*-Tf **binding assay on U2OS cells**
U2OS cells were subjected to VLP*-Tf particles with or without the presence of serum. The unbound VLPs were coated on plates and detected by ELISA assay. The data were normalized by calculation of the difference in absorbance values between VLPs with and without serum. Standard deviations were calculated from triplicates.

Further, we performed the flow cytometry study on U2OS cell. Being aware of the fact, that fluorescent day could substantially influence the interaction of VLPs with cells (see minor interaction of **VLP*** labeled with rhodamine in Fig 5.6. and high interaction of VLP* labeled with Alexa Fluor 488 in Fig. 5.12B), we compared binding of VLP* and VLP*-T.Red on U2OS cells. These particles were prepared (from the same stock) as negative controls to VLP*-Tf (chap. 4.2.4.3). VLP* and VLP*-T.Red particles were subjected to U2OS cells for 1 hour with or without the presence of free human transferrin (Tf+), 10% FBS or 55% FBS (Fig. 5.20). As could be seen from the graph (Fig. 5.20), the conjugation of Texas Red to VLPs labeled with AF488 completely changed their behavior and diminished the high (and probably unspecific) interaction of VLP* with cells. Interestingly, the addition of Texas Red dye with neutral charge led to masking of AF488 conjugated to VLP surface. Considering this finding, we used VLP*-T.Red as a negative control in the following experiments because VLPs labeled only with AF488 (VLP*) were partially aggregated (Fig. 5.16) and showed high unspecific interaction with U2OS cells (Fig, 5.20).

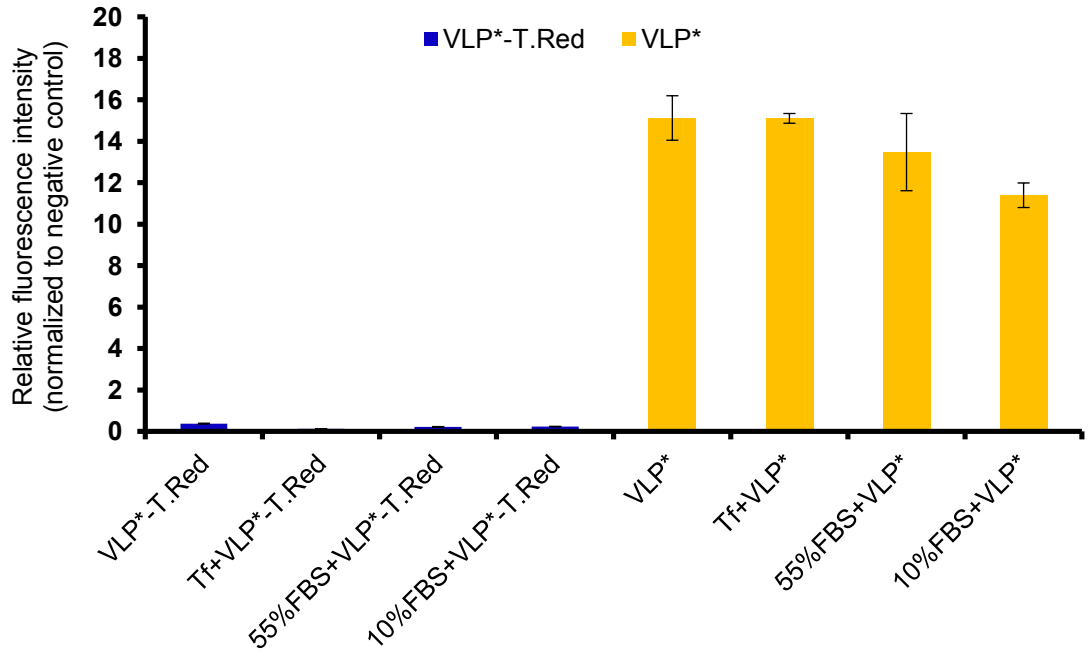

Figure 5.20: **Flow cytometry study of VLPs uptake by U2OS**
The cells were subjected to VLP*-T.Red and VLP* with or without the presence of fetal bovine serum (FBS) or free transferrin (Tf+). The data represent the median of AF488 fluorescence intensity normalized to autofluorescence of control cells. Standard deviations of both graphs were calculated from quadruplicates (two independent experiments in duplicates).

In the following test, we used two types of VLPs; VLP*-Tf and VLP*-T.Red. Both transferrin positive VLP*-Tf and negative VLP*-T.Red particles as well as labeled transferrin Tf-AF488 were subjected to U2OS cells for 1 hour with or without the presence of 10% or 55% FBS (Fig. 5.21). Incubation with free unmodified transferrin (Tf+) was used as an internal control. The acquired data were normalized to autofluorescence of control cells. The data showed that uptake of VLP*-Tf particles was not constrained by FBS, while Tf-AF488 internalization was about 25 % lower. The interaction of VLP*-T.Red particles with U2OS cells was negligible.

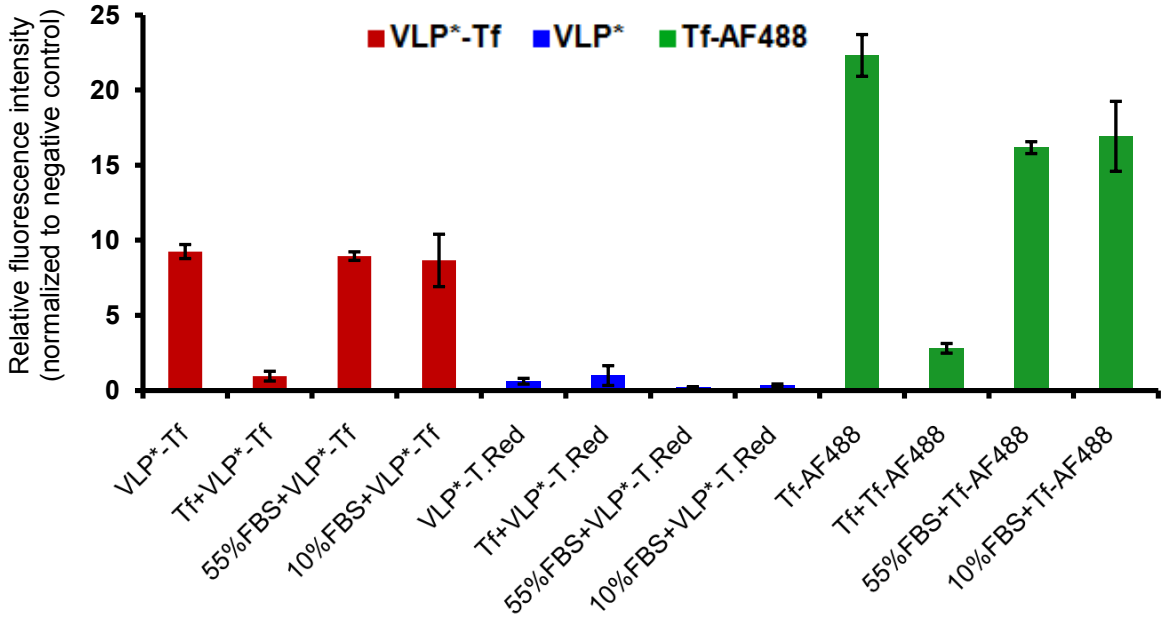

Figure 5.21: **Flow cytometry study of VLPs uptake by U2OS**
The cells were subjected to VLP*-Tf or VLP*-T.Red or Tf-AF488 with or without the presence of fetal bovine serum (FBS) or free transferrin (Tf+). The data represent the median of AF488 fluorescence intensity normalized to autofluorescence of control cells. Standard deviations of both graphs were calculated from quadruplicates (two independent experiments in duplicates).

The investigation of VLP*-Tf uptake by U2OS cells in the presence of human serum required the elimination of free transferrin from the solution. We tested the affinity methods with monoclonal antibody against human transferrin (AbαTf), such as immunoprecipitation with protein A coated magnetic beads and incubation on nitrocellulose membrane, however, both methods required huge amount of the antibody and did not remove the transferrin completely. Therefore, we implemented the titration assay of 10% HS and AbαTf. The goal was to find the optimal concentration of antibody that eliminates free transferrin from the serum. For the assay, U2OS cells were grown on ELISA plate and incubated for 1 hour either with VLP*-Tf particles only or with the combination of 10% HS and AbαTf. 10% HS was preincubated in RT with shaking (400 rpm) for 1 hour with either PBS or with diluted AbαTf (from 0.05 to 0.3 µg/µl). A gradual decrease of binding inhibition is visible from the acquired data (Fig. 5.22) until the antibody concentration reached 0.25 µg/µl. Higher concentration of AbαTf exceeded the concentration of serum Tf and free antibodies efficiently blocked the interaction of VLP*-Tf particles with TfR.

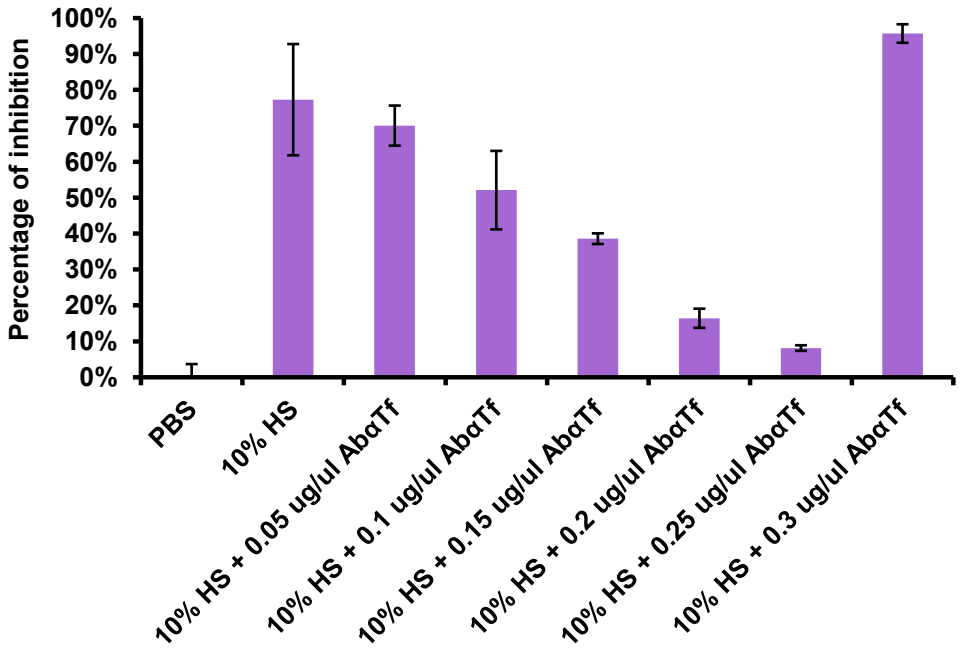

Figure 5.22: **Calibration of AbαTf concentration on U2OS cells**
The graph represents data from ELISA assay performed with U2OS cells. These cells were subjected to VLP*-Tf particles with or without the presence of 10% human serum. The serum was preincubated with various concentrations of antibody against Tf (from 0.05 to 0.3 µg/µl). The data were normalized by calculation of the difference in absorbance value between VLPs with serum and VLPs without serum (PBS; the positive control). Standard deviations were calculated from triplicates.

The optimal concentration of AbαTf (0.25 µg/µl) was further utilized in flow cytometry of U2OS with human serum (Fig. 5.23). Both transferrin positive VLP*-Tf and negative VLP*-T.Red particles or labeled transferrin Tf-AF488 were subjected to U2OS cells for 1 hour with or without the presence of 10% or 55% HS. In addition, 10% HS was either not preincubated or preincubated with 0.25 µg/µl AbαTf for 1 hour before mixing with VLP*-Tf solution. The obtained data were normalized to autofluorescence of control cells (Fig. 5.23). The results showed inhibition of VLP*-Tf binding in the presence of HS. However, the binding was restored by the preincubation with AbαTf. Similarly, the interaction of the positive control, Tf-AF488, was restricted by the presence of serum. The interaction of VLP*-T.Red particles with U2OS cells was very low, regardless of serum presence or absence.

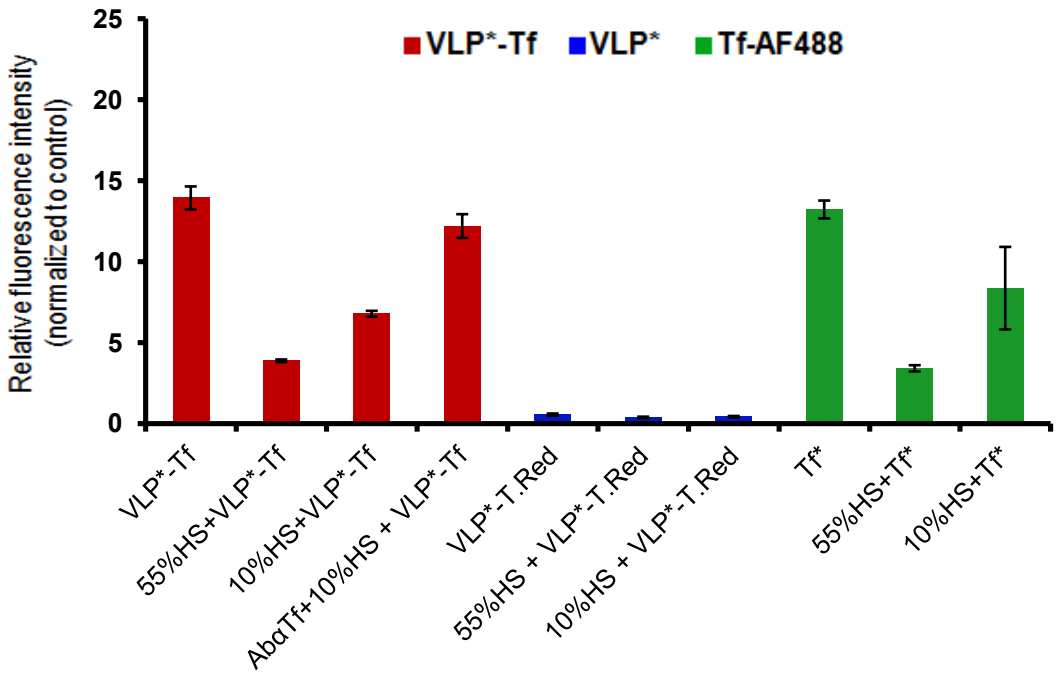

Figure 5.23: **Flow cytometry study of VLPs uptake by U2OS**
The cells were subjected to VLP*-Tf, VLP*-T.Red and Tf-AF488 without or with the presence of human serum (HS) or with the presence of serum preincubated with AbαTf.The data represent the median of AF488 fluorescence intensity normalized to autofluorescence of control cells. Standard deviations of both graphs were calculated from quadruplicates (two independent experiments in duplicates).

6. Discussion

Retargeting of MPyV VLPs to TfR

Our laboratory has studied mouse polyomavirus based VLPs, their properties (Forstová et al., 1995; Štokrová et al., 1999), cell trafficking (Mannova and Forstova, 2003; Richterová et al., 2001), immunogenic properties (Frič et al., 2008) and their genetic manipulations (Bouřa et al., 2005; Fraiberk et al., 2017) for years. The main goal of this thesis was to investigate the potential of chemical modifications of mouse polyomavirus VLPs with aim to develop novel nanoparticles retargeted to specific cells or tissues, carrying a chemically conjugated retargeting moiety on their surface, for their utilization in bioapplications such as the delivery of diagnostic and therapeutic compounds, gene therapy or immunotherapy. Similar types of modification were previously used for other types of viral particles such as bacteriophages (Chung et al., 2014; Rhee et al., 2012) or plant viruses (Bruckman and Steinmetz, 2014; Strable and Finn, 2009) and also for VLPs based on SV40 virus (Kitai et al., 2011). The first experiments using chemical conjugation of targeting molecules through oxime bond, did not lead to efficient retargeting of MPyV VLPs, even though we have tested various conditions and ligands (data not shown). After multiple testing, the problem was identified in the selected type of modification, as the negative control modified by nicotinic acid hydrazide had increased unspecific binding of MPyV VLPs. Thus, we selected a new type of chemical modification based on copper catalyzed azide/alkyne cycloaddition ("click" chemistry), well described for VLPs based on bacteriophages (Banerjee et al., 2010; Chung et al., 2014; Patel and Swartz, 2011; Pokorski et al., 2011).

Firstly we applied the "click" chemistry on the VLPs for installation of model targeting moiety, human transferrin (Tf). The obtained load of transferrin (labeled with AF488) on VLPs labeled with rhodamine was 35±2 Tf molecules/VLP, which provided approximately 24% coverage of VLP surface (**VLP*-Tf*** particles). The efficiency of conjugation was partially increased during the next preparation of these VLPs, achieving the load of 51±3 Tf molecules/VLP and ~35% coverage (VLP*-Tf particles). The higher efficacy might be connected with different modification of transferrin molecule, as this time, we used transferrin not labeled with AF488 dye. The coverage in both cases were similar to previously prepared constructs of VLPs bearing transferrin molecules (Banerjee et al., 2010; Huang et al., 2006; Yildiz et al., 2012).

For the subsequent test of **VLP*-Tf*** and VLP*-Tf interactions with transferrin receptor, we prepared also various types of control particles that were fluorescently labeled, however, did not bear transferrin molecules. Three types of control particles were

produced: VLPs labeled with rhodamine (**VLP***), VLPs labeled with AF488 (VLP*) and VLPs labeled with AF488 and Texas Red (VLP*-T.Red). Surprisingly, the interaction of these VLPs with a model human cancer cell line U2OS was greatly different. The interaction of VLPs labeled with rhodamine as well as T.Red was negligible, contrary to high unspecific binding of VLPs with AF488 (40 times higher than VLP*-T.Red). As the difference between VLP* and VLP*-T.Red lies only in the conjugation of T.Red, we suppose that the change in ability of interaction with cells is driven by the charge of conjugated dye as the overall charge is positive for rhodamine dye, neutral for T.Red and negative for AF488. Interestingly, the comparative study of interactions of water-soluble dyes (including 32 dyes) with lipid bilayer showed that the negatively charged AF488 does not bind to bilayer, whereas the zwitterionic dyes tetramethylrhodamine (TAMRA) and sulphorhodamine B (T.Red) bound lipid bilayer very efficiently (Hughes et al., 2014). However, in another comparative study, the authors revealed that there is a difference between interactions of a free or conjugated dye with cells. The cells treated with TAMRA dye conjugated to cell penetrating peptide (penetratin) exhibited a number of small fluorescent dots in the cytoplasm, whereas no interaction was visible for the native TAMRA dye (Birch et al., 2017). This is in contrast with the data obtained for this dye on a lipid bilayer (Hughes et al., 2014). All these data confirmed that not only charge but also many other factors influence the interaction of the dye and membrane, such as the chemical structure, conjugation of the dye, chemical and physical properties of the carrier and testing method. The effect of labeling on the nanoparticle behavior was not examined yet and thus, our findings are novel in this field. From our experiment, we can conclude that the labeling with AF488 (negative charge) is not suitable for uptake studies of MPyV VLPs. With respect to this finding, the uptake studies on U2OS cells were performed with **VLP*** and VLP*-T.Red particles, together with VLP*-Tf* and VLP*-Tf particles. The data from flow cytometry and confocal microscopy showed substantial increase in uptake of VLPs with transferrin. The saturation of TfR by incubation with free Tf led to complete block of the interaction, indicating the selective binding of these particles through the TfR. The control particles without Tf conjugations retained their ability to bind cells in VP1-specific manner and the interaction was not influenced by preincubation with free Tf. In summary, the coverage of VLP surface by Tf molecules sterically blocked the interaction of VP1 protein with its natural receptor. The similar data were obtained also with CCRF-CEM lymphoblastoid human cancer cell line, whereas the interaction with human endothelial non-cancerous cell line HUVEC was negligible, confirming a high affinity and selectivity of VLPs with transferrin to cancer cells overexpressing TfR.

Furthermore, we analyzed whether the conjugation of transferrin to the VLP surface could influence the way of uptake of the VLPs by human cancer cells. The natural endocytic pathway of MPyV VLPs encompasses membrane raft derived smooth endocytic vesicles (Richterová et al., 2001). On the other hand, transferrin molecules are internalized through clathrin-coated pits (Dautry-Varsat, 1986). It was previously published that polyomavirus meets free transferrin in perinuclear space in recycling endosomes not sooner than 3 hour post infection (Liebl et al., 2006; Mannova and Forstova, 2003), while MPyV VLPs with conjugated transferrin are fastly internalized and transported, being mostly detected in the perinuclear area, already 1 hour post infection (Zackova Suchanova et al., 2017). Therefore, we decided to treat the cells with chlorpromazine, a clathrin-specific inhibitor that translocates clathrin from the cell surface to intracellular endosomes (Dutta and Donaldson, 2012) and does not influence the entry of mouse polyomavirus (Gilbert and Benjamin, 2000). The protocol published for studying the role of clathrin in endocytosis of vesicular stomatitis virus was adjusted and applied to human epithelial cancer cells HeLa (Sun et al., 2005). HeLa cells that were utilized in our experiment were much more sensitive to concentration of chlorpromazine. In our hands, HeLa cells died after treatment with chlorpromazine concentrations higher than 30 μg/ml. However, this concentration was sufficient for blocking of clathrin endocytic pathway as both VLP*-Tf and Tf* proteins were not internalized. VLP* without installed transferrin molecules bound to and enter cells irrespectively to chlorpromazine presence, confirming the retargeting of VLP*-Tf particles from their natural endocytic pathway comprising smooth, often caveolin-rich vesicles to transferrin specific pathway through clathrin-coated pits.

In conclusion, the polyomaviral VLPs could be retargeted to cancer cells by chemical modification leading to conjugation of Tf molecules onto the VLP surface. The surface architecture of VLP modification encompassing surface exposed lysines and ligation approach utilizing “click” chemistry was firstly used for VLPs derived from a representative of *Polyomaviridae* family. The only chemically modified VLPs from this family were SV40 VLPs; however, these VLPs required previous genetic modification to incorporate new amino acid into VP1 sequence (Kitai et al., 2011). The inserted cysteines served for conjugation of epidermal growth factor receptor, so the conjugation molecule and strategy was different from ours. The conjugation of Tf to polyomavirus based VLPs now expand the family of VLPs that were designed in similar way to interact specifically with numerous cancer cell lines. These include VLPs based on brome mosaic virus (Yildiz et al., 2012), various bacteriophages (Banerjee et al., 2010; Galaway and Stockley, 2013; Huang et al., 2006; Khalaj-Kondori et al., 2016, 2011; Wu et al., 2005) and other member

of the group of small non-enveloped DNA viruses, adenovirus (Campos, 2004; Kreppel et al., 2005; Oh et al., 2005). In our hands the interaction of transferrin-bearing MPyV VLPs with TfR overexpressed on cancer cells was selective and efficient. Moreover, the installation of Tf molecules clearly diminished the undesirable interaction of VLPs with their natural receptor containing the ubiquitously distributed sialic acid residue that broadens the cell and tissue tropism of these VLPs (Krauzewicz et al., 2000). Based on the cellular uptake studies, we suggest that Tf molecules bound to the VLP surface masks the VP1-specific interactions responsible for recognition of sialic acid. The strong avidity and binding selectivity can lead to efficient targeting of transferrin coated VLPs *in vivo*.

Influence of serum proteins on targeting of MPyV VLPs

During the recent years, it was found that the biological identity of targeted nanoparticles could be changed in the blood serum by formation of a protein corona. The corona covers the nanoparticle surface, masks the targeting ligands and can cause mistargeting. Salvati et al., 2013 published a comprehensive study about the influence of serum proteins on silica nanoparticles modified with transferrin molecules. They found out that as the concentration of serum increases, the interaction of Tf modified nanoparticles (NPs) with TfR decreases. The similar results were obtained also for polystyrene beads decorated with transferrin (Xiao et al., 2018). Moreover, this group evaluated the influence of the size of targeting moieties on the formation of protein corona around NPs. Two different ligands, a bulky transferrin protein and a small RGD peptide, were applied in this study. The data revealed a more significant decrease of cellular uptake of NPs with RGD, indicating the small size of RGD peptide to be more prone to formation of protein corona. According to these findings, we decided to investigate the targeting abilities of VLP*-Tf particles in the presence of serum proteins (chap. 5.3).

To study the interactions of serum treated VLP*-Tf particles with transferrin receptor (TfR) in detail, we utilized the ELISA assay in two different set ups; (i) with adsorbed recombinant TfR, (ii) with adherent osteosarcoma cells U2OS allowing the investigation of influence of serum proteins on VLP*-Tf/TfR interaction in context of cells. However, serum contains a high concentration of free transferrin that might inhibit the interaction of VLP*-Tf and TfR. We have chosen three species; human (HS), mouse (MS) and fetal bovine serum (FBS) to be examined in this assay. Human serum highly inhibited the interaction of VLP*-Tf particles. It was published previously that HS contains a high amount of free human transferrin that interferes with the binding of engineered Tf

molecules, whose affinity to TfR is affected by various modifications (Leverence et al., 2010). Partial inhibition was achieved also with mouse serum that also contains Tf molecules. The sequence analysis of mouse and human transferrin amino acid composition revealed 73% identity (Clustal O, version 1.2.4) and also their molecular weight is similar (Welch, 1990). Nevertheless, the interaction of human Tf with human TfR is affected by the amino acid composition in the N2 subdomain of Tf (positions 142-145, PRKP sequence) and according to sequence alignment of Tf from different species, it could be predicted, whether they have the ability to interact with human TfR (Wally et al., 2006). Mouse Tf has one substitution in this sequence; lysine is exchanged by serine that belongs also to polar amino acids but with neutral charge. This could be the reason of decreased affinity of mouse Tf to human TfR. Otherwise, the evolutionary branch for mouse Tf is the same as for rabbit Tf (Welch, 1990) that was proved to bind well to human TfR (Cheng et al., 2004). Bovine Tf has 69% sequence identity with human Tf. However, except of the first proline, the binding important sequence PRKP is different and therefore bovine Tf does not interfere with binding to human TfR (Wally et al., 2006). Nevertheless, the presence of transferrin might not be the only limiting factor of NP interaction, as the relative proportion of protein composition of sera differs among mammalian species (Zeitlinger et al., 2011). Based on this finding and achieved data, we focused on the influence of human and bovine serum as they are the most divergent among the tested species.

Firstly, interaction of VLP*-Tf particles with or without the presence of 10% or 55% FBS were analyzed by flow cytometry using U2OS cells. Free Tf was used as an internal control of efficient inhibition. The acquired data revealed that binding of VLP*-Tf particles is not constrained by FBS, while interaction of positive control, Tf protein labeled by AF488, was decreased in 25 %. The non-specific binding of negative control particles VLP*-T.Red to U2OS cells was negligible, irrespectively to presence of serum. Correspondingly, the confocal microscopy study on HeLa cells treated with chlorpromazine in the presence of 10% FBS confirmed that bovine serum does not influence the binding of VLP*-Tf particles and that these VLPs retained their specificity of interaction with TfR and were internalized by clathrin-mediated endocytic pathway.

Secondly, the influence of human serum on targeting of VLP*-Tf particles was examined. However, before investigation of influence of HS proteins on VLP*-Tf uptake by U2OS.cells, the elimination of free Tf from the serum was necessary. The implemented titration assay with 10% HS and monoclonal antibody against human transferrin (AbαTf)

revealed the optimal concentration of AbαTf for sterical blockade of free Tf together with no effect on interaction of VLP*-Tf and TfR. The same assay was conducted also with high concentrated human serum (55%). However, the molar ratio of serum Tf exceeded the maximal usable concentration of AbαTf (data not shown). The antibody treated human serum was used in flow cytometry study of VLP interactions with U2OS cells. The results showed a little influence of human serum pretreated with AbαTf on VLP*-Tf interaction with U2OS cells, contrary to serum without AbαTf, that caused a distinct inhibition. Similarly, the restriction of Tf-AF488 uptake in the presence of HS was visible. VLP*-T.Red particles did not interact with U2OS cells. These findings are consistent with our hypothesis that inhibition of VLP*-Tf and TfR interaction is mediated exclusively by the presence of free transferrin in human serum, without the influence of protein corona formation. The resistance to interaction of proteins from biological fluids is a crucial feature for targeted nanoparticle delivery. Masking of particle surface by PEG linkers employed in some studies (Bao et al., 2013; Harvie et al., 2000; Mishra, 2004) does not seem to be the optimal way of modification and could have a detrimental effect on nanoparticle targeting (reviewed in Moghimi and Szebeni, 2003; Verhoef and Anchordoquy, 2013). The requirement of new approaches to stealth the NP surface is not necessary in case of polyomaviral VLPs that naturally eliminated the association with serum proteins. In conclusion, polyomaviral VLPs grafting the targeting molecule involve the simple biorecognition of corresponding receptor and have the capacity to discriminate the target even in the biological milieu.

The formation of protein corona around the nanoparticle surface was studied also on diverse types of non-targeted nanoparticles, which represented a miscellaneous rate of protein association. The most abundant protein corona was achieved by hard matter nanoparticles, such as silica NPs (Ghavami et al., 2012), gold NPs (Piella et al., 2017), and magnetic NPs (Yallapu et al., 2015). Lower interaction was observed for synthetic nanoparticles comprising copolymer NPs (Cedervall et al., 2007), chitosan NPs (Varnamkhasti et al., 2015) and polystyrene NPs (Ghavami et al., 2012; Lundqvist et al., 2008). The lowest association with serum proteins accomplished virus-like particles based on Tobacco Mosaic Virus (TMV) (Pitek et al., 2018, 2016). It was found that TMV VLPs form a hard protein corona around their surface, similarly to silica nanoparticles, although the composition is different and the quantity is 6-fold lower (Pitek et al., 2016). Nevertheless, these VLPs were derived from plant viruses and therefore their behavior in biological environment could be different from mammalian viruses that naturally evolved

to eliminate the influence of protein corona. To verify this hypothesis we decided to investigate the behavior of unmodified polyomaviral VLPs in the presence of serum proteins (chap. 5.3).

We implemented the comparative study of MPyV VLPs and commercially produced polystyrene nanoparticles. Both particles were incubated in 55% HS and consecutively purified by dialysis and centrifugation against 20% sucrose cushion. The analysis of obtained fractions revealed that polyomaviral VLPs; contrary to polystyrene nanoparticles, do not interact with proteins of human serum. To further verify the ability of polyomaviral VLPs to eliminate the formation of protein corona, we utilized 10% and 55% serum from various species. Two different cell lines, mouse fibroblasts 3T6 and human osteosarcoma U2OS were treated with MPyV VLPs with or without the presence of serum. The inhibition of VLP and cell interaction was very low in all cases, reaching the highest inhibition in 55% HS: 6.4% for 3T6 and 9.1% for U2OS, respectively. The low inhibition in a variety of serum proteins confirmed that polyomaviral VLPs are superior to other types of nanoparticles and could potentially serve as a universal tool in animal and human bioapplications.

In conclusion, we demonstrated that targeted MPyV VLPs are not influenced by the formation of protein corona on their surface and that this feature in not granted by the type of conjugated molecule but it is a natural characteristic of MPyV VLPs. We thus suppose that MPyV VLPs with their unique targeting capabilities can become a modular and efficient platform for drug delivery devices.

Retargeting of MPyV VLPs to GCPII

Following the retargeting of MPyV VLPs to a broadly distributed cancer marker, TfR, we decided to investigate the potential of polyomaviral VLPs for targeting of prostate cancer cells through a type-specific cancer marker. The molecule selected for retargeting was inhibitor of glutamate carboxypeptidase II (iGCPII), that is overexpressed on prostate cancer cells (Tykvart et al., 2014). The strategy of targeting by specific inhibitor was previously proved successful for other types of nanoparticles (Banerjee et al., 2017; Chen et al., 2016; Sanna et al., 2011; Xu et al., 2017). This aim was closely related to modification of MPyV VLPs by transferrin molecule; however, this time, we did not conjugate a bulky globular protein but a small chemical compound. Targeting with small molecules is usually a more challenging approach that requires optimization and is novel for polyomavirus based VLPs.

For installation of inhibitor to VLP surface, we used "click" chemistry as it was proved to be successful method for MPyV VLPs modification. To the prepared retargeting VLP*-iGCPII particles, control particles, VLP*, labeled with AF488 and particles with conjugated 13 polyethylene glycol linker ended with carboxyl residue (VLP*-PEG) were prepared. The PEG linker was used for masking of negatively charged AF488 dye. Similarly to conjugation of T.Red, this modification avoided unspecific interactions, aggregation and VP1-specific interaction with widely distributed sialic acid residues. The characterization of prepared VLPs revealed the rough load of iGCPII molecules on VLP*-iGCPII to 540 and 1,080 PEG molecules on VLP*-PEG. The MALDI measurement also confirmed the covalent attachment of these molecules to the VLP surface.

The interaction between VLP*-iGCPII and GCPII was firstly analyzed *in vitro* by surface plasmon resonance (SPR). The data revealed a very efficient binding of VLP*-iGCPII to GCPII, indicating a strong interaction that is mediated by creation of multiple bonds between ligand and layer (avidity). Once we have verified the interaction of modified particles with GCPII, we focused on binding specificity to GCPII in context of cancer cells. For cellular uptake studies, we utilized glioblastoma cell line U251 MG with switchable expression of GCPII. Therefore, we had only one type of cells and the study could be realized in a very consistent way. VLP*-iGCPII were effectively uptaken by U251 MG cells with GCPII expression (U251 MG^+) while turning off the GCPII expression (U251 MG^-) diminished the interaction. In contrast, VLP* had very strong interaction to U251 MG irrespectively to GCPII presence. The intensive VLP* binding to glioblastoma cells represents probably not only the unwanted unspecific binding but also specific interaction as these cells abundantly express complex gangliosides (Schnaar et al., 2014; Yates et al., 1988), the natural receptors of MPyV. The negligible interaction was obtained with VLP*-PEG particles proving the successful prevention of VP1 specific interaction by PEG conjugation. The confocal microscopy images confirmed that VLP*-iGCPII particles were highly internalized into U251 MG^+ but, no particles binding and internalization in U251 MG^- cells was observed. Control VLP* interacted with both cell types.

In conclusion, we proved the possibility of retargeting of MPyV VLPs to cancer cells by conjugation of small molecule to the VLP surface, which was a part of our comprehensive comparative study of diverse range of inhibitor-bearing nanoparticles to investigate the versatility and limitations of GCPII targeting (Neburkova et al., 2018).

Virus-like particles based either on mouse polyomavirus or bacteriophage Qβ, polymer-coated nanodiamonds and polymeric nanoparticles coated with GCPII inhibitor were tested for their ability to interact with GCPII. Utilization of one cell type model for testing of NP interaction enabled the comparison of targeting in a very consistent way. The obtained data proved that all NPs with installed inhibitor were able to bind GCPII, irrespective to nanoparticle size, structure, polydispersity, type of conjugation chemistry and load of inhibitor. However, any nanomaterial has advantages and disadvantages. If we compare the designed NPs with focus on MPyV VLPs, we should definitely highlight their ability to load various cargos by simple encapsidation and biodegradability that lowers the risk of tissue persistence compared to some synthetic materials. On the other hand, the efficiency of cellular uptake was the lowest from all tested NPs and the surface modification was necessary to hide the VP1 broad tropism. A high load of short PEG linker lowered the VP1-specific interaction of MPyV VLPs and conjugation of iGCPII to the end of this linker retargeted VLPs to prostate specific marker, GCPII.

In general, the specificity of interaction is not the only limitation of targeted therapeutic nanoparticles; it is also either the unspecificity or unwanted side specificity of NPs. In this regard, polyomaviral VLPs need to be modified by the way which prevents the VP1-specific binding. Another possibility is the genetic modification of VP1 surface loops responsible for most of VP1 interactions. Such a modification, eliminating VP1 interaction with sialic acid (without any effect on assembly and stability of VLPs), was already realized in our laboratory.

7. Summary

Goal 1. Preparation of VLPs with conjugated transferrin and analysis of their efficiency to interact with cancer cells.

a) We have produced high amount of polyomaviral VLPs in insect cells Sf9 with utilization of baculovirus expression system. The stability and purity of these particles were verified by electron microscopy.

b) The transferrin protein was successfully conjugated to the surface of VLPs by "click" chemistry.

c) Characterization of prepared particles was done by multiple methods. Firstly, the stability was verified by transmission electron microscopy and DLS measurement. Secondly, the efficacy of transferrin conjugation was counted from SDS-PAGE followed with densitometry analysis.

d) The binding efficiency of modified VLPs to cancer cells was analyzed by confocal microscopy and flow cytometry. Both methods proved that conjugation of transferrin molecule retargeted polyomaviral VLPs to cancer cells overexpressing transferrin receptor (U2OS and CCRF-CEM). Moreover, the conjugation also protected modified VLPs from the recognition of their natural receptor containing sialic acid residues.

Goal 2. Preparation of VLPs with conjugated inhibitor of GCPII and analysis of their efficiency to interact with cancer cells.

a) Unmodified VLPs were produced by baculovirus expression system. The stability and purity of these particles were verified by TEM.

b) The inhibitor of GCPII was efficiently conjugated to the surface of VLPs by "click" chemistry.

c) Various methods were used for characterization of modified VLPs. Stability and homogeneity were verified by TEM and DLS measurement, the efficacy of iGCPII conjugation was investigated by SPR measurement and counted according to the data obtained from MALDI analysis.

d) Confocal microscopy and flow cytometry proved that conjugation of iGCPII molecule retargeted polyomaviral VLPs to cells overexpressing GCPII (U251 MG^{+}).

Moreover, the conjugation protected modified VLPs from VP1-specific binding to sialic acid residues.

Goal 3. Characterization of polyomavirus VLPs in context of serum proteins.

a) MPyV VLPs were examined in the presence of serum and the interaction with serum proteins was studied. The comparative study with polystyrene nanoparticles showed that MPyV VLPs, contrary to polystyrene NPs, associate with a minimum of serum proteins and these proteins has no influence on VLP/cell interaction.

b) New batch of VLPs with conjugated transferrin was prepared. VLP*-Tf particles were further incubated with 55% and 10% serum from different species and their interaction with TfR in the presence of serum was characterized. *In vitro* binding assay proved the inhibition effect of transferrin, abundantly present protein in serum, on VLP binding.

c) The analysis of cellular uptake of VLP*-Tf particles with serum proteins by flow cytometry and ELISA binding assay revealed the resistance of these particles to protein corona driven mistargeting.

8. Involvement in the publications

List of publications enclosed in this doctoral thesis:

This thesis is based upon two first author publications and one manuscript:

1) Zackova Suchanova J, Neburkova J, Spanielova H, Forstova J, Cigler P. **Retargeting Polyomavirus-Like Particles to Cancer Cells by Chemical Modification of Capsid Surface.** *Bioconjugate Chemistry* 28(2):307–13.

    - First author publication
    - Contribution of the author: 75%
    - I was significantly involved in conceiving the experiments that were predominantly done by myself. I also significantly contributed to data analysis and manuscript preparation.

2) Neburkova J[#], Sedlak F[#], Zackova Suchanova J[#], Kostka L, Sacha P, Subr V, Etrych T, Simon P, Barinkova J, Krystufek R, Spanielova H, Forstova J, Konvalinka J, Cigler P **Inhibitor-GCPII interaction: selective and robust system for targeting cancer cells with structurally diverse nanoparticles.** *Molecular Pharmaceutics* 2018, doi:10.1021/acs.molpharmaceut.7b00889

    - First author publication (shared)
    - Contribution of the author: 30%
    - I was involved in conceiving the experiments. I prepared all types of MPyV VLPs and assisted with characterization of all prepared nanoparticles together with measurement of their cellular uptake. I also contributed to data analysis and manuscript preparation.

3) **Targeting of Polyomavirus Based Nanoparticles is not Influenced by Formation of Protein Corona.**

    - Manuscript in preparation
    - First author publication
    - Contribution of the author: 90%

I hereby confirm that the author of this thesis, Jiřina Žáčková Suchanová, have substantially contributed to the publications listed above. In case of her first-author publication (unshared), she did the majority of experimental work and contributed to the manuscript preparation.

RNDr. Hana Španielová, Ph.D.

……..

9. List of References

Abbing, A., Blaschke, U.K., Grein, S., Kretschmar, M., Stark, C.M.B., Thies, M.J.W., Walter, J., Weigand, M., Woith, D.C., Hess, J., Reiser, C.O.A., 2004. Efficient intracellular delivery of a protein and a low molecular weight substance via recombinant polyomavirus-like particles. J. Biol. Chem. 279, 27410–27421. https://doi.org/10.1074/jbc.M313612200

Armstrong, J.K., Wenby, R.B., Meiselman, H.J., Fisher, T.C., 2004. The Hydrodynamic Radii of Macromolecules and Their Effect on Red Blood Cell Aggregation. Biophys. J. 87, 4259–4270. https://doi.org/10.1529/biophysj.104.047746

Banerjee, D., Liu, A.P., Voss, N.R., Schmid, S.L., Finn, M.G., 2010. Multivalent Display and Receptor-Mediated Endocytosis of Transferrin on Virus-Like Particles. ChemBioChem 11, 1273–1279. https://doi.org/10.1002/cbic.201000125

Banerjee, S.R., Foss, C.A., Horhota, A., Pullambhatla, M., McDonnell, K., Zale, S., Pomper, M.G., 2017. 111In- and IRDye800CW-Labeled PLA–PEG Nanoparticle for Imaging Prostate-Specific Membrane Antigen-Expressing Tissues. Biomacromolecules 18, 201–209. https://doi.org/10.1021/acs.biomac.6b01485

Bao, Y., Jin, Y., Chivukula, P., Zhang, J., Liu, Y., Liu, J., Clamme, J.-P., Mahato, R.I., Ng, D., Ying, W., Wang, Y., Yu, L., 2013. Effect of PEGylation on biodistribution and gene silencing of siRNA/lipid nanoparticle complexes. Pharm. Res. 30, 342–351. https://doi.org/10.1007/s11095-012-0874-6

Birch, D., Christensen, M.V., Staerk, D., Franzyk, H., Nielsen, H.M., 2017. Fluorophore labeling of a cell-penetrating peptide induces differential effects on its cellular distribution and affects cell viability. Biochim. Biophys. Acta BBA - Biomembr. 1859, 2483–2494. https://doi.org/10.1016/j.bbamem.2017.09.015

Blundell, E.L.C.J., Healey, M.J., Holton, E., Sivakumaran, M., Manstana, S., Platt, M., 2016. Characterisation of the protein corona using tunable resistive pulse sensing: determining the change and distribution of a particle's surface charge. Anal. Bioanal. Chem. 408, 5757–5768. https://doi.org/10.1007/s00216-016-9678-6

Bolen, J.B., Anders, D.G., Trempy, J., Consigli, R.A., 1981. Differences in the subpopulations of the structural proteins of polyoma virions and capsids: biological functions of the multiple VP1 species. J. Virol. 37, 80–91.

Bostwick, D.G., Iczkowski, K.A., Amin, M.B., Discigil, G., Osborne, B., 1998. Malignant lymphoma involving the prostate: report of 62 cases. Cancer 83, 732–738.

Bouřa, E., Liebl, D., Špíšek, R., Frič, J., Marek, M., Štokrová, J., Holáň, V., Forstová, J., 2005. Polyomavirus EGFP-pseudocapsids: Analysis of model particles for introduction of proteins and peptides into mammalian cells. FEBS Lett. 579, 6549–6558. https://doi.org/10.1016/j.febslet.2005.10.062

Bruckman, M.A., Steinmetz, N.F., 2014. Chemical Modification of the Inner and Outer Surfaces of Tobacco Mosaic Virus (TMV). Methods Mol. Biol. Clifton NJ 1108, 173–185. https://doi.org/10.1007/978-1-62703-751-8_13

Buck, C.B., Van Doorslaer, K., Peretti, A., Geoghegan, E.M., Tisza, M.J., An, P., Katz, J.P., Pipas, J.M., McBride, A.A., Camus, A.C., McDermott, A.J., Dill, J.A., Delwart, E., Ng, T.F.F., Farkas, K., Austin, C., Kraberger, S., Davison, W., Pastrana, D.V., Varsani, A., 2016. The Ancient Evolutionary History of Polyomaviruses. PLoS Pathog. 12. https://doi.org/10.1371/journal.ppat.1005574

Campos, S., 2004. Avidin-based targeting and purification of a protein IX-modified, metabolically biotinylated adenoviral vector. Mol. Ther. 9, 942–954. https://doi.org/10.1016/j.ymthe.2004.03.006

Carbone, M., Ascione, G., Chichiarelli, S., Garcia, M.-I., Eufemi, M., Amati, P., 2004. Chromosome-protein interactions in polyomavirus virions. J. Virol. 78, 513–519.

Caruso, M., Belloni, L., Sthandier, O., Amati, P., Garcia, M.-I., 2003. α4β1 Integrin Acts as a Cell Receptor for Murine Polyomavirus at the Postattachment Level. J. Virol. 77, 3913–3921. https://doi.org/10.1128/JVI.77.7.3913-3921.2003

Casals, E., Pfaller, T., Duschl, A., Oostingh, G.J., Puntes, V., 2010. Time evolution of the nanoparticle protein corona. ACS Nano 4, 3623–3632. https://doi.org/10.1021/nn901372t

Catrice, E.V.B., Sainsbury, F., 2015. Assembly and Purification of Polyomavirus-Like Particles from Plants. Mol. Biotechnol. 57, 904–913. https://doi.org/10.1007/s12033-015-9879-9

Cedervall, T., Lynch, I., Foy, M., Berggård, T., Donnelly, S.C., Cagney, G., Linse, S., Dawson, K.A., 2007. Detailed Identification of Plasma Proteins Adsorbed on Copolymer Nanoparticles. Angew. Chem. Int. Ed. 46, 5754–5756. https://doi.org/10.1002/anie.200700465

Chang, D., Cai, X., Consigli, R.A., 1993. Characterization of the DNA binding properties of polyomavirus capsid protein. J. Virol. 67, 6327–6331.

Chao, C.-N., Huang, Y.-L., Lin, M.-C., Fang, C.-Y., Shen, C.-H., Chen, P.-L., Wang, M., Chang, D., Tseng, C.-E., 2015. Inhibition of human diffuse large B-cell lymphoma growth by JC polyomavirus-like particles delivering a suicide gene. J. Transl. Med. 13. https://doi.org/10.1186/s12967-015-0389-0

Chao, C.-N., Yang, Y.-H., Wu, M.-S., Chou, M.-C., Fang, C.-Y., Lin, M.-C., Tai, C.-K., Shen, C.-H., Chen, P.-L., Chang, D., Wang, M., 2018. Gene therapy for human glioblastoma using neurotropic JC virus-like particles as a gene delivery vector. Sci. Rep. 8. https://doi.org/10.1038/s41598-018-19825-w

Chen, L.S., Wang, M., Ou, W.C., Fung, C.Y., Chen, P.L., Chang, C.F., Huang, W.S., Wang, J.Y., Lin, P.Y., Chang, D., 2010. Efficient gene transfer using the human JC virus-like particle that inhibits human colon adenocarcinoma growth in a nude mouse model. Gene Ther. 17, 1033–1041.

Chen, X.S., Garcea, R.L., Goldberg, I., Casini, G., Harrison, S.C., 2000. Structure of small virus-like particles assembled from the L1 protein of human papillomavirus 16. Mol. Cell 5, 557–567.

Chen, X.S., Stehle, T., Harrison, S.C., 1998. Interaction of polyomavirus internal protein VP2 with the major capsid protein VP1 and implications for participation of VP2 in viral entry. EMBO J. 17, 3233–3240.

Chen, Z., Penet, M.-F., Krishnamachary, B., Banerjee, S.R., Pomper, M.G., Bhujwalla, Z.M., 2016. PSMA-specific theranostic nanoplex for combination of TRAIL gene and 5-FC prodrug therapy of prostate cancer. Biomaterials 80, 57–67. https://doi.org/10.1016/j.biomaterials.2015.11.048

Cheng, Y., Zak, O., Aisen, P., Harrison, S.C., Walz, T., 2004. Structure of the Human Transferrin Receptor-Transferrin Complex. Cell 116, 565–576. https://doi.org/10.1016/S0092-8674(04)00130-8

Chithrani, B.D., Ghazani, A.A., Chan, W.C.W., 2006. Determining the Size and Shape Dependence of Gold Nanoparticle Uptake into Mammalian Cells. Nano Lett. 6, 662–668. https://doi.org/10.1021/nl052396o

Choi, C.H.J., Alabi, C.A., Webster, P., Davis, M.E., 2010. Mechanism of active targeting in solid tumors with transferrin-containing gold nanoparticles. Proc. Natl. Acad. Sci. U. S. A. 107, 1235–1240. https://doi.org/10.1073/pnas.0914140107

Chou, M.-I., Hsieh, Y.-F., Wang, M., Chang, J.T., Chang, D., Zouali, M., Tsay, G.J., 2010. In vitro and in vivo targeted delivery of IL-10 interfering RNA by JC virus-like particles. J. Biomed. Sci. 17, 51. https://doi.org/10.1186/1423-0127-17-51

Chung, W.-J., Lee, D.-Y., Yoo, S.Y., 2014. Chemical modulation of M13 bacteriophage and its functional opportunities for nanomedicine. Int. J. Nanomedicine 9, 5825–5836. https://doi.org/10.2147/IJN.S73883

Dai Qin, Walkey Carl, Chan Warren C. W., 2014. Polyethylene Glycol Backfilling Mitigates the Negative Impact of the Protein Corona on Nanoparticle Cell Targeting. Angew. Chem. Int. Ed. 53, 5093–5096. https://doi.org/10.1002/anie.201309464

Dalianis, T., Hirsch, H.H., 2013. Human polyomaviruses in disease and cancer. Virology 437, 63–72. https://doi.org/10.1016/j.virol.2012.12.015

Daniels, T.R., Delgado, T., Rodriguez, J.A., Helguera, G., Penichet, M.L., 2006. The transferrin receptor part I: Biology and targeting with cytotoxic antibodies for the treatment of cancer. Clin. Immunol. Orlando Fla 121, 144–158. https://doi.org/10.1016/j.clim.2006.06.010

Das Gupta, A., Shah, V.I., 1990. Correlation of transferrin receptor expression with histologic grade and immunophenotype in chronic lymphocytic leukemia and non-Hodgkin's lymphoma. Hematol. Pathol. 4, 37–41.

Dashti, N.H., Abidin, R.S., Sainsbury, F., 2018. Programmable In Vitro Coencapsidation of Guest Proteins for Intracellular Delivery by Virus-like Particles. ACS Nano 12, 4615–4623. https://doi.org/10.1021/acsnano.8b01059

Dautry-Varsat, A., 1986. Receptor-mediated endocytosis: the intracellular journey of transferrin and its receptor. Biochimie 68, 375–381.

Deng, Y.-N., Zeng, J.-Y., Su, H., Qu, Q.-M., 2015. Recombinant VLP-Z of JC Polyomavirus: A Novel Vector for Targeting Gene Delivery. Intervirology 58, 363–368. https://doi.org/10.1159/000443832

Dilworth, S.M., 1990. Cell alterations induced by the large T-antigens of SV40 and polyoma virus. Semin. Cancer Biol. 1, 407–414.

Docter, D., Westmeier, D., Markiewicz, M., Stolte, S., Knauer, S.K., Stauber, R.H., 2015. The nanoparticle biomolecule corona: lessons learned – challenge accepted? Chem. Soc. Rev. 44, 6094–6121. https://doi.org/10.1039/C5CS00217F

Dutta, D., Donaldson, J.G., 2012. Search for inhibitors of endocytosis. Cell. Logist. 2, 203–208. https://doi.org/10.4161/cl.23967

Enomoto, T., Kawano, M., Fukuda, H., Sawada, W., Inoue, T., Haw, K.C., Kita, Y., Sakamoto, S., Yamaguchi, Y., Imai, T., Hatakeyama, M., Saito, S., Sandhu, A., Matsui, M., Aoki, I., Handa, H., 2013. Viral protein-coating of magnetic nanoparticles using simian virus 40 VP1. J. Biotechnol. 167, 8–15. https://doi.org/10.1016/j.jbiotec.2013.06.005

Enomoto, T., Kukimoto, I., Kawano, M., Yamaguchi, Y., Berk, A.J., Handa, H., 2011. In vitro reconstitution of SV40 particles that are composed of VP1/2/3 capsid proteins and nucleosomal DNA and direct efficient gene transfer. Virology 420, 1–9. https://doi.org/10.1016/j.virol.2011.08.014

Eriksson, M., Andreasson, K., Weidmann, J., Lundberg, K., Tegerstedt, K., Dalianis, T., Ramqvist, T., 2011. Murine Polyomavirus Virus-Like Particles Carrying Full-Length Human PSA Protect BALB/c Mice from Outgrowth of a PSA Expressing Tumor. PLoS ONE 6, e23828. https://doi.org/10.1371/journal.pone.0023828

Fields, B.N., Knipe, D.M., Howley, P.M., 2007. Fields virology. Wolters Kluwer Health/Lippincott Williams & Wilkins, Philadelphia.

Fluck, M.M., Schaffhausen, B.S., 2009. Lessons in signaling and tumorigenesis from polyomavirus middle T antigen. Microbiol. Mol. Biol. Rev. MMBR 73, 542–563, Table of Contents. https://doi.org/10.1128/MMBR.00009-09

Forstová, J., Krauzewicz, N., Sandig, V., Elliott, J., Palková, Z., Strauss, M., Griffin, B.E., 1995. Polyoma virus pseudocapsids as efficient carriers of heterologous DNA into mammalian cells. Hum. Gene Ther. 6, 297–306. https://doi.org/10.1089/hum.1995.6.3-297

Forstova, J., Krauzewicz, N., Wallace, S., Street, A.J., Dilworth, S.M., Beard, S., Griffin, B.E., 1993. Cooperation of structural proteins during late events in the life cycle of polyomavirus. J. Virol. 67, 1405–1413.

Fraiberk, M., Hájková, M., Krulová, M., Kojzarová, M., Drda Morávková, A., Pšikal, I., Forstová, J., 2017. Exploitation of stable nanostructures based on the mouse

polyomavirus for development of a recombinant vaccine against porcine circovirus 2. PLoS ONE 12. https://doi.org/10.1371/journal.pone.0184870

Frič, J., Marek, M., Hrušková, V., Holáň, V., Forstová, J., 2008. Cellular and humoral immune responses to chimeric EGFP-pseudocapsids derived from the mouse polyomavirus after their intranasal administration. Vaccine 26, 3242–3251. https://doi.org/10.1016/j.vaccine.2008.04.006

Galaway, F.A., Stockley, P.G., 2013. MS2 Viruslike Particles: A Robust, Semisynthetic Targeted Drug Delivery Platform. Mol. Pharm. 10, 59–68. https://doi.org/10.1021/mp3003368

Gao, D., Lin, X.-P., Zhang, Z.-P., Li, W., Men, D., Zhang, X.-E., Cui, Z.-Q., 2016. Intracellular cargo delivery by virus capsid protein-based vehicles: From nano to micro. Nanomedicine Nanotechnol. Biol. Med. 12, 365–376. https://doi.org/10.1016/j.nano.2015.10.023

Gao, D., Zhang, Z.-P., Li, F., Men, D., Deng, J.-Y., Wei, H.-P., Zhang, X.-E., Cui, Z.-Q., 2013. Quantum dot-induced viral capsid assembling in dissociation buffer. Int. J. Nanomedicine 8, 2119–2128. https://doi.org/10.2147/IJN.S44534

Ge, C., Tian, J., Zhao, Y., Chen, C., Zhou, R., Chai, Z., 2015. Towards understanding of nanoparticle–protein corona. Arch. Toxicol. 89, 519–539. https://doi.org/10.1007/s00204-015-1458-0

Ghavami, M., Saffar, S., Emamy, B.A., Peirovi, A., Shokrgozar, M.A., Serpooshan, V., Mahmoudi, M., 2012. Plasma concentration gradient influences the protein corona decoration on nanoparticles. RSC Adv. 3, 1119–1126. https://doi.org/10.1039/C2RA22093H

Gilbert, J.M., Benjamin, T.L., 2000. Early Steps of Polyomavirus Entry into Cells. J. Virol. 74, 8582–8588.

Gillock, E.T., Rottinghaus, S., Chang, D., Cai, X., Smiley, S.A., An, K., Consigli, R.A., 1997. Polyomavirus major capsid protein VP1 is capable of packaging cellular DNA when expressed in the baculovirus system. J. Virol. 71, 2857–2865.

Gleiter, S., Lilie, H., 2001. Coupling of antibodies via protein Z on modified polyoma virus-like particles. Protein Sci. 10, 434–444.

Gleiter, S., Stubenrauch, K., Lilie, H., 1999. Changing the surface of a virus shell fusion of an enzyme to polyoma VP1. Protein Sci. 8, 2562–2569.

Goldmann, C., Stolte, N., Nisslein, T., Hunsmann, G., Lüke, W., Petry, H., 2000. Packaging of small molecules into VP1-virus-like particles of the human polyomavirus JC virus. J. Virol. Methods 90, 85–90.

Gossen, M., Bujard, H., 1992. Tight control of gene expression in mammalian cells by tetracycline-responsive promoters. Proc. Natl. Acad. Sci. U. S. A. 89, 5547–5551.

Gref, null, Lück, null, Quellec, null, Marchand, null, Dellacherie, null, Harnisch, null, Blunk, null, Müller, null, 2000. "Stealth" corona-core nanoparticles surface modified by polyethylene glycol (PEG): influences of the corona (PEG chain length and surface density) and of the core composition on phagocytic uptake and plasma protein adsorption. Colloids Surf. B Biointerfaces 18, 301–313.

Griffith, J.P., Griffith, D.L., Rayment, I., Murakami, W.T., Caspar, D.L., 1992. Inside polyomavirus at 25-A resolution. Nature 355, 652–654. https://doi.org/10.1038/355652a0

Günther, C., Schmidt, U., Rudolph, R., Böhm, G., 2001. Protein and peptide delivery via engineered polyomavirus-like particles. FASEB J. https://doi.org/10.1096/fj.00-0645fje

Gupta, A.K., Gupta, M., 2005. Synthesis and surface engineering of iron oxide nanoparticles for biomedical applications. Biomaterials 26, 3995–4021. https://doi.org/10.1016/j.biomaterials.2004.10.012

Gupta, S.S., Kuzelka, J., Singh, P., Lewis, W.G., Manchester, M., Finn, M.G., 2005. Accelerated Bioorthogonal Conjugation: A Practical Method for the Ligation of Diverse Functional Molecules to a Polyvalent Virus Scaffold. Bioconjug. Chem. 16, 1572–1579. https://doi.org/10.1021/bc050147l

Hamad, I., Al-Hanbali, O., Hunter, A.C., Rutt, K.J., Andresen, T.L., Moghimi, S.M., 2010. Distinct polymer architecture mediates switching of complement activation pathways at the nanosphere-serum interface: implications for stealth nanoparticle engineering. ACS Nano 4, 6629–6638. https://doi.org/10.1021/nn101990a

Harvie, P., Wong, F.M.P., Bally, M.B., 2000. Use of Poly(ethylene glycol)–Lipid Conjugates to Regulate the Surface Attributes and Transfection Activity of Lipid–DNA Particles. J. Pharm. Sci. 89, 652–663. https://doi.org/10.1002/(SICI)1520-6017(200005)89:5<652::AID-JPS11>3.0.CO;2-H

Heidari, S., Krauzewicz, N., Kalantari, M., Vlastos, A., Griffin, B.E., Dalianis, T., 2000. Persistence and tissue distribution of DNA in normal and immunodeficient mice inoculated with polyomavirus VP1 pseudocapsid complexes or polyomavirus. J. Virol. 74, 11963–11965.

Hermanson, G.T., 2008. Bioconjugate techniques. Academic Press, Amsterdam.

Hong, V., Presolski, S.I., Ma, C., Finn, M.G., 2009. Analysis and Optimization of Copper-Catalyzed Azide-Alkyne Cycloaddition for Bioconjugation. Angew. Chem. Int. Ed. 48, 9879–9883. https://doi.org/10.1002/anie.200905087

Hrusková, V., Morávková, A., Babiarová, K., Ludvíková, V., Fric, J., Vonka, V., Forstová, J., 2009. Bcr-Abl fusion sequences do not induce immune responses in mice when administered in mouse polyomavirus based virus-like particles. Int. J. Oncol. 35, 1247–1256.

Huang, R.K., Steinmetz, N.F., Fu, C.-Y., Manchester, M., Johnson, J.E., 2006. Transferrin-mediated targeting of bacteriophage HK97 nanoparticles into tumor cells. Nanomed. 6, 55–68. https://doi.org/10.2217/nnm.10.99

Hughes, L.D., Rawle, R.J., Boxer, S.G., 2014. Choose Your Label Wisely: Water-Soluble Fluorophores Often Interact with Lipid Bilayers. PLoS ONE 9, e87649. https://doi.org/10.1371/journal.pone.0087649

Java, Anuja, Cheng, X., Brennan, D.C., 2012. Polyomavirus Infections of Humans., in: Encyclopedia of Life Sciences. John Wiley & Sons, Chichester.

Jiang, W., Kim, B.Y.S., Rutka, J.T., Chan, W.C.W., 2008. Nanoparticle-mediated cellular response is size-dependent. Nat. Nanotechnol. 3, 145–150. https://doi.org/10.1038/nnano.2008.30

Khalaj-Kondori, M., Kavoosi, M., Rahmati-Yamchi, M., Kadivar, M., 2016. Preparation of a transferrin-targeted M13-based gene nanocarrier and evaluation of its efficacy for gene delivery and expression in eukaryote cells. Turk. J. Biol. 40, 561–570. https://doi.org/10.3906/biy-1503-16

Khalaj-Kondori, M., Sadeghizadeh, M., Behmanesh, M., Saggio, I., Monaci, P., 2011. Chemical coupling as a potent strategy for preparation of targeted bacteriophage-derived gene nanocarriers into eukaryotic cells: Chemically targeted bacteriophage-derived gene nanocarriers. J. Gene Med. 13, 622–631. https://doi.org/10.1002/jgm.1617

Khlebtsov, N., Bogatyrev, V., Dykman, L., Khlebtsov, B., Staroverov, S., Shirokov, A., Matora, L., Khanadeev, V., Pylaev, T., Tsyganova, N., Terentyuk, G., 2013. Analytical and Theranostic Applications of Gold Nanoparticles and Multifunctional Nanocomposites. Theranostics 3, 167–180. https://doi.org/10.7150/thno.5716

Kimchi-Sarfaty, C., Brittain, S., Garfield, S., Caplen, N.J., Tang, Q., Gottesman, M.M., 2005. Efficient delivery of RNA interference effectors via in vitro-packaged SV40 pseudovirions. Hum. Gene Ther. 16, 1110–1115. https://doi.org/10.1089/hum.2005.16.1110

Kimchi-Sarfaty, C., Gottesman, M.M., 2012. SV40 in vitro packaging: a pseudovirion gene delivery system. Cold Spring Harb. Protoc. 2012, 1019–1023. https://doi.org/10.1101/pdb.prot071043

Kimchi-Sarfaty, C., Gottesman, M.M., 2004. SV40 pseudovirions as highly efficient vectors for gene transfer and their potential application in cancer therapy. Curr. Pharm. Biotechnol. 5, 451–458.

Kitai, Y., Fukuda, H., Enomoto, T., Asakawa, Y., Suzuki, T., Inouye, S., Handa, H., 2011. Cell selective targeting of a simian virus 40 virus-like particle conjugated to epidermal growth factor. J. Biotechnol. 155, 251–256. https://doi.org/10.1016/j.jbiotec.2011.06.030

Kler, S., Asor, R., Li, C., Ginsburg, A., Harries, D., Oppenheim, A., Zlotnick, A., Raviv, U., 2012. RNA encapsidation by SV40-derived nanoparticles follows a rapid two-state mechanism. J. Am. Chem. Soc. 134, 8823–8830. https://doi.org/10.1021/ja2110703

Knop, K., Hoogenboom, R., Fischer, D., Schubert, U.S., 2010. Poly(ethylene glycol) in drug delivery: pros and cons as well as potential alternatives. Angew. Chem. Int. Ed Engl. 49, 6288–6308. https://doi.org/10.1002/anie.200902672

Kondo, K., Noguchi, M., Mukai, K., Matsuno, Y., Sato, Y., Shimosato, Y., Monden, Y., 1990. Transferrin receptor expression in adenocarcinoma of the lung as a histopathologic indicator of prognosis. Chest 97, 1367–1371.

Krauzewicz, N., Cox, C., Soeda, E., Clark, B., Rayner, S., Griffin, B.E., 2000. Sustained ex vivo and in vivo transfer of a reporter gene using polyoma virus pseudocapsids. Gene Ther. 7, 1094–1102.

Kreppel, F., Gackowski, J., Schmidt, E., Kochanek, S., 2005. Combined Genetic and Chemical Capsid Modifications Enable Flexible and Efficient De- and Retargeting of Adenovirus Vectors. Mol. Ther. 12, 107–117. https://doi.org/10.1016/j.ymthe.2005.03.006

Kristensen, C.B., Gram, L.F., 2009. Equilibrium Dialysis for Determination of Protein Binding of Imipramine - Evaluation of a Method. Acta Pharmacol. Toxicol. (Copenh.) 50, 130–136. https://doi.org/10.1111/j.1600-0773.1982.tb00954.x

Lee, K.L., Shukla, S., Wu, M., Ayat, N.R., El Sanadi, C.E., Wen, A.M., Edelbrock, J.F., Pokorski, J.K., Commandeur, U., Dubyak, G.R., Steinmetz, N.F., 2015. Stealth filaments: polymer chain length and conformation affect the in vivo fate of PEGylated potato virus X. Acta Biomater. 19, 166–179. https://doi.org/10.1016/j.actbio.2015.03.001

Leverence, R., Mason, A.B., Kaltashov, I.A., 2010. Noncanonical interactions between serum transferrin and transferrin receptor evaluated with electrospray ionization mass spectrometry. Proc. Natl. Acad. Sci. U. S. A. 107, 8123–8128. https://doi.org/10.1073/pnas.0914898107

Li, F., Chen, H., Zhang, Y., Chen, Z., Zhang, Z.-P., Zhang, X.-E., Wang, Q., 2012. Three-Dimensional Gold Nanoparticle Clusters with Tunable Cores Templated by a Viral Protein Scaffold. Small 8, 3832–3838. https://doi.org/10.1002/smll.201201047

Li, F., Gao, D., Zhai, X., Chen, Y., Fu, T., Wu, D., Zhang, Z.-P., Zhang, X.-E., Wang, Q., 2011. Tunable, Discrete, Three-Dimensional Hybrid Nanoarchitectures. Angew. Chem. Int. Ed. 50, 4202–4205. https://doi.org/10.1002/anie.201007433

Li, F., Li, K., Cui, Z.-Q., Zhang, Z.-P., Wei, H.-P., Gao, D., Deng, J.-Y., Zhang, X.-E., 2010. Viral Coat Proteins as Flexible Nano-Building-Blocks for Nanoparticle Encapsulation. Small 6, 2301–2308. https://doi.org/10.1002/smll.201001078

Li, F., Zhang, Z.-P., Peng, J., Cui, Z.-Q., Pang, D.-W., Li, K., Wei, H.-P., Zhou, Y.-F., Wen, J.-K., Zhang, X.-E., 2009. Imaging Viral Behavior in Mammalian Cells with Self-Assembled Capsid-Quantum-Dot Hybrid Particles. Small 5, 718–726. https://doi.org/10.1002/smll.200801303

Li, J., Zhu, J.-J., 2013. Quantum dots for fluorescent biosensing and bio-imaging applications. The Analyst 138, 2506–2515. https://doi.org/10.1039/c3an36705c

Liddington, R.C., Yan, Y., Moulai, J., Sahli, R., Benjamin, T.L., Harrison, S.C., 1991. Structure of simian virus 40 at 3.8-Å resolution. Nature 354, 278–284. https://doi.org/10.1038/354278a0

Liebl, D., Difato, F., Hornikova, L., Mannova, P., Stokrova, J., Forstova, J., 2006. Mouse Polyomavirus Enters Early Endosomes, Requires Their Acidic pH for Productive Infection, and Meets Transferrin Cargo in Rab11-Positive Endosomes. J. Virol. 80, 4610–4622. https://doi.org/10.1128/JVI.80.9.4610-4622.2006

Lin, M.-C., Wang, M., Fang, C.-Y., Chen, P.-L., Shen, C.-H., Chang, D., 2014. Inhibition of BK virus replication in human kidney cells by BK virus large tumor antigen-specific shRNA delivered by JC virus-like particles. Antiviral Res. 103, 25–31. https://doi.org/10.1016/j.antiviral.2013.12.013

Lin, Z.J., Musiano, D., Abbot, A., Shum, L., 2005. In vitro plasma protein binding determination of flunarizine using equilibrium dialysis and liquid chromatography–tandem mass spectrometry. J. Pharm. Biomed. Anal. 37, 757–762. https://doi.org/10.1016/j.jpba.2004.10.050

Liu, H., Moy, P., Kim, S., Xia, Y., Rajasekaran, A., Navarro, V., Knudsen, B., Bander, N.H., 1997. Monoclonal Antibodies to the Extracellular Domain of Prostate-specific Membrane Antigen Also React with Tumor Vascular Endothelium. Cancer Res. 57, 3629–3634.

Liu, H., Rajasekaran, A.K., Moy, P., Xia, Y., Kim, S., Navarro, V., Rahmati, R., Bander, N.H., 1998. Constitutive and antibody-induced internalization of prostate-specific membrane antigen. Cancer Res. 58, 4055–4060.

Lund, P.E., Hunt, R.C., Gottesman, M.M., Kimchi-Sarfaty, C., 2010. Pseudovirions as vehicles for the delivery of siRNA. Pharm. Res. 27, 400–420. https://doi.org/10.1007/s11095-009-0012-2

Lundqvist, M., Stigler, J., Elia, G., Lynch, I., Cedervall, T., Dawson, K.A., 2008. Nanoparticle size and surface properties determine the protein corona with possible implications for biological impacts. Proc. Natl. Acad. Sci. U. S. A. 105, 14265–14270. https://doi.org/10.1073/pnas.0805135105

Lynch, I., Dawson, K.A., 2008. Protein-nanoparticle interactions. Nano Today 3, 40–47. https://doi.org/10.1016/S1748-0132(08)70014-8

Maffre, P., Nienhaus, K., Amin, F., Parak, W.J., Nienhaus, G.U., 2011. Characterization of protein adsorption onto FePt nanoparticles using dual-focus fluorescence correlation spectroscopy. Beilstein J. Nanotechnol. 2, 374–383. https://doi.org/10.3762/bjnano.2.43

Mahmoudi, M., Lynch, I., Ejtehadi, M.R., Monopoli, M.P., Bombelli, F.B., Laurent, S., 2011. Protein-nanoparticle interactions: opportunities and challenges. Chem. Rev. 111, 5610–5637. https://doi.org/10.1021/cr100440g

Mannova, P., Forstova, J., 2003. Mouse Polyomavirus Utilizes Recycling Endosomes for a Traffic Pathway Independent of COPI Vesicle Transport. J. Virol. 77, 1672–1681. https://doi.org/10.1128/JVI.77.3.1672-1681.2003

Mannová, P., Liebl, D., Krauzewicz, N., Fejtová, A., Stokrová, J., Palková, Z., Griffin, B.E., Forstová, J., 2002. Analysis of mouse polyomavirus mutants with lesions in the minor capsid proteins. J. Gen. Virol. 83, 2309–2319.

Maurer, T., Eiber, M., Schwaiger, M., Gschwend, J.E., 2016. Current use of PSMA-PET in prostate cancer management. Nat. Rev. Urol. 13, 226–235. https://doi.org/10.1038/nrurol.2016.26

Mishra, S., 2004. PEGylation significantly affects cellular uptake and intracellular trafficking of non-viral gene delivery particles. Eur. J. Cell Biol. 83, 97–111. https://doi.org/10.1078/0171-9335-00363

Moens, U., Calvignac-Spencer, S., Lauber, C., Ramqvist, T., Feltkamp, M.C.W., Daugherty, M.D., Verschoor, E.J., Ehlers, B., 2017. ICTV Virus Taxonomy Profile: Polyomaviridae. J. Gen. Virol. 98, 1159–1160. https://doi.org/10.1099/jgv.0.000839

Moghimi, S.M., Szebeni, J., 2003. Stealth liposomes and long circulating nanoparticles: critical issues in pharmacokinetics, opsonization and protein-binding properties. Prog. Lipid Res. 42, 463–478. https://doi.org/10.1016/S0163-7827(03)00033-X

Monopoli, M.P., Aberg, C., Salvati, A., Dawson, K.A., 2012. Biomolecular coronas provide the biological identity of nanosized materials. Nat. Nanotechnol. 7, 779–786. https://doi.org/10.1038/nnano.2012.207

Monopoli, M.P., Walczyk, D., Campbell, A., Elia, G., Lynch, I., Bombelli, F.B., Dawson, K.A., 2011. Physical-chemical aspects of protein corona: relevance to in vitro and in vivo biological impacts of nanoparticles. J. Am. Chem. Soc. 133, 2525–2534. https://doi.org/10.1021/ja107583h

Montross, L., Watkins, S., Moreland, R.B., Mamon, H., Caspar, D.L., Garcea, R.L., 1991. Nuclear assembly of polyomavirus capsids in insect cells expressing the major capsid protein VP1. J. Virol. 65, 4991–4998.

Moreland, R.B., Montross, L., Garcea, R.L., 1991. Characterization of the DNA-binding properties of the polyomavirus capsid protein VP1. J. Virol. 65, 1168–1176.

Nakanishi, A., Chapellier, B., Maekawa, N., Hiramoto, M., Kuge, T., Takahashi, R., Handa, H., Imai, T., 2008. SV40 vectors carrying minimal sequence of viral origin with exchangeable capsids. Virology 379, 110–117. https://doi.org/10.1016/j.virol.2008.06.032

Nakase, M., Inui, M., Okumura, K., Kamei, T., Nakamura, S., Tagawa, T., 2005. p53 gene therapy of human osteosarcoma using a transferrin-modified cationic liposome. Mol. Cancer Ther. 4, 625–631.

Neburkova, J., Sedlak, F., Zackova Suchanova, J., Kostka, L., Sacha, P., Subr, V., Etrych, T., Simon, P., Barinkova, J., Krystufek, R., Spanielova, H., Forstova, J., Konvalinka, J., Cigler, P., 2018. Inhibitor–GCPII Interaction: Selective and Robust System for Targeting Cancer Cells with Structurally Diverse Nanoparticles. Mol. Pharm. https://doi.org/10.1021/acs.molpharmaceut.7b00889

Neugebauer, M., Walders, B., Brinkman, M., Ruehland, C., Schumacher, T., Bertling, W.M., Geuther, E., Reiser, C.O.A., Reichel, C., Strich, S., Hess, J., 2006. Development of a vaccine marker technology: Display of B cell epitopes on the surface of recombinant polyomavirus-like pentamers and capsoids induces peptide-specific antibodies in piglets after vaccination. Biotechnol. J. 1, 1435–1446. https://doi.org/10.1002/biot.200600149

Nguyen, V.H., Lee, B.-J., 2017. Protein corona: a new approach for nanomedicine design. Int. J. Nanomedicine 12, 3137–3151. https://doi.org/10.2147/IJN.S129300

Niikura, K., Sugimura, N., Musashi, Y., Mikuni, S., Matsuo, Y., Kobayashi, S., Nagakawa, K., Takahara, S., Takeuchi, C., Sawa, H., Kinjo, M., Ijiro, K., 2013. Virus-like particles with removable cyclodextrins enable glutathione-triggered drug release in cells. Mol. Biosyst. 9, 501. https://doi.org/10.1039/c2mb25420d

Oh, K.S., Engler, J.A., Joung, I., 2005. Enhancement of gene delivery to cancer cells by a retargeted adenovirus. J. Microbiol. 43, 179–182.

O'Keefe, D.S., Bacich, D.J., Heston, W.D.W., 2001. Prostate Specific Membrane Antigen, in: Prostate Cancer, Contemporary Cancer Research. Humana Press, Totowa, NJ, pp. 307–326. https://doi.org/10.1007/978-1-59259-009-4_18

Oppenheim, A., Sandalon, Z., Peleg, A., Shaul, O., Nicolis, S., Ottolenghi, S., 1992. A cis-acting DNA signal for encapsidation of simian virus 40. J. Virol. 66, 5320–5328.

Otsuka, H., Nagasaki, Y., Kataoka, K., 2003. PEGylated nanoparticles for biological and pharmaceutical applications. Adv. Drug Deliv. Rev. 55, 403–419.

Patel, K.G., Swartz, J.R., 2011. Surface Functionalization of Virus-Like Particles by Direct Conjugation Using Azide–Alkyne Click Chemistry. Bioconjug. Chem. 22, 376–387. https://doi.org/10.1021/bc100367u

Perry, J.L., Reuter, K.G., Kai, M.P., Herlihy, K.P., Jones, S.W., Luft, J.C., Napier, M., Bear, J.E., DeSimone, J.M., 2012. PEGylated PRINT Nanoparticles: The Impact of PEG Density on Protein Binding, Macrophage Association, Biodistribution, and Pharmacokinetics. Nano Lett. 12, 5304–5310. https://doi.org/10.1021/nl302638g

Petrini, M., Pelosi-Testa, E., Sposi, N.M., Mastroberardino, G., Camagna, A., Bottero, L., Mavilio, F., Testa, U., Peschle, C., 1989. Constitutive expression and abnormal glycosylation of transferrin receptor in acute T-cell leukemia. Cancer Res. 49, 6989–6996.

Piella, J., Bastús, N.G., Puntes, V., 2017. Size-Dependent Protein–Nanoparticle Interactions in Citrate-Stabilized Gold Nanoparticles: The Emergence of the Protein Corona. Bioconjug. Chem. 28, 88–97. https://doi.org/10.1021/acs.bioconjchem.6b00575

Pino, P. del, Pelaz, B., Zhang, Q., Maffre, P., Nienhaus, G.U., Parak, W.J., 2014. Protein corona formation around nanoparticles – from the past to the future. Mater. Horiz. 1, 301–313. https://doi.org/10.1039/C3MH00106G

Pitek, A.S., O'Connell, D., Mahon, E., Monopoli, M.P., Baldelli Bombelli, F., Dawson, K.A., 2012. Transferrin Coated Nanoparticles: Study of the Bionano Interface in Human Plasma. PLoS ONE 7. https://doi.org/10.1371/journal.pone.0040685

Pitek, A.S., Veliz, F.A., Jameson, S.A., Steinmetz, N.F., 2018. Interactions Between Plant Viral Nanoparticles (VNPs) and Blood Plasma Proteins, and Their Impact on the VNP In Vivo Fates, in: Virus-Derived Nanoparticles for Advanced Technologies, Methods in Molecular Biology. Humana Press, New York, NY, pp. 591–608. https://doi.org/10.1007/978-1-4939-7808-3_38

Pitek, A.S., Wen, A.M., Shukla, S., Steinmetz, N.F., 2016. The protein corona of plant virus nanoparticles influences their dispersion properties, cellular interactions and in vivo fates. Small Weinh. Bergstr. Ger. 12, 1758–1769. https://doi.org/10.1002/smll.201502458

Pokorski, J.K., Hovlid, M.L., Finn, M.G., 2011. Cell Targeting with Hybrid Qβ Virus-Like Particles Displaying Epidermal Growth Factor. ChemBioChem 12, 2441–2447. https://doi.org/10.1002/cbic.201100469

Pozzi, D., Colapicchioni, V., Caracciolo, G., Piovesana, S., Capriotti, A.L., Palchetti, S., De Grossi, S., Riccioli, A., Amenitsch, H., Laganà, A., 2014. Effect of polyethyleneglycol (PEG) chain length on the bio-nano-interactions between PEGylated lipid nanoparticles and biological fluids: from nanostructure to uptake in cancer cells. Nanoscale 6, 2782–2792. https://doi.org/10.1039/c3nr05559k

Presolski, S.I., Hong, V.P., Finn, M.G., 2011. Copper-Catalyzed Azide-Alkyne Click Chemistry for Bioconjugation. Curr. Protoc. Chem. Biol. 3, 153–162. https://doi.org/10.1002/9780470559277.ch110148

Prior, R., Reifenberger, G., Wechsler, W., 1990. Transferrin receptor expression in tumours of the human nervous system: relation to tumour type, grading and tumour growth fraction. Virchows Arch. A Pathol. Anat. Histopathol. 416, 491–496.

Prutki, M., Poljak-Blazi, M., Jakopovic, M., Tomas, D., Stipancic, I., Zarkovic, N., 2006. Altered iron metabolism, transferrin receptor 1 and ferritin in patients with colon cancer. Cancer Lett. 238, 188–196. https://doi.org/10.1016/j.canlet.2005.07.001

Qu, Q., Sawa, H., Suzuki, T., Semba, S., Henmi, C., Okada, Y., Tsuda, M., Tanaka, S., Atwood, W.J., Nagashima, K., 2004. Nuclear Entry Mechanism of the Human Polyomavirus JC Virus-like Particle ROLE OF IMPORTINS AND THE NUCLEAR PORE COMPLEX. J. Biol. Chem. 279, 27735–27742. https://doi.org/10.1074/jbc.M310827200

Rahman, M., Laurent, S., Tawil, N., Yahia, L., Mahmoudi, M., 2013. Nanoparticle and Protein Corona, in: Protein-Nanoparticle Interactions, Springer Series in Biophysics. Springer Berlin Heidelberg, pp. 21–44. https://doi.org/10.1007/978-3-642-37555-2_2

Rehor, I., Lee, K.L., Chen, K., Hajek, M., Havlik, J., Lokajova, J., Masat, M., Slegerova, J., Shukla, S., Heidari, H., Bals, S., Steinmetz, N.F., Cigler, P., 2015. Plasmonic Nanodiamonds: Targeted Core-Shell Type Nanoparticles for Cancer Cell Thermoablation. Adv. Healthc. Mater. 4, 460–468. https://doi.org/10.1002/adhm.201400421

Rhee, J.-K., Baksh, M., Nycholat, C., Paulson, J.C., Kitagishi, H., Finn, M.G., 2012. Glycan-Targeted Virus-like Nanoparticles for Photodynamic Therapy. Biomacromolecules 13, 2333–2338. https://doi.org/10.1021/bm300578p

Richardson, D.R., Ponka, P., 1997. The molecular mechanisms of the metabolism and transport of iron in normal and neoplastic cells. Biochim. Biophys. Acta BBA-Rev. Biomembr. 1331, 1–40.

Richterova, Z., Liebl, D., Horak, M., Palkova, Z., Stokrova, J., Hozak, P., Korb, J., Forstova, J., 2001. Caveolae Are Involved in the Trafficking of Mouse Polyomavirus Virions and Artificial VP1 Pseudocapsids toward Cell Nuclei. J. Virol. 75, 10880–10891. https://doi.org/10.1128/JVI.75.22.10880-10891.2001

Richterová, Z., Liebl, D., Horák, M., Palková, Z., Štokrová, J., Hozák, P., Korb, J., Forstová, J., 2001. Caveolae Are Involved in the Trafficking of Mouse Polyomavirus Virions and Artificial VP1 Pseudocapsids toward Cell Nuclei. J. Virol. 75, 10880–10891. https://doi.org/10.1128/JVI.75.22.10880-10891.2001

Ryschich, E., Huszty, G., Knaebel, H.P., Hartel, M., Büchler, M.W., Schmidt, J., 2004. Transferrin receptor is a marker of malignant phenotype in human pancreatic cancer and in neuroendocrine carcinoma of the pancreas. Eur. J. Cancer Oxf. Engl. 1990 40, 1418–1422. https://doi.org/10.1016/j.ejca.2004.01.036

Šácha, P., Knedlík, T., Schimer, J., Tykvart, J., Parolek, J., Navrátil, V., Dvořáková, P., Sedlák, F., Ulbrich, K., Strohalm, J., Majer, P., Šubr, V., Konvalinka, J., 2016. iBodies: Modular Synthetic Antibody Mimetics Based on Hydrophilic Polymers Decorated with Functional Moieties. Angew. Chem. Int. Ed. 55, 2356–2360. https://doi.org/10.1002/anie.201508642

Saha, K., Moyano, D.F., Rotello, V.M., 2013. Protein coronas suppress the hemolytic activity of hydrophilic and hydrophobic nanoparticles. Mater. Horiz. 1, 102–105. https://doi.org/10.1039/C3MH00075C

Salunke, D.M., Caspar, D.L.D., Garcea, R.L., 1986. Self-assembly of purified polyomavirus capsid protein VP1. Cell 46, 895–904. https://doi.org/10.1016/0092-8674(86)90071-1

Salvati, A., Pitek, A.S., Monopoli, M.P., Prapainop, K., Bombelli, F.B., Hristov, D.R., Kelly, P.M., Åberg, C., Mahon, E., Dawson, K.A., 2013. Transferrin-functionalized nanoparticles lose their targeting capabilities when a biomolecule corona adsorbs on the surface. Nat. Nanotechnol. 8, 137–143. https://doi.org/10.1038/nnano.2012.237

Sanna, V., Pintus, G., Roggio, A.M., Punzoni, S., Posadino, A.M., Arca, A., Marceddu, S., Bandiera, P., Uzzau, S., Sechi, M., 2011. Targeted biocompatible nanoparticles for the delivery of (-)-epigallocatechin 3-gallate to prostate cancer cells. J. Med. Chem. 54, 1321.

Schmidt, U., Kenklies, J., Rudolph, R., Böhm, G., 1999. Site-specific fluorescence labelling of recombinant polyomavirus-like particles. Biol. Chem. 380, 397–401. https://doi.org/10.1515/BC.1999.053

Schmidt, U., Rudolph, R., Böhm, G., 2001. Binding of external ligands onto an engineered virus capsid. Protein Eng. 14, 769–774.

Schnaar, R.L., Gerardy-Schahn, R., Hildebrandt, H., 2014. Sialic Acids in the Brain: Gangliosides and Polysialic Acid in Nervous System Development, Stability, Disease,

and Regeneration. Physiol. Rev. 94, 461–518. https://doi.org/10.1152/physrev.00033.2013
Schowalter, R.M., Buck, C.B., 2013. The Merkel Cell Polyomavirus Minor Capsid Protein. PLoS Pathog 9, e1003558. https://doi.org/10.1371/journal.ppat.1003558
Seymour, G.J., Walsh, M.D., Lavin, M.F., Strutton, G., Gardiner, R.A., 1987. Transferrin receptor expression by human bladder transitional cell carcinomas. Urol. Res. 15, 341–344.
Shin, Y.C., Folk, W.R., 2003. Formation of Polyomavirus-Like Particles with Different VP1 Molecules That Bind the Urokinase Plasminogen Activator Receptor. J. Virol. 77, 11491–11498. https://doi.org/10.1128/JVI.77.21.11491-11498.2003
Silver, D.A., Pellicer, I., Fair, W.R., Heston, W.D., Cordon-Cardo, C., 1997. Prostate-specific membrane antigen expression in normal and malignant human tissues. Clin. Cancer Res. 3, 81–85.
Skrastina, D., Bulavaite, A., Sominskaya, I., Kovalevska, L., Ose, V., Priede, D., Pumpens, P., Sasnauskas, K., 2008. High immunogenicity of a hydrophilic component of the hepatitis B virus preS1 sequence exposed on the surface of three virus-like particle carriers. Vaccine 26, 1972–1981. https://doi.org/10.1016/j.vaccine.2008.02.030
Soldatova, I., Prilepskaja, T., Abrahamyan, L., Forstová, J., Huérfano, S., 2018. Interaction of the Mouse Polyomavirus Capsid Proteins with Importins Is Required for Efficient Import of Viral DNA into the Cell Nucleus. Viruses 10. https://doi.org/10.3390/v10040165
Sontag, E., Fedorov, S., Kamibayashi, C., Robbins, D., Cobb, M., Mumby, M., 1993. The interaction of SV40 small tumor antigen with protein phosphatase 2A stimulates the map kinase pathway and induces cell proliferation. Cell 75, 887–897.
Spanielová, H., Fraiberk, M., Suchanová, J., Soukup, J., Forstová, J., 2014. The encapsidation of polyomavirus is not defined by a sequence-specific encapsidation signal. Virology 450–451, 122–131. https://doi.org/10.1016/j.virol.2013.12.010
Španielová, H., Fraiberk, M., Suchanová, J., Soukup, J., Forstová, J., 2014. The encapsidation of polyomavirus is not defined by a sequence-specific encapsidation signal. Virology 450–451, 122–131. https://doi.org/10.1016/j.virol.2013.12.010
Stehle, T., Gamblin, S.J., Yan, Y., Harrison, S.C., 1996. The structure of simian virus 40 refined at 3.1 A resolution. Struct. Lond. Engl. 1993 4, 165–182.
Stehle, T., Harrison, S.C., 1996. Crystal structures of murine polyomavirus in complex with straight-chain and branched-chain sialyloligosaccharide receptor fragments. Struct. Lond. Engl. 1993 4, 183–194.
Stehle, T., Yan, Y., Benjamin, T.L., Harrison, S.C., 1994. Structure of murine polyomavirus complexed with an oligosaccharide receptor fragment. Nature 369, 160–163. https://doi.org/10.1038/369160a0
Štokrová, J., Palková, Z., Fischer, L., Richterová, Z., Korb, J., Griffin, B.E., Forstová, J., 1999. Interactions of heterologous DNA with polyomavirus major structural protein, VP1. FEBS Lett. 445, 119–125. https://doi.org/10.1016/S0014-5793(99)00003-4
Strable, E., Finn, M.G., 2009. Chemical modification of viruses and virus-like particles. Curr. Top. Microbiol. Immunol. 327, 1–21.
Stubenrauch, K., Gleiter, S., Brinkman, U., Rudolph, R., Lilie, H., 2001. Conjugation of an antibody Fv fragment to a virus coat protein: cell-specific targeting of recombinant polyoma-virus-like particles. Biochem J 356, 867–873.
Su, S.L., Huang, I.-P., Fair, W.R., Powell, C.T., Heston, W.D.W., 1995. Alternatively Spliced Variants of Prostate-specific Membrane Antigen RNA: Ratio of Expression as a Potential Measurement of Progression. Cancer Res. 55, 1441–1443.
Suchanova, J., 2012. Targeting prostate tumor cells by polyomavirus virus-like particles. Diploma thesis, Faculty of Science, Charles University, Prague.

Suchanova, J., Spanielova, H., Forstova, J., 2015. Applications of Viral Nanoparticles Based on Polyomavirus and Papillomavirus Structures, in: Viral Nanotechnology. CRC Press, pp. 303–362.

Sun, X., Yau, V.K., Briggs, B.J., Whittaker, G.R., 2005. Role of clathrin-mediated endocytosis during vesicular stomatitis virus entry into host cells. Virology 338, 53–60. https://doi.org/10.1016/j.virol.2005.05.006

Takahashi, R., Kanesashi, S., Inoue, T., Enomoto, T., Kawano, M., Tsukamoto, H., Takeshita, F., Imai, T., Ochiya, T., Kataoka, K., Yamaguchi, Y., Handa, H., 2008. Presentation of functional foreign peptides on the surface of SV40 virus-like particles. J. Biotechnol. 135, 385–392. https://doi.org/10.1016/j.jbiotec.2008.05.012

Tegerstedt, K., Franzén, A., Ramqvist, T., Dalianis, T., 2007. Dendritic cells loaded with polyomavirus VP1/VP2Her2 virus-like particles efficiently prevent outgrowth of a Her2/neu expressing tumor. Cancer Immunol. Immunother. 56, 1335–1344. https://doi.org/10.1007/s00262-007-0281-8

Tegerstedt, K., Lindencrona, J.A., Curcio, C., Andreasson, K., Tullus, C., Forni, G., Dalianis, T., Kiessling, R., Ramqvist, T., 2005. A Single Vaccination with Polyomavirus VP1/VP2Her2 Virus-Like Particles Prevents Outgrowth of HER-2/neu–Expressing Tumors. Cancer Res. 65, 5953–5957.

Tenzer, S., Docter, D., Kuharev, J., Musyanovych, A., Fetz, V., Hecht, R., Schlenk, F., Fischer, D., Kiouptsi, K., Reinhardt, C., Landfester, K., Schild, H., Maskos, M., Knauer, S.K., Stauber, R.H., 2013. Rapid formation of plasma protein corona critically affects nanoparticle pathophysiology. Nat. Nanotechnol. 8, 772–781. https://doi.org/10.1038/nnano.2013.181

Tenzer, S., Docter, D., Rosfa, S., Wlodarski, A., Kuharev, J., Rekik, A., Knauer, S.K., Bantz, C., Nawroth, T., Bier, C., Sirirattanapan, J., Mann, W., Treuel, L., Zellner, R., Maskos, M., Schild, H., Stauber, R.H., 2011. Nanoparticle size is a critical physicochemical determinant of the human blood plasma corona: a comprehensive quantitative proteomic analysis. ACS Nano 5, 7155–7167. https://doi.org/10.1021/nn201950e

Touzé, A., Bousarghin, L., Ster, C., Combita, A.-L., Roingeard, P., Coursaget, P., 2001. Gene transfer using human polyomavirus BK virus-like particles expressed in insect cells. J. Gen. Virol. 82, 3005–3009.

Treuel, L., Brandholt, S., Maffre, P., Wiegele, S., Shang, L., Nienhaus, G.U., 2014. Impact of protein modification on the protein corona on nanoparticles and nanoparticle-cell interactions. ACS Nano 8, 503–513. https://doi.org/10.1021/nn405019v

Treuel, L., Docter, D., Maskos, M., Stauber, R.H., 2015. Protein corona – from molecular adsorption to physiological complexity. Beilstein J. Nanotechnol. 6, 857–873. https://doi.org/10.3762/bjnano.6.88

Tsai, B., Gilbert, J.M., Stehle, T., Lencer, W., Benjamin, T.L., Rapoport, T.A., 2003. Gangliosides are receptors for murine polyoma virus and SV40. EMBO J. 22, 4346–4355. https://doi.org/10.1093/emboj/cdg439

Tykvart, J., Šácha, P., Bařinka, C., Knedlík, T., Starková, J., Lubkowski, J., Konvalinka, J., 2012. Efficient and versatile one-step affinity purification of in vivo biotinylated proteins: Expression, characterization and structure analysis of recombinant human glutamate carboxypeptidase II. Protein Expr. Purif. 82, 106–115. https://doi.org/10.1016/j.pep.2011.11.016

Tykvart, J., Schimer, J., Bařinková, J., Pachl, P., Poštová-Slavětínská, L., Majer, P., Konvalinka, J., Šácha, P., 2014. Rational design of urea-based glutamate carboxypeptidase II (GCPII) inhibitors as versatile tools for specific drug targeting and delivery. Bioorg. Med. Chem. 22, 4099–4108. https://doi.org/10.1016/j.bmc.2014.05.061

van Agthoven, A., Goridis, C., Naquet, P., Pierres, A., Pierres, M., 1984. Structural characteristics of the mouse transferrin receptor. Eur. J. Biochem. 140, 433–440.

Varnamkhasti, B.S., Hosseinzadeh, H., Azhdarzadeh, M., Vafaei, S.Y., Esfandyari-Manesh, M., Mirzaie, Z.H., Amini, M., Ostad, S.N., Atyabi, F., Dinarvand, R., 2015. Protein corona hampers targeting potential of MUC1 aptamer functionalized SN-38 core–shell nanoparticles. Int. J. Pharm. 494, 430–444. https://doi.org/10.1016/j.ijpharm.2015.08.060

Verhoef, J.J.F., Anchordoquy, T.J., 2013. Questioning the Use of PEGylation for Drug Delivery. Drug Deliv. Transl. Res. 3, 499–503.

Voronkova, T., Kazaks, A., Ose, V., Özel, M., Scherneck, S., Pumpens, P., Ulrich, R., 2007. Hamster polyomavirus-derived virus-like particles are able to transfer in vitro encapsidated plasmid DNA to mammalian cells. Virus Genes 34, 303–314. https://doi.org/10.1007/s11262-006-0028-1

Walker, R.A., Day, S.J., 1986. Transferrin receptor expression in non-malignant and malignant human breast tissue. J. Pathol. 148, 217–224. https://doi.org/10.1002/path.1711480305

Wally, J., Halbrooks, P.J., Vonrhein, C., Rould, M.A., Everse, S.J., Mason, A.B., Buchanan, S.K., 2006. The crystal structure of iron-free human serum transferrin provides insight into inter-lobe communication and receptor binding. J. Biol. Chem. 281, 24934–24944. https://doi.org/10.1074/jbc.M604592200

Wang, T., Zhang, Z., Gao, D., Li, F., Wei, H., Liang, X., Cui, Z., Zhang, X.-E., 2011. Encapsulation of gold nanoparticles by simian virus 40 capsids. Nanoscale 3, 4275. https://doi.org/10.1039/c1nr10568j

Welch, S., 1990. A comparison of the structure and properties of serum transferrin from 17 animal species. Comp. Biochem. Physiol. B 97, 417–427.

Weyermann, J., Lochmann, D., Zimmer, A., 2004. Comparison of antisense oligonucleotide drug delivery systems. J. Controlled Release 100, 411–423. https://doi.org/10.1016/j.jconrel.2004.08.027

Wong, S.S., 1991. Chemistry of Protein Conjugation and Cross-Linking. CRC Press.

Wu, M., Sherwin, T., Brown, W.L., Stockley, P.G., 2005. Delivery of antisense oligonucleotides to leukemia cells by RNA bacteriophage capsids. Nanomedicine Nanotechnol. Biol. Med. 1, 67–76. https://doi.org/10.1016/j.nano.2004.11.011

Xiao, W., Xiong, J., Zhang, S., Xiong, Y., Zhang, H., Gao, H., 2018. Influence of ligands property and particle size of gold nanoparticles on the protein adsorption and corresponding targeting ability. Int. J. Pharm. 538, 105–111. https://doi.org/10.1016/j.ijpharm.2018.01.011

Xu, X., Wu, J., Liu, Y., Saw, P.E., Tao, W., Yu, M., Zope, H., Si, M., Victorious, A., Rasmussen, J., Ayyash, D., Farokhzad, O.C., Shi, J., 2017. Multifunctional Envelope-Type siRNA Delivery Nanoparticle Platform for Prostate Cancer Therapy. ACS Nano 11, 2618–2627. https://doi.org/10.1021/acsnano.6b07195

Yallapu, M.M., Chauhan, N., Othman, S.F., Khalilzad-Sharghi, V., Ebeling, M.C., Khan, S., Jaggi, M., Chauhan, S.C., 2015. Implications of protein corona on physico-chemical and biological properties of magnetic nanoparticles. Biomaterials 46, 1–12. https://doi.org/10.1016/j.biomaterials.2014.12.045

Yang, D.C., Wang, F., Elliott, R.L., Head, J.F., 2001. Expression of transferrin receptor and ferritin H-chain mRNA are associated with clinical and histopathological prognostic indicators in breast cancer. Anticancer Res. 21, 541–549.

Yashunsky, V., Lirtsman, V., Golosovsky, M., Davidov, D., Aroeti, B., 2010. Real-Time Monitoring of Epithelial Cell-Cell and Cell-Substrate Interactions by Infrared Surface Plasmon Spectroscopy. Biophys. J. 99, 4028–4036. https://doi.org/10.1016/j.bpj.2010.10.017

Yates, A.J., Markowitz, D.L., Stephens, R.E., Pearl, D.K., Whisler, R.L., 1988. Growth inhibition of cultured human glioma cells by beta-interferon is not dependent on changes in ganglioside composition. J. Neuropathol. Exp. Neurol. 47, 119–127.

Yildiz, I., Tsvetkova, I., Wen, A.M., Shukla, S., Masarapu, M.H., Dragnea, B., Steinmetz, N.F., 2012. Engineering of Brome mosaic virus for biomedical applications. RSC Adv. 2, 3670. https://doi.org/10.1039/c2ra01376b

Zackova Suchanova, J., Neburkova, J., Spanielova, H., Forstova, J., Cigler, P., 2017. Retargeting Polyomavirus-Like Particles to Cancer Cells by Chemical Modification of Capsid Surface. Bioconjug. Chem. 28, 307–313. https://doi.org/10.1021/acs.bioconjchem.6b00622

Zeitlinger, M.A., Derendorf, H., Mouton, J.W., Cars, O., Craig, W.A., Andes, D., Theuretzbacher, U., 2011. Protein Binding: Do We Ever Learn? Antimicrob. Agents Chemother. 55, 3067–3074. https://doi.org/10.1128/AAC.01433-10

10. Supplements